Medizinische Klinik 1 und Poliklinik

Direktoren: Herr Prof. Dr. Gerhard Ehninger und Herr Prof. Dr. Martin Bornhäuser

---

Bone marrow niche-mimetics modulate hematopoietic stem cell function via adhesion signaling *in vitro*.

D i s s e r t a t i o n s s c h r i f t

zur Erlangung des akademischen Grades

Doctor rerum medicinalium

(Dr. rer. medic.)

vorgelegt

der Medizinischen Fakultät Carl Gustav Carus

der Technischen Universität Dresden

von

Martin Kräter M.Sc.

geboren am 10.09.1986

in Lutherstadt Wittenberg

Dresden 2017

1. Gutachter: Prof. Dr. Martin Bornhäuser

2.Gutachter: Prof. Dr. Ben Wielockx

Tag der mündlichen Prüfung: (Verteidigungstermin)

gez.: --

Vorsitzender der Promotionskommission

Anmerkung:

Die Eintragung der Gutachter und Tag der mündlichen Prüfung (Verteidigung) erfolgt nach Festlegung von Seiten der Medizinischen Fakultät Carl Gustav Carus der Technischen Universität Dresden. Die oben genannten Eintragungen werden durch die Doktoranden nach der Verteidigung zwecks Übergabe der fünf Pflichtexemplare an die Zweigbibliothek Medizin in gedruckter Form oder handschriftlich vorgenommen.

List of contents

Inhalt

List of contents

List of figures

List of figures

List of tables

Abbreviations

A	Alpha
AFM	Atomic force microscopy
amino-silan	3-aminopropyl-triethoxy-silane
AP	Alkaline phosphatase
APC	Allophycocyanin
APS	Ammonium persulfate
Arg	Arginine
Asp	Aspartic acid
AT	Attached
B	Beta
BCA	Bicinchoninic Acid
BFU-E	Burst forming erythrocyte
BM	Bone marrow
BMP	Bone morphogenic protein
BMT	Bone marrow transplantation
BrdU	Bromdesoxyuridin
BSA	Bovine Serum Albumin
CAM	Cell adhesion molecule
CD	Cluster of differentiation
cDNA	complementary Deoxyribonucleic acid
CFSE	Carboxyfluorescein succinimidyl ester
CFU	Colony forming unit
CFU-E	Colony forming unit erythrocyte
CFU-F	Colony forming unit fibroblasts
CFU-G	Colony forming unit granulocyte
CFU-M	Colony forming unit monocyte
CFU-GM	Colony forming unit granulocyte/monocyte
CFU-GEMM	Colony forming unit granulocyte/erythrocyte/monocyte/megakaryocyte
CLP	Common lymphoid progenitor

Abbreviations

CMP	Common myeloid progenitor
CO_2	Carbon dioxide
CXCL12, SDF-1	CXC-motiv-chemokin 12
CXCR4	C-X-C chemokine receptor type 4
Cy2 / 3	Cyanine Dye 2 / 3
DAPI	4',6-diamidino-2-phenylindole
DMSO	Dimethyl sulfoxide
DMEM	Dulbecco´s Modified Eagle Medium
DNA	Deoxyribonucleic acid
ECL	Enhanced chemiluminescence
ECM	Extracellular matrix
EDTA	Ethylenediaminetetraacetic acid
EGF	Epidermal growth factor
ELISA	Enzyme-linked immunosorbent assay
Epo	Erythropoietin
F-actin	Filamentous actin
FACS	Fluorescence-activated cell scanning / sorting
FAK	Focal adhesion kinase
FCS	Fetal Calf Serum
FGF	Fibroblast growth factor
FITC	Fluorescein isothiocyanate
FLT-3	FMS related tyrosine kinase 3
FN	Fibronectin
GAPDH	Glyceraldehyde-3-phosphate Dehydrogenase
G-CSF	Granulocyte-colony stimulating factor
Gly	Glycine
GMP	Granulocyte/macrophage progenitors
Gran	Granulocytes
HGF	Hepatocyte growth factor
H_2O_2	Hydrogen peroxide

Abbreviations

HPC	Hematopoietic progenitor cell
HRP	Horseradish peroxidase
HSA	Human Serum Albumin
HSC	Hematopoietic stem cell
HSPC	Hematopoietic stem and progenitor cell
hTERT	Human telomerase reverse transcriptase
IF	Immunofluorescence
IgG	Immunoglobulin G
IL-3	Interleukin 3
IL-8	Interleukin 8
ITG	Integrin
ISCT	International Society for Cellular Therapy
LB	Lysogeny Broth
LFA-1	Lymphocyte function-associated antigen 1
Lym	Lymphocytes
MC	Methylcellulose
MEP	Megakaryocyte/erythrocyte progenitors
MNC	Mononucleated cell
Mon	Monocytes
MSC	Mesenchymal stromal cell
NaCL	Sodium chloride
PB	Peripheral blood
PBS	Phosphate buffered saline
PCD	Plastic culture dish
PCR	Polymerase chain reaction
PDMS	Polydimethylsiloxane
PE	Phycoerythrin
PEI	Polyethylenimine
PFA	Paraformaldehyde
PI	Propidium iodide

Abbreviations

PI3K	Phosphatidylinositol-4,5-bisphosphate 3-kinase
POMA	Poly(octadecene alt maleic anhydride)
PTH	Parathyroid hormone
Puro	Puromycin
RBC	Red blood cell
RGD	Tripeptide (Arginine, Glycine and Aspartic acid)
RNA	Ribonucleic acid
RT	Room temperature
RT-DC	Real-time deformability cytometry
SCF	Stem Cell Factor
SCP-1	Single-cell picked clone 1
SD	Standard deviation
SDS	sodium dodecyl sulfate
S.E.M.	Standard error of the mean
shRNA	short hairpin Ribonucleic acid
SN	Supernatant
TGF-β	Transforming growth factor-β
THF	Tetrahydrofuran
TEMED	Tetramethylethylenediamine
Tyr	Tyrosine
VCAM1	Vascular cell-adhesion molecule 1
VGF	VGF nerve growth factor inducible protein
VLA-4	Very late antigen-4
VLA-5	Very Late Antigen-5
w/o	Without

1 Introduction

To develop and maintain a cohesive and complex biological entity from a single cell, such as specialized tissues consisting of billions of cells, necessitates the presence of multiple highly orchestrated processes and suitable scaffolds. In mammals, a gradual evolution from the zygote to more specialized cells takes place during the process of development (Evans, 2011), and multiple cells with the capacity to theoretically differentiate into all tissue-specific lineages need to evolve. Ernst Haeckel named these cells 'Stammzelle' in 1868 from which the term 'stem cells' has been derived. These stem cells can be classified as having various levels of differentiation capabilities depending on the cell types they give rise to. Thus, the zygote and the cells of the early blastomere are known as totipotent stem cells and they have the ability to generate an entire organism. Next, embryonic stem cells can be obtained from the inner cell mass of the blastocyst, are known as pluripotent stem cells, and are capable of differentiating into all three germ layers except the trophectoderm, which is extraembryonic (Rippon and Bishop, 2004). In contrast, tissue residing stem cells refer to cells that have a comparatively limited differentiation capacity, are therefore more specialized, and are called multipotent stem cells. They have the capacity to generate various lineages and give rise to specific progenitors, e.g. hematopoietic stem cells (HSCs; Eaves, 2015) or mesenchymal stem/stromal cells (MSCs; Zuk et al., 2002). Three more stem cell sub-classifications also exists, namely, oligopotent stem cells that refer to progenitors and can differentiate into subsets of mature tissue specific cells. Unipotent stem cells that can differentiate into only a single cell type (de Kretser, 2007), and induced pluripotent stem cells. These latter stem cells are artificially reprogramed somatic cells that demonstrate characteristics of pluripotent stem cells, including expression of characteristic markers, are capable of forming all three germ layers, and can differentiate into different tissues (Yu et al., 2007). Therefore, stem cells, in general, are defined as clonogenic cells that are distinguished by their unspecialized self-renewing phenotype and inducible differentiation capacity.

Stem cell division

Human adult multipotent stem cells are present in nearly all tissues and organs where they usually multiply and differentiate to replace or repair the tissue they reside in. However, in some cases, stem cells of a specific tissue give rise to cells of a completely different tissue. This phenomenon is known as stem cell plasticity. A common source of transdifferentiating stem cells is the bone marrow (Quesenberry et al., 2004). Stem cell division occurs due to multiple intrinsic and extrinsic factors that are either present or are transported to the environment the cells reside in. These factors lead to symmetric or asymmetric division, which give rise to two identical (same fate) or two different daughter cells, respectively. For example, Self-renewing stem cells divide symmetrically to produce stem cells with the cell

fate of the primary cell while asymmetric division results in a stem cell and a more mature cell type, such as a progenitor cell (Figure 1-1). In the hematopoietic system, stem cells constantly divide to renew blood cells at the rate of more than one million cells per second (Ogawa, 1993; Bryder et al., 2006). Therefore, HSCs differentiate to hematopoietic progenitor cells (HPCs) that are capable of self-renewal and therefore, give rise to dividing cells that multiply the number of repopulating units. Interestingly, stem cells from different tissues divide and generate progeny at non-identical rates. Thus, specific tissues can be regenerated diverse effectively. As described HSCs and HPCs constantly renew blood frequently; however, to activate residing stem cells during brain or heart regeneration, specialized conditions are needed (Taupin and Gage, 2002; Beltrami et al., 2003).
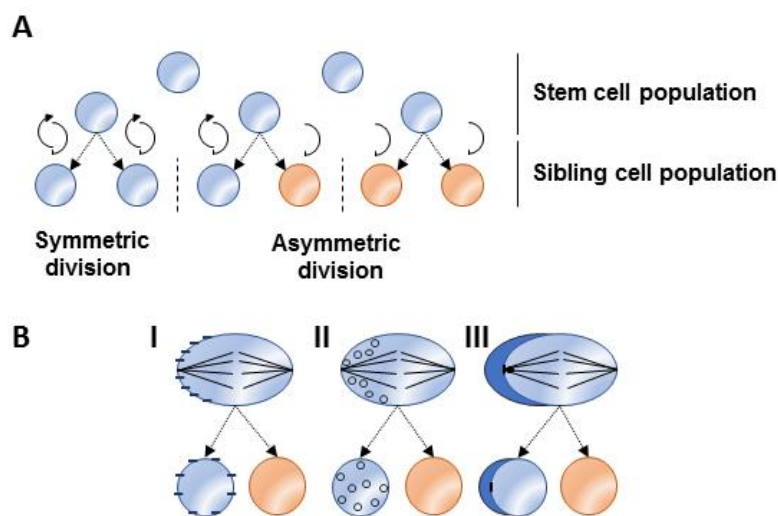
Figure 1-1: Stem cell division strategies (adopted from Morrison and Kimble, 2006**)**
A) The stem cell population (blue) can either divide by symmetric or asymmetric division. Symmetric division leads to siblings with the same cell fate as the dividing cell, i.e. self-renewal. Asymmetric division can produce two sets of progeny, i.e., one set with one stem cell and one mature cell or another set with two mature cells (orange). (B) Asymmetric division is defined by cell polarity and lead to stem cells (blue) or more mature/differentiated cells (orange). Three mechanisms are plausible. I: Regulators of cell polarity are asymmetrically distributed along the membrane (dark blue lines). II: Cell fate regulators (dark blue circles) are associated with the membrane, the centrosome, or a cell compartment that is asymmetrically distributed. III: The mitotic spindle is oriented toward the stem cell niche (dark blue area), and thereby regulates the accessibility of only one of the daughter cells to extrinsic signals required to maintain stem cell fate.

Asymmetric division, in this context, represents an attractive strategy for stem cells because it simultaneously facilitates self-renewal and differentiation. The mechanisms governing asymmetric division can be separated into intrinsic signals (fate determinants) that partition the dividing cell to assemble polarity (Figure 1-1B I-II) and extrinsic signals that optimize cell positioning towards environmental cues that enable polarization (Figure 1-1B II). However, asymmetric division represents a major drawback during development (Morrison et al., 1995) or stem cell loss after injury (Bodine et al., 1996), as the stem cell pool cannot be expanded (Morrison and Kimble, 2006). In such situations, symmetric division can repopulate stem cells in the developing embryo or in the stem cell compartment of adults and result in tissue

homeostasis (Yang et al., 2015). Moreover, in regenerative medicine regimens that use autologous or allogenic stem cell transplantation such as bone marrow (BM) HSC transplantation (HSCT), symmetric division of HSCs allows complete reconstitution of the BM blood producing compartment.

An emerging alternative method of generating stem cells is dedifferentiation, where mature cells receive signals to reverse their state of differentiation to acquire stem- or progenitor-cell properties. This can be facilitated *in vitro* by inducing the expression of the so-called 'Yamanaka factors' (Oct4, Sox2, cMyc, Klf4). Using a retroviral expression system Yamanaka and colleagues could show that induction of these four transcription factors resulted in induced pluripotency in human and mouse fibroblasts (Takahashi and Yamanaka, 2006; Nakagawa et al., 2007; Takahashi et al., 2007). A common *in vivo* dedifferentiation process is known to occur in tumor and tumor stem cell development (Friedmann-Morvinski and Verma, 2014), but stem cell plasticity can also be partially mediated by dedifferentiation during human tissue development. For example, in the small intestine, the expression of Myc is induced by the Wnt/β-Catenin pathway, which could lead to stem cell transformation from somatic cells within the tissue (Finch et al., 2009).
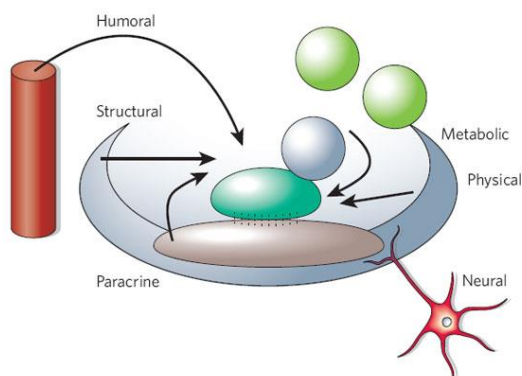
Figure 1-2: The stem cell niche (Scadden, 2006) The stem cell niche is presented as a local environment in tissues. Stem cells (in cyan) are influenced and regulated by multiple signals including neuronal input, contact with sibling cells (light blue and green) and other niche cells (gray) as well as metabolic, paracrine, and endocrine signals from local or distant sources. Moreover, structural constrains and physical cues in the extracellular environment are critical factors that tightly regulate stem cell systems.

Nevertheless, cell division and differentiation processes are controlled by factors that are provided by a specialized microenvironment where the stem cells reside. This environment is called the stem cell niche. This niche comprises cellular and extracellular features that orchestrate stem cell function using paracrine and metabolic signals or physical and structural cues, as depicted in Figure 1-2.

1.1 The stem cell microenvironment

Stem cell niches are believed to be well-defined environments that are present in almost all tissues where the stem cells are anchored and receive multiple regulatory signals to fulfill the homeostatic requirements of the tissues they reside in. Contrarily, stem cells are conceptually defined by their response to niche signals to self-renew and differentiate in order to regenerate specific tissues. This definition pointed stem cells of limited interest when

not integrated to this particularly regulating environment (Scadden, 2006). Schofield (1978) presented his idea of a specialized environment where stem cells are located and where their activity and self-renewal are controlled. He hypothesized that this environment promotes differentiation and stem cell maintenance by association with other cell types. This scenario also assures the presence of progeny as long the cell is in contact with this locally restricted environment or to a similar 'stem cell niche'. This idea was proposed in reference to hematopoiesis and was based on inconsistent findings that showed that the mouse spleen colony-forming cells could not be primary hematopoietic stem cells because these cells showed an "age-structure". This concept is explained as follows. Evolutionarily, the spleen or kidney function as hematopoietic organs in lower animals such as fish (Catton, 2012; Kobayashi et al., 2016), in mice hematopoiesis only partially occurs in the spleen (Wolber et al., 2002), while in humans, the spleen functions as secondary HSC niche (Freedman and Saunders, 1981; Dor et al., 2006) only under disease condition (e.g. osteopetrosis) . The mammalian hematopoietic niche has been definitively located in the BM of the large hollow bones.

Besides the multiple cell types in the hematopoietic stem cell niche, chemokines like stem cell derived factor 1 (SDF-1) and cytokines such as stem cell factor (SCF) are known to play a major role in stem cell maintenance and hematopoietic regulation (Mendelson and Frenette 2014). Additionally, the extracellular matrix (ECM), a dense protein mesh secreted by niche cells such as the mesenchymal stromal cells (MSCs), is described to provide a natural reservoir for soluble growth factors and environmental, structural, and physical cues (Klein, 1995). This view represents a significant extension of the Schofield model and highlights the complexity of the hematopoietic stem cell microenvironment within the BM (Figure 1-3).
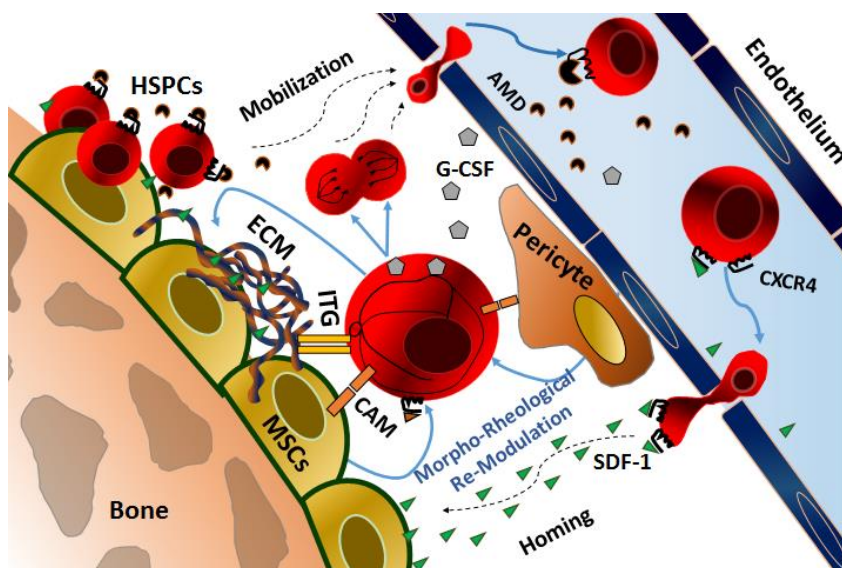
Figure 1-3: The hematopoietic stem cell microenvironment
The cartoon details components of the hematopoietic stem cell niche and the cell mechanical features that are needed to regulate stem cell function. Hematopoietic stem and progenitor cells (HSPCs; red)

reside in the BM niche next to cells like MSCs (yellow), endothelial cells (blue), pericytes (orange), and ECM components; cells and the ECM mediate adhesion via cell adhesion molecules (CAMs) or integrins (ITG). A feature of HSPCs is their mobilization into the blood stream in response to granulocyte-colony stimulating factor (G-CSF) or therapeutic factors like plerixafor (AMD), while homing occurs towards an SDF-1 gradient. Thus, HSPCs receive niche signals, including biochemical, biomechanical, and structural cues from the ECM scaffold, which result in mechanical and morphological adaptations, implicating these cues as biomarkers for stem cell properties, including cell division and differentiation.

Within the BM, two distinct HSPCs niches have been proposed: the endosteal niche and the vascular niche (Wilson and Trumpp, 2006). The vascular niche comprises endothelial cells and pericytes, where the endothelial cells form the sinusoids and arterioles and the pericytes stabilize the vascular tubes. HSC and endothelial interaction appear very likely since both cell types derive from the hemangioblast, a common embryonic precursor (Huber et al., 2004). Interestingly, only BM located endothelial cells exhibit HSC interaction and maintenance factors such as vascular cell-adhesion molecule 1 (VCAM1) or SDF-1 (Sipkins et al., 2005) and can promote clonal HSC *ex vivo* expansion (Li et al., 2003). It is believed that the vascular niche provides an environment conducive for activated HSCs, as sinusoids and venules allow HSC passage in and out of circulation. Nevertheless, *in vivo* imaging revealed a subpopulation of dormant HSCs in the sinusoidal endothelial cells, indicating homeostasis between the vascular and the endosteal niche in the healthy BM (Kiel et al., 2005). The endosteal niche is anatomically located in BM cavities of the trabecular regions of the bone (Lord et al., 1975). Here, a layer of MSCs and MSC-derived osteoblasts cover the bone surface, and interact with dormant HSCs. MSCs and osteoblasts reportedly maintain HSC function as well as expansion, as identified by genetic stimulation of osteoblast proliferation *in vivo* (Calvi et al., 2003), and can also facilitate *in vitro* HSC expansion in co-cultures (Taichman and Emerson, 1998). These findings point towards a direct correlation between increasing osteoblast numbers and primary HSC numbers, suggesting that with increasing numbers of osteoblast, there is a proportional increase in niche space.

Figure 1-3 depicts both niches during BM homeostasis; however, under mobilizing conditions, the vascular niche could become more relevant for HSCs as they move between the blood and the BM (Wright, 2001). Additionally, it could be hypothesized that HSC localization close to the blood stream would permit comprehensive monitoring of the individual's hematopoietic status reflected by the concentration of blood-borne factors. Thus, fast proliferating short term HSCs could reside in the vascular niche, quickly mobilize in response to hematopoietic alterations (Wilson and Trumpp, 2006). In general, the concept of two HSC niches within the BM is still under debate and multiple studies have presented evidence supporting the presence of the vascular niche (Kiel et al., 2005; Kobayashi et al., 2010; Itkin et al., 2016) and the endosteal niche (Zhang et al., 2003; Visnjic, 2004; Nilsson, 2005). However, the current view is that MSC-derived cells play a central role in both niches

(Smith and Calvi, 2013). Therefore, in this thesis, we have analyzed the interaction between primary human HSCs and MSC-derived ECM scaffolds. These scaffolds are cell free, covalently adhere to glass slides, and indeed model the endosteal niche as glass has a bone-like elastic modulus in the range of several GPa (Hutmacher, 2001; Liu et al., 2013). Additionally, it is acknowledged that 2D *in vitro* MSC cultures result in progressively osteogenic differentiation (Bruder et al., 1997; Banfi et al., 2002; Wagner et al., 2008; Bara et al., 2014). Hence, we will focus on the endosteal bone marrow niche.

1.1.1 The cellular endosteal bone marrow microenvironment

The BM comprises of two different types of stem cells mentioned before; namely, the hematopoietic stem cells and the mesenchymal stem cells. MSCs are capable of differentiating into various mesenchymal tissues including fat, cartilage, and tendon, can form marrow cells, and differentiate into bone-forming osteoblasts. Additionally, they can be found in several other tissues like neural tissue, heart, skin, liver, and muscle, which suggests that they possess enormous plasticity (Friedenstein, 1976; Horwitz et al., 2006; Spees et al., 2016). HSCs reconstitute all blood components by differentiating along several self-renewing multipotent progenitor cell lineages. Two major branches develop from these cells and are known as the common lymphoid progenitor (CLP) and the common myeloid progenitor (CMP). CLPs give rise to T and B-cells as well as natural killer cells, while erythrocytes, platelets, granulocytes, and macrophages derive from CMPs (Bryder et al., 2006; Seita and Weissman, 2010; Trumpp et al., 2010). Thus, the endosteal niche comprises MSCs and HSCs, as well as their progenies including osteoblasts, CLPs, and CMPs (Figure 1-4).

However, an additional cell type, known as the osteoclast, is crucial for formation of the bone and the regulation of its mass. Osteoclasts anchor to bone-specific ECMs and form polarized, ruffled, membrane surfaces. Between this membrane and the bone an acidic micro-milieu (pH approx. 4.5) develops that subsequently digests the bone surface. Osteoclasts derive from the fusion of macrophages and are, therefore, multinucleated cells. In order for this fusion to occur exclusively in the bone-forming areas, proximity of macrophages and osteoblasts is required. Osteoclastogenesis is controlled through parathyroid hormone (PTH) secreted by the parathyroid glands that regulate the blood calcium concentration. Osteoblasts express and present a receptor for PTH, which, after activation, induces the production of secreted osteoclastogenesis factors including the macrophage colony-stimulating factor. These factors then interact with receptors on macrophages and induce commitment towards the osteoclast phenotype (Teitelbaum, 2000). Therefore, these cells are said to derive, in a broader sense, from HSCs, by a direct interplay between osteoblasts and macrophages.

1.1.1.1 Mesenchymal stem/stromal cells

MSCs represent one of two stem cell fractions in the BM (Prockop, 1997). Almost all non-hematopoietic cells like fibroblasts, osteoblasts, adipocytes, etc. derive from MSCs (Cordeiro-Spinetti et al., 2015); however, whether all BM stromal cells represent biologically active stem cells for mesenchymal tissue regeneration is still under debate (Horwitz et al., 2006). Therefore, the International Society for Cellular Therapies (ISCT) has termed these cells mesenchymal stromal cells, which allows their continued identification as MSCs (Horwitz et al., 2005). Additionally, for reproducible identification of MSCs, the ISCT has proposed minimal criteria for defining multipotent mesenchymal stromal cells. When maintained in standard culture conditions, MSCs must be plastic-adherent in standard tissue culture, must express CD105, CD73, and CD90, and lack expression of CD45, CD34, CD14 or CD11b, CD79α or CD19, and HLA-DR. Furthermore, MSCs must be able to differentiate into osteoblasts, adipocytes, and chondroblasts, under appropriate stimuli (Dominici et al., 2006).

When Friedenstein et al. (1968) described MSCs for the first time, they found these cells to be a clonogenic subpopulation of BM MNCs and referred them to as colony forming unit fibroblasts (CFU-F). MSCs can be isolated from various tissues and the BM is commonly used as the source for clinical and research purposes (Horwitz et al., 2006). However, only 0.001 – 0.01% of BM mononucleated cells (MNC) are MSCs (Boeker et al., 2008). In order to isolate MSCs MNCs are cultured, the adherent spindle-shaped fraction is passaged to remove contaminating hematopoietic cells and subsequently collected; this process is termed "adherent selection" (Colter et al., 2000; Jiang et al., 2002). Beside these minimal criteria, multiple surface molecules have been proposed to identify, characterize, and localize MSCs, both within the BM and other tissues (Lv et al., 2014).

Interestingly, MSCs were identified as the most potent cells to regulate HSPC function by cell-cell interaction via N-cadherin, very late antigen 4 (VLA4), or cell adhesion molecules (CAMs) (Bianco et al., 2008). They secrete large amounts of ECM molecules including fibronectins (FN) and collagens that act as scaffolds for cell adhesion and migration. Furthermore, these molecules can provide physical and structural constraints that regulate HSPC function. Additionally, MSCs and osteoblasts secrete HSPC-regulating cytokines and chemokines (Taichman and Emerson, 1998), including SDF-1, Wint-ligands, SCF, bone morphogenic protein (BMP), and Notch-ligands. This close interaction of HSPCs and MSCs is reminiscent of synaptic interactions and was accordingly termed by Wilson and Trumpp (2006) as the "niche-stem-cell-synapse".

These observations pointed to the possibility of using MSCs as a feeder layer for HSPC co-culture (Dexter et al., 1977a) and led, very early on, to the development of immortalized cell lines (Roecklein and Torok-Storb, 1995). In 2008, Boeker et al. introduced the human BM-

derived MSC cell line, single cell picked clone 1 (SCP-1), in which expression of the human telomerase reverse transcriptase (hTERT) abolished telomere shortening and the senescence-associated phenotype that led to unlimited proliferation of these MSCs. However, SCP-1 cells did not undergo neoplastic transformation. Furthermore, classical MSC functions, including multi-lineage differentiation capacity and HSPC support, were not altered. Additionally, SCP-1 cells were found to secret considerable levels of SDF-1 (Arabanian et al., 2014) and ECM proteins (Kräter et al., 2017).

1.1.1.2 Hematopoietic stem and progenitor cells

Hematopoietic stem cells represent the second stem cell population located in the BM microenvironment (Arroyo et al., 1999; Mitjavila-Garcia et al., 2002; Boisset et al., 2013). These cells are defined by their self-renewing capacity and their ability to give rise to all mature blood cells (Osawa et al., 1996; Notta et al., 2011). Figure 1-4 illustrates the developmental hierarchy of human and mouse HSPCs as most knowledge was gained in mice, including the first descriptions of hematopoietic colony formation in the mouse spleen after marrow transplantation (Till and McCulloch, 1961; Becker et al., 1963). These initial findings identified HSPCs as clonogenic cells with extramedullary niches beside the BM with the capacity to find and home to their niches after transplantation (Seita and Weissman, 2010). They also represent the first tissue-specific stem cells that could be isolated (Spangrude et al., 1988) and their discovery led to the fundamental development of experimental systems for stem cell expansion, lineage potential evaluation, and fluorescence activated cell sorting (Coulombel, 2004; Bryder et al., 2006).
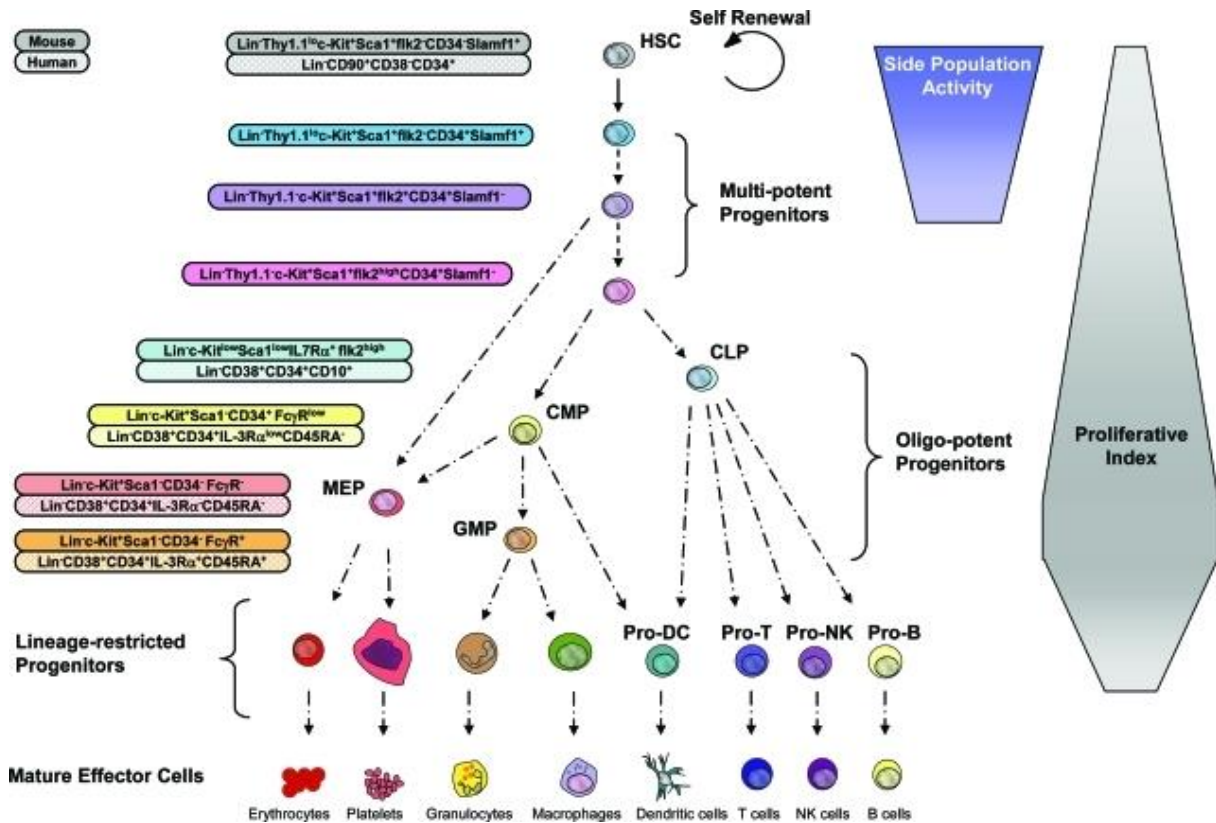
Figure 1-4: Hematopoietic development (Bryder et al., 2006)
In this model of the hematopoietic development hierarchy, self-renewing HSCs are located at the top and give rise to common progenitors (CLP and CMP) via multipotent progenitors that show loss of side population activity (measured by efflux of Hoechst 33342) during maturation. Additionally, the proliferative capacity of the cells increases to the level of progenitors, including the granulocyte/macrophage progenitors (GMP) and the megakaryocyte/erythrocyte progenitors (MEP), which derive from CMP in order to increase the number of repopulating units. GMPs and MEPs further differentiate into erythrocytes, platelets, granulocytes, and macrophages. CLPs give rise to T cells, B cells, and NK cells. CMPs and CLPs also give rise to dendritic cells. These cell populations can be classified by surface marker expression, as presented for both mouse and human cells.

In translational medicine, HSPCs are the only stem cell source available for routine clinical application; e.g., the current standard therapy for multiple hematopoietic disorders is autologous stem cell transplantation (Mendelson and Frenette, 2014). As shown in Figure 1-4 the cell surface marker expression profile is used to identify various stem and progenitor cell populations of the hematopoietic system. Early HSPCs are defined as negative for lineage (Lin) markers, CD34$^+$, CD90$^+$, and CD38$^-$. However, many other markers like CD133 have been described to identify subsets of highly potent HSPCs (Yin et al., 1997). Moreover, several surface-expressed integrins (ITG) could be used to identify HSPCs as they confer stem cell properties via adhesion signaling. ITGβ1 and β2 were shown to promote HSPC anchoring to the BM stroma (Teixido et al., 1992). ITGα2 was found to promote HSPC maintenance (Boisset et al., 2013). ITGβ3 was found to correlate with properties of quiescent HSC (Umemoto et al., 2006) and was required for BM homing (Umemoto et al., 2012). Additionally, ITGβ3 can be used to enrich long-term repopulating HSPCs (Umemoto et al., 2008). Therefore, it is still difficult to distinguish between HSCs and early progenitors by

surface molecule expression alone. Nevertheless, HSPCs can be isolated from 3 major sources, umbilical cord blood, bone marrow, and peripheral blood (PB) (Cheuk, 2013) and can be enriched by sorting based on the surface antigen CD34 before clinical or tissue engineering applications (Gordon, 2008). Mobilization of stem cells into the peripheral blood is facilitated by the administration of cytokines like granulocyte colony stimulating factor (G-CSF). Additionally, combined administration strategies that use G-CSF and plerixafor (AMD3100), a C-X-C-motive chemokine receptor 4 (CXCR4) antagonist, increase mobilization efficiency (Cashen et al., 2007; Giralt et al., 2014). HSPCs express CXCR4, which is the receptor for SDF-1. SDF-1 is produced by BM-MSCs and BM-endothelial cells, and serves as a gradient for HSPC homing to the BM. It has been shown that HSPCs actively migrate towards this gradient, both *in vivo* and *in vitro* (Aiuti et al., 1997). As these cells are few in number from most graft sources and the number of usable cells is limited, *ex vivo* expansion-cultures have been established using cytokine cocktails like SCF, interleukin 3 (IL-3) and fms-related tyrosine kinase 3 (FLT-3) (Dexter et al., 1977b; Delaney et al., 2010; Csaszar et al., 2012) or small molecules like prostaglandin E2 (North et al., 2007). However, *in vitro* suspension culture of HSPCs leads to heterogeneous cell populations with undefined cellular identities (Blank et al., 2008). These findings indicate that a more complex cultivation method remodeling the naïve stem cell environment could increase stem cell number and be used to understand HSPC regulation *ex vivo*.

1.1.2 Extracellular bone marrow microenvironment

Besides the cellular environment present in the BM niche, extracellular components like ECM proteins, morphogens, cytokines, and chemokines are also key regulators of HSPCs. The ECM plays a major role in generating and modulating these exogenous factors by presenting appropriate adhesion sides, physical and structural cues, and facilitating the storage and release of signaling molecules like growth factors (Hynes 2014). Therefore, tissue-engineering approaches focused on the ECM to develop artificial niches for HSPCs. However, naïve reconstitution of *in vitro* systems, including maintenance of structural and functional properties, is rarely achieved due to its inherent complexity (Rosso et al., 2004), as described in the following sections.

1.1.2.1 Extracellular matrix

The ECM within the BM niche is a macromolecular structure consisting of multiple proteins including fibronectins, collagens, proteoglycans, laminins, and others. Its fibrillar structure is insoluble, highly crosslinked, and provides adhesion and guidance structures for cell migration. Additionally, its elastic properties can regulate HSPC expansion and MSC differentiation (Coulombe et al., 1988; Seib et al., 2009a). Thereby, the ECM is secreted by cells residing in the tissue; mostly MSCs in the BM. All cells remain in contact with the ECM, and this results in tissue-specific ECM composition (Gattazzo et al., 2014). Figure 1-5 represents the major components and the integrin-mediated cell-ECM interactions.
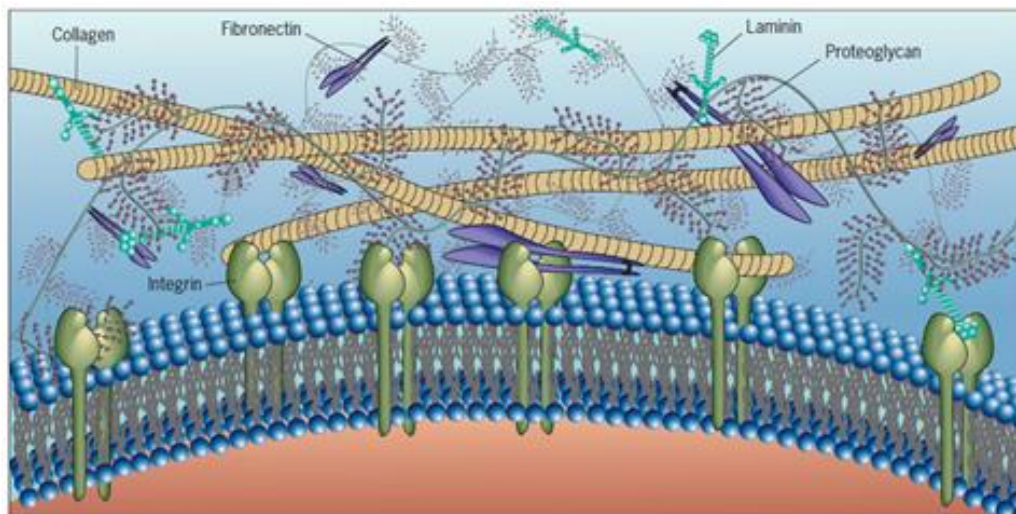
Figure 1-5: ECM components and cell interactions (Karp, 2008)
The macromolecular structure of the ECM is mainly assembled by major protein components like collagens, fibronectins, laminins, and proteoglycans. Cells interact with these structures through integrin-mediated adhesions.

Owing to its tissue-specific composition, the ECM guides intercellular interactions and cell-matrix communication, and thereby acts as a major determinant of cell proliferation and differentiation during tissue homeostasis. Nevertheless, besides provision of structural stability the ECM is biodegradable and this degradation is mediated by cell-secreted proteinases, which then permits cell migration. Proteolytic degradation of the ECM is highly conserved between invertebrates and vertebrates and has been shown to be a key process in development, tissue homeostasis, and disease progression (Daley et al., 2008; Brown, 2011; Lu et al., 2011). However, due to the functional diversity of ECM proteins, various molecular interactions, and synergistic effects (Figure 1-6), a functional classification of single ECM components is almost impossible. Nevertheless, several proteins are known to mediate cellular adhesion and cell function regulation and these will be discussed in the following sections.

Chemokines and Cytokines

Apart from structural integrity, the BM ECM stores multiple chemokines and cytokines via ECM protein binding (Zhang and Lodish in 2008;

Figure 1-6). Therefore, the ECM is involved in the regulation of HSPC activity by furnishing local chemokine/growth factor availability and by establishing appropriate biochemical
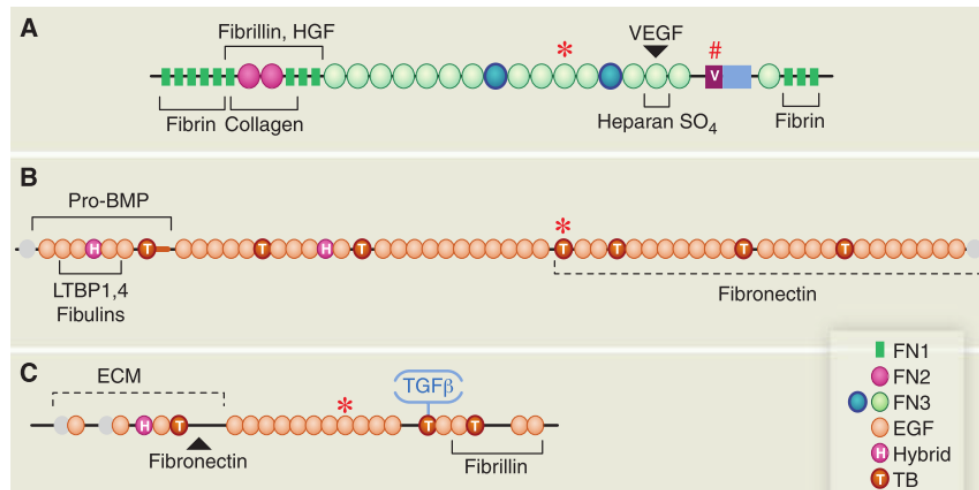
gradients (Hynes, 2012).

Figure 1-6: Domain structures of several ECM proteins (Hynes, 2012)
Representative ECM proteins show highly complex domain structures and binding sites for multiple other ECM proteins and growth factors resulting in a highly crosslinked, complex, 3-dimensional scaffold. (A) Fibronectin binds to various growth factors, e.g. hepatocyte growth factor (HGF) and vascular endothelial growth factor (VEGF), common ECM proteins such as collagen and fibrillin, and presents an RGD-motive (asterisk) for cell-matrix interaction. (B) Fibrillin-1 exhibits high crosslinking capability with fibronectin and fibulins, and consists of multiple epidermal growth factor (EGF) binding repeats. (C) Latent TGF-β binding protein-1 (TGBP-1) presents TGF-β binding sides, and interacts with fibrillin and fibronectin.

Known ECM-associated growth factors are SDF-1, hepatocyte growth factor (HGF), fibroblast growth factor (FGF), transforming growth factor-β (TGF-β), interleukin-8 (IL-8), and VEGF. FGF and VEGF can bind to heparin and heparan sulfate components of the proteoglycans. These sulfates are described to be cytokine reservoirs, and cytokine release is mediated by proteolytic ECM degradation. Additionally, FGF receptor binding depends on co-binding of heparan chains (Mohammadi et al., 2005) and is identical for TGF-β signaling (Shi and Massagué, 2003). During HSC-niche development, orchestrated signaling of bone morphogenic protein (BMP) by its native antagonist FGF in the subaortic mesenchyme was shown to restrict HSC specification (Pouget et al., 2014). Both cytokines are usually secreted by MSCs and anchored to the ECM proteins, implying specific localization within the ECM to regulate cellular function.

A major chemoattractant stored within the BM-specific ECM is SDF1, whose function includes lymphocyte homing, mature blood cell activation, and stem cell growth inhibition (Whetton and Spooncert, 1998). MSC and osteoblast-derived SDF-1 is anchored on ECM

molecules to form a SDF-1 gradient from the endosteal niche to the blood vessels, as presented in Figure 1-3 (Jung et al., 2008; Greenbaum et al., 2013; Thon, 2014). SDF-1 knock out mice display an embryonic lethal phenotype due to lack of migration of HSPCs from the fetal liver to the BM (Nagasawa et al., 1996). It was shown that addition of SDF-1 to *in vitro* HSPC cultures on ECM components like FN increases random cell migration (Lee-Thedieck et al., 2012) and survival of progenitor cells (Broxmeyer et al., 2003).

There is emerging evidence on crosstalk and synergistic signaling between growth factors and integrins. Rahman et al. (2005) reported the presence of HGF binding domains on FN and vitronectin, which coordinate HGF receptor signaling and Phosphatidylinositol-4,5-bisphosphate 3-kinase (PI3K)-mediated enhanced migration. This indicates induction of integrin signaling via HGF receptor; vice versa, cellular adhesion to ECM structures via integrins might enhance growth factor signaling.

Cell adhesion to ECM

Multiple receptors such as P- and E-selectins, VE-cadherins, and integrins were found to mediate HSPC adhesion to endothelial cells, MSCs, and the corresponding ECM. These findings correlate with HSPC homing and retention in the bone marrow (Sahin and Buitenhuis, 2012). Essentially, integrins (ITGs) are the most important mediators of the cell-ECM crosstalk. These glycoproteins form heterodimeric transmembrane receptors consisting of 18 α-subunits and 8 β-subunits. Each β subunit is bound to a specific α integrin subset, thereby resulting in 24 different combinations that are expressed on almost all cell types with a specific expression pattern (Hynes, 2002). Integrins were found to sense and transduce the bio-chemical nature of the environment into the cell. Moreover, physical cues generated by external and internal forces were transduced via ITGs. Therefore, cells can sense mechanical properties, the nanostructure and shear forces in the surrounding environment (Geiger et al., 2009). An overview of this signaling is presented and described in Figure 1-7.
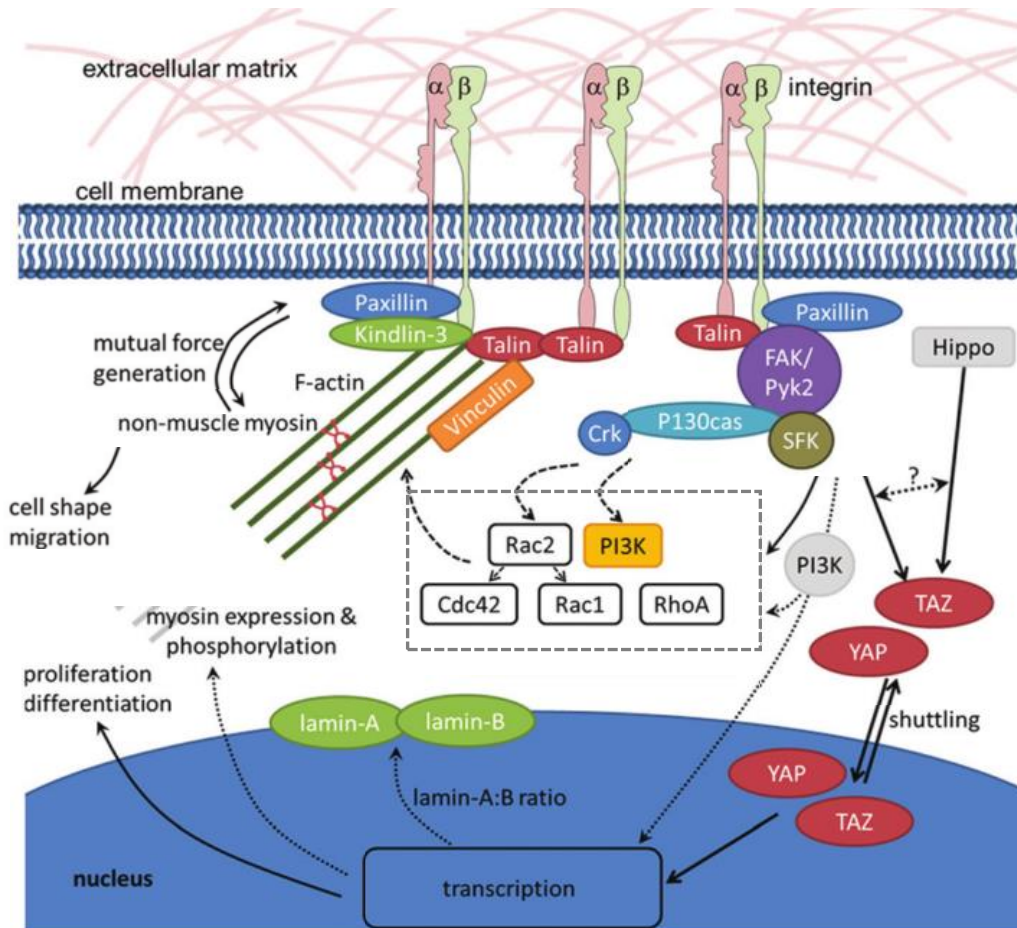
Figure 1-7: Mechanosensing in HSPCs (adapted from Lee-Thedieck and Spatz, 2014**)**
This schema illustrates integrin-mediated signaling in HSPCs. ITG subunits heterodimerize after ligand recognition and recruit several proteins, including focal adhesion kinase (FAK), paxillin, and vinculin to the inner cell membrane. These complexes can either interact with the acto-myosin cytoskeleton to adapt cell shape and promote migration via vinculin, or mediate kinase signaling via paxillin and FAK phosphorylation. Moreover, crosstalk between the acto-myosin pathway and the kinase pathway was demonstrated by cell division control protein 42 homolog (Cdc42) signaling. Cytoskeletal rearrangement, through ITG signaling, remodel cell shape, which promotes mechanical signal transduction into the nucleus and results in regulation of cellular transcription.

In addition to cytokines, HSPC phenotype can be maintained by cell-matrix adhesions viaat adhesion receptors such as integrins. *Ex vivo* co-cultures of HSPCs and BM niche cells like MSCs were used to mimic these interactions, whichhas proven to be a promising tool for stem cell expansion (Freund et al., 2006a; Jang et al., 2006; Jing et al., 2010; de Lima et al., 2012). However, in co-cultures it is nearly impossible to distinguish between cell-cell mediated and cell-ECM mediated signaling. ECM components coated on plastic culture dishes showed that biomechanical forces of the surrounding environment were transduced to cells via integrin signaling (Ross et al., 2013), and that these forces controlled HSPC fate *in vitro* (Engler et al., 2006; Holst et al., 2010; Naba et al., 2014). Thus, these physical aspects were shown to be markers for differentiation (Yu et al., 2010) that also drive cell fate decisions (Lautenschlaeger et al., 2009; Ekpenyong et al., 2012).

Following this line, it was found that HSPCs favor anchorage to stiff substrates and exhibit random migration as demonstrated by hydrogel scaffolds with different mechanical

properties. Generally, gels with an elastic modulus greater than 38 kPa represent hard surfaces while those with less than 20 kPa represent soft surfaces (Lee-Thedieck et al., 2012). The authors demonstrated that ITGα5, ITGβ1, and ITGαVβ3 were responsible for HSPC adhesion to fibronectin coatings on hydrogels, and this was inhibited by the addition of linear RGD motives. Further, they found that adhesion and migration were inhibited by blocking PI3K activity. These findings support the fact of ITG mediated ECM component recognition. Transduction of mechanical signals via the acto-myosin cytoskeleton and signaling via kinases recruited to ITGs is shown in Figure 1-7. These cross interacting pathways lead to morphological and mechanical adaptations in cell shape and increased migration (Lee-Thedieck et al., 2012; Lee-Thedieck and Spatz, 2014). Whether adhesion to stiff or soft substrates regulates proliferation and differentiation, and thereby functional properties described by Holst et al. (2010), is an interesting question in this context. Additionally, the transduction of environmental mechanical properties into cell mechanical properties via ITG and focal adhesion kinase (FAK) signaling, as demonstrated by Bae et al. (2014) in mouse embryonic fibroblasts, would uncover the nature of cellular alignment to substrate physical cues, and help establish HSPC mechanical properties as functional marker, both *in vivo* and *in vitro.*

As described above, multiple ITGs in destingt expression patterns are found on HSPCs, and their suitablitiy as HSPC markers was analyzed (Potocnik et al., 2000; Carstanjen et al., 2005; Qian et al., 2006). However, ITGs are not exclusively expressed on HSPCs, but are also present on mature blood cells. Umemoto et al. (2012) described ITGαVβ3 signaling as a regulator for thrombopoietin-mediated HSPC maintenance. ITGαII2b was found to play a role in the maintenance of HSC activity in the mouse embryonic aorta (Boisset et al., 2013) and ITGβ3, was found to enrich long term repopulating HSPCs (Umemoto et al., 2008). On the other hand, ITGβ3 expression correlates with megakaryocyte–erythroid progenitor cell differentiation and is strongly expressed on platelets. Thus, suitable models are required to identify stem cell interaction with pure BM-derived ECMs to uncover ITG signaling in the context of HSPC regulation.

Taken together, the ECM provides multiple signals to the HSPCs as illustrated in Figure 1-8. These signals control cell fate decisions and proliferation, and mediate tissue homeostasis, highlighting the need to decipher and understand cell-ECM interaction in detail to develop successful tissue engineering approaches with improved clinical cell replacement therapies.
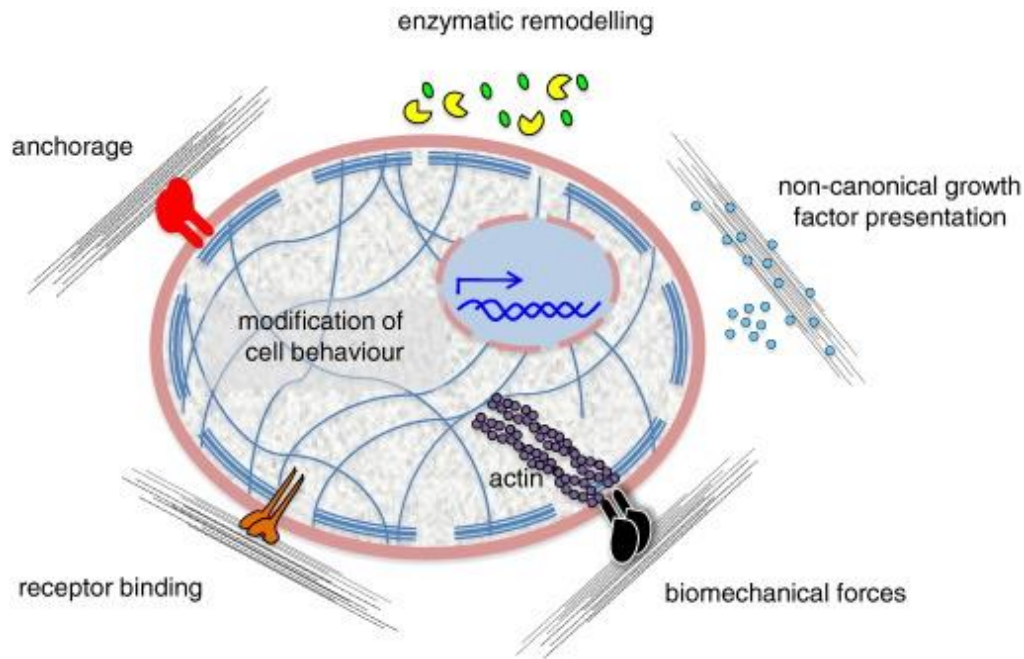
Figure 1-8: ECM mediated cell regulation (Gattazzo et al., 2014)
The ECM is a direct target of cellular receptors that transduce biomechanical forces into the cell via actin fibers, anchors the cell to its environment, and provides tissue stability. The ECM stores and presents growth factors to the cell and can be remodeled by cell-derived enzymes. These features result in intracellular signaling followed by cellular adaptation.

1.2 Native *ex vivo* ECM scaffolds

As described above, the ECM represents a versatile, stability providing compartment with tissue-specific properties and cell-regulatory functions (Roskelley et al., 1994). As an example, it was shown *ex vivo* that BM-ECM promotes osteogenic lineage differentiation of adipose derived stromal cells; a scenario that is hardly possible in classic tissue culture using cytokines (Zhang et al., 2015). Interestingly, these findings also indicate that tissue-specific signaling is conserved even in *ex vivo* experiments. Multiple studies have demonstrated functional preservation and organ-specific constitution of ECMs after decellularization of whole tissue samples or organs (Gilbert et al., 2006). Additionally, it was shown that decellularized ECMs have the potential to induce cellular phenotypes (Furuyama and Mochitate, 2000) and prevent *ex vivo* embryonic stem cell differentiation (Klimanskaya et al., 2005).

However, the generation of tissue-like ECMs represents a major challenge with respect to the BM environment due to its low density and smooth properties. Prewitz et al. (2013) introduced a novel technique to generate decellularized ECMs derived from human BM MSCs. The approach uses standard microscopy glass slides as culture carriers. Slides were oxidized, aminosilanized, and spin coated with a 0.16% (w/v) poly(octadecen-*alt*-maleic anhydrate) in tetra hydro furan solution, as shown in Figure 1-9. These thin films of

covalently bound copolymers were then activated by a tempering for 2 h at 120°C to covalently link fibronectin. For ECM production, primary MSCs were cultured on these modified glass slides, secreted ECM proteins linked to covalently bound fibronectin to prevent detachment from the culture carrier during decellularization. The resulting ECMs were used as culture scaffold. This technique did not alter naïve protein cross-linking, as demonstrated by formalin-fixed approaches (Beacham et al., 2007) and matrices were characterized biochemically, biophysically, and functionally as tissue-mimetic culture substrates (Figure 1-9; Seib et al., 2009b; Prewitz et al., 2013, 2015).
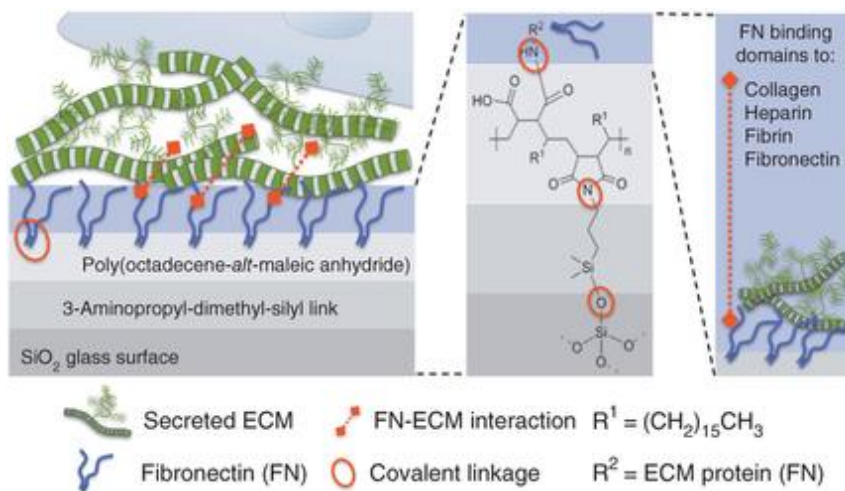
Figure 1-9: Surface preparation for cell derived ECM scaffolds (Prewitz et al., 2013)
Freshly oxidized glass slides were coated with 3-Aminopropyl-dimethyl-silyl (aminosilan) and fibronectin-functionalized poly(octadecen-alt-maleic anhydrate) (POMA) to generate a covalent link between the glass surface and fibronectin. MSCs were cultured on these modified glass slides, and after 10 days, secreted ECM remained immobilized to the glass surface, even during decellulariation.

It has been reported that matrices derived from primary human MSCs possess homogeneous topography with a thickness of approximately 1 µm and a stiffness of approximately 0.1 kPa, measured by atomic force microscopy (Prewitz et al., 2013, 2015), which represents BM bio-mechanical properties (Jansen et al., 2015). Moreover, proteomic analyses identified over 500 proteins within the ECM structures with over 50% of these annotated as ECM proteins and ECM structural constituents by gene ontology. Additionally, anchorage and continued release of BM-related cytokines, including HGF (Takai et al., 1997), FGF (Choi et al., 2008), IL-8 (Rougier et al., 1998), and VEGF (Asahara et al., 1999) were detected. These observations suggest, a native molecular signature of MSC-derived ECMs, which served as a naïve reconstituted environment for MSCs (Seib et al., 2009a) and HSPCs, and supported both stem cell expansion with the capacity of *in vivo* repopulation of immunodeficient NSG mice (Prewitz et al., 2013).

We used this technique to model the HSPC niche *ex vivo* and analyze the HSPC-ECM interaction with respect to contact-mediating structures. However, as it was shown that ECM molecules secreted by primary MSCs are highly versatile (Amable et al., 2014) and donor dependent (Kalinina et al., 2015), therefore, the use of a reproducible model system such as SCP-1 cells to generate consistent ECM scaffolds is recommended.

Targeted modulation of ECM components

To identify key components of the extracellular HSPC niche, genetic modification of the SCP-1 cell secretome can help investigate the role of individual ECM proteins in HSPC maintenance or expansion. Lentiviral vectors can be used to achieve stable expression of shRNAs in SCP-1 cells. We adapted a protocol published by Stopp et al. (2013) to effectively transduce SCP-1 cells with shRNAs to induce RNA interference, and consequently, a known-down of a protein of interest. Adequate candidates were identified based on a mass spectrometry screen of the MSC secretome (Prewitz et al., 2013) and on functional relevance for HSPCs described in literature. A promising candidate was fibulin-1.

The extracellular matrix protein fibulin-1 was found to negatively regulate HSPC proliferation and differentiation. MSCs and osteoblasts strongly express fibulin-1, which keeps HSPCs in a quiescent state and maintains their stem cell character (Hergeth et al., 2008). Moreover, fibulin-1 is known to interfere with cell migration in the ECM of the endosteal HSPC niche (Kluge et al., 1990; Hergeth et al., 2008). The fibulin protein family consists of seven members, Fibulin-1 to -7. In humans, four alternative splicing variants of fibulin-1 exist: Fibulin-1A, B, C, and D. Compared to variants C and D, variants A and B are expressed at lower levels. Splicing variant D was found to co-localize with fibronectin and to inhibit cell adhesion by inducing the exposure of anti-adhesive sites on fibronectin (Twal et al., 2015). The N-terminal domain-I consists of anaphylatoxin domains, followed by domain-II composed of EGF-like modules with high calcium-binding capacity (de Vega et al., 2009). Calcium complexation is thought to be important for maintaining HSCs within the niche (Adams et al., 2006). The fibulin-1 knockout has a perinatal lethal phenotype, demonstrating a crucial role for this protein in development (Kostka et al., 2001).

2   Aim of the study

Regenerative medicine is an increasingly interdisciplinary field that strives to combine knowledge from biology, physics, chemistry, engineering, and medicine. It aims at developing novel cellular therapies that can restore or regenerate normal tissue and organs and their functions in response to tissue degeneration or malignant diseases. Classical reconstruction attempts include stem cell transplantation. However, several complications such as graft-rejection or donor site morbidity need to be overcome. In this context, the unique properties of stem cells to differentiate towards multiple tissue lineages and cell types offer great potential and become highly interesting. For the treatment of malignant blood disorders like lymphoma or leukemia, hematopoietic stem cell transplantation has become standard therapy. Hematopoietic stem cells are defined by their self-renewing capacity and their ability to give rise to all mature blood cells (Osawa M, Hanada KI, Hamada H and H, 1996; Notta et al., 2011). They reside in a specialized microenvironment in the BM called the hematopoietic stem cell niche (Arroyo et al., 1999; Mitjavila-Garcia et al., 2002; Boisset et al., 2013). This niche coordinates differentiation and self-renewal, i.e., division without differentiation. However, a major drawback is their low numbers and, therefore, the availability of healthy stem cells. Only one in around 10,000 BM cells is a hematopoietic stem cell with the ability to support long term hematopoiesis after transplantation. To collect HSPCs, BM aspiration or G-CSF stimulated proliferation and mobilization into the peripheral blood are common techniques. Nevertheless, to achieve therapeutically relevant amounts, *in vitro* expansion of HSPCs has become a major interdisciplinary goal in translational medicine. However, the effective translation of knowledge gained on cell communication and regulation within the BM niche that is suitable to culture techniques for HSPCs is still unavailable.

Therefore, the overall goal of this study was to improve the naïve *in vitro* culture systems based on decellularized ECM scaffolds, as described by Prewitz et al. 2013, for HSPC maintenance and to identify the functional regulators of the HSPC-ECM interaction. Thus, four major aims were defined and addressed in this thesis:

- For classical *in vitro* expansion, CD34$^+$ HSPCs isolated from G-CSF mobilized peripheral blood suspension cultures were used. Nevertheless, in the BM, cells are connected to each other via a complex network of extracellular matrix components. Prewitz et al. (2013) described primary human MSC-secreted ECMs as BM naïve culture substrates. As these ECMs undergo alterations due to MSC donor variations and cell senescence, we aimed at using SCP-1 cell line to gain highly reproducible ECM scaffolds. SCP-1 is a

primary human MSC-derived cell line that was shown to possess all major features of MSCs, including surface marker expression and differentiation capacity (Boeker et al., 2008). Thus, the ECM scaffolds derived from SCP-1 cells should be tested to verify if they serve as support structures and natural microenvironments for HSPC expansion.

- The extracellular matrix in the BM stores and presents multiple growth factors and cytokines. It also provides physical cues and adhesion sides that may serve as migration-guiding structures. Cell-matrix interactions between HSPCs and BM-mimetic ECM scaffolds can remodel cell shape and physical properties, which are both major regulators of HSPC function. These morphological and biophysical parameters of the ECM cultured HSPCs should be described and compared to suspension cultured HSPCs and HSPC-SCP-1 co-cultures.

- The CXCR4/SDF-1 axis is known to mediate BM homing and retention of HSPCs through a bioactive SDF-1 chemokine gradient produced mainly by MSCs. However, it is known that adhesion of HSPCs to stromal extracellular components is achieved primarily by integrin-mediated focal adhesions. Therefore, ECM scaffolds derived from SCP-1 cells were analyzed for SDF-1 incorporation and bio-active presentation. Moreover, mediators of the HSPC-ECM interaction via adhesion receptors and formation of signaling focal contacts should be identified.

- In the BM, the osteoblast-derived ECM is mainly present in the endosteal hematopoietic stem cell niche, and SCP-1 cells can undergo osteogenic differentiation using appropriate stimuli. We aimed at identifying the influence of osteogenic induced ECMs on HSPC proliferation and adhesion. Additionally, SCP-1 cells are known to be susceptible to lentiviral shRNA transduction, which could be used for targeted modulation of ECM components by knocking down proteins of interest. We, therefore, aimed to increase HSPC adhesion by down regulating fibulin-1, an ECM protein known to form anti-adhesive sides on fibronectin. The lentiviral shRNA knock down should be established in SCP-1 cells, and the adhesion and proliferation of HSPCs on knock down ECMs should be analyzed.

The observations and conclusions from the study can help increase our understanding of HSPC regulation when cells adhere to the BM niche and lead to a tunable *in vitro* expansion system for long term repopulating HSPC with homing and effective BM lodgement.

3 Materials and methods

3.1 Materials

Table 3-1: Materials

Material	Company
25 gauge needle	BD microlance, USA
30 - 50 gauge needle	Braun, Germany
6-well plates	Greiner-Bio One, Austria
12-well plates	Greiner-Bio One, Austria
24-well plates	Corning, USA
BD FalconTM tubes	BD Biosciences, USA
Blunt end filling needle	BD Biosciences, USA
ChemoTx disposable chemotaxis system	NeuroProbe, USA
Cell culture plate (6 well)	Greiner-Bio One, Austria
Cell culture plate (12 well)	Greiner-Bio One, Austria
Cell culture flask (T25)	Greiner-Bio One, Austria
Cell culture flask (T75)	Greiner-Bio One, Austria
Cell culture flask (T175)	Greiner-Bio One, Austria
ECM glass coverslips (6 - 32 mm)	Thermo Fischer Scientific, Menzel-Gläser, USA
FACS tubes	VWR, USA
LS columns	Milteniy Biotec, Germany
Luer-Lock syringes 1 ml – 5 ml	BD Biosciences, USA
Microscopy glass coverslips	Greiner-Bio One, Austria
Microscopy slides	Thermo Fischer Scientific, USA
Microfluidic chips – FLIC20	Zellmechanik Dresden
Nunc Cryo Tubes	Sigma-Aldrich, USA
Parafilm	Sigma-Aldrich, USA
Petri dish (round)	Greiner-Bio One, Austria
Petri dish (square)	Thermo Fischer Scientific, USA
Pre-separations filters	Milteniy Biotec, Germany
Reaction Tubes	Eppendorf, Germany
Stripette 5 ml – 50 ml	Sigma-Aldrich, USA
Vacuum filter (0.22 µm pore size, 500 ml)	Corning, USA

3.1.1 Chemicals and reagents

Table 3-2: Chemicals and reagents

Chemical/ Reagent	Company
2-phospho-ascorbic acid	Sigma-Aldrich, USA
3-aminopropyl-triethoxy-silane (amino-silan)	ABCR, Germany
4',6-diamidino-2-phenylindole (DAPI)	Sigma-Aldrich, USA

Materials and Methods

Acetic acid	Merck, Germany
Acetone	Sigma-Aldrich, USA
Acrylamide (40%) (w/v)	GE Healthcare, UK
Agarose	Sigma-Aldrich, USA
Alexa Fluor 488 phalloidin	Thermo Fischer Scientific, USA
Alexa Fluor 647 phalloidin	Thermo Fischer Scientific, USA
Ammonia solution	Sigma-Aldrich, USA
Ammonium persulfate (APS)	Carl Roth, Germany
β-glycerol-phosphate	Sigma-Aldrich, USA
Bisacryamide (2% w/v)	GE Healthcare, UK
Biocoll 1.077 g/ml	Merck, Germany
Blocking solution	Santa Cruz Biotechnology, USA
Bovine Serum Albumin (BSA)	Sigma-Aldrich, USA
Cellcarrier A / B	Zellmechanik Dresden, Germany
Coomassie blue	Merck, Germany
CXC-motiv-chemokin 12 (CXCL12, SDF-1)	PeproTech, USA
Dexamethasone	Sigma-Aldrich, USA
Dimethylsolfoxid (DMSO)	Merck, Germany
ECL plus western blotting detection reagents	Amersham, UK
Ethanol (absolute)	Merck, Germany
Fetal Calf Serum (FCS)	Biochrom, Germany
Fibronectin (FN)	Roche, Germany
FMS-like tyrosine kinase 3 ligand (FLT3) human	Miltenyi Biotec, Germany
GeneRuler 100bp DNA ladder	Thermo Fischer Scientific, USA
Granulocyte-colony stimulating factor (G-CSF)	Peprotec, USA
Glycine	Carl Roth, Germany
Human Serum Albumin (HSA) 200g/ ml	Baxter, Germany
Hydrogen peroxide (H_2O_2)	Merck, Germany
Interleukin 3 (IL-3)	Milteniy Biotec, Germany
Isopropanol	Merck, Germany
LB medium	VWR chemicals, USA
Methanol	Merck, Germany
Milk powder	Carl Roth, Germany
Milli-Q Water purified and deionized water	Millipore, Germany
Paraformaldehyde (PFA)	Sigma-Aldrich, USA
Polyethylenimine (PEI)	Sigma-Aldrich, USA
Percoll 1.073 g/ml	Biochrome, USA
Phosphate buffered saline (PBS)	Thermo Fischer Scientific, Gibco, USA
ply(octadecene alt maleic anhydride) (POMA)	Polysciences Inc., USA
Potassium chloride	Sigma-Aldrich, USA
Prestained Protein Ladder PageRuler	Thermo Fischer Scientific, USA

Propidium Iodide (PI)	Thermo Fischer Scientific, Invitrogen, USA
Puromycin	Sigma-Aldrich, USA
PVDF membrane	GE Healthcare, UK
RedSafe	iNtRON Biotechnology, Korea
Roti®-Load 2 –buffer	Carl Roth, Germany
SDS	Carl Roth, Germany
Sodium chloride (NaCL)	Carl Roth, Germany
Sodium citrate 4%	Fenwalinc, USA
Sodium Hydroxide (NaOH)	Merck, Germany
Stem Cell Factor (SCF) human	Milteniy Biotec, Germany
Tetrahydrofuran (THF)	Sigma-Aldrich, USA
Tetramethylethylenediamine (TEMED)	Carl Roth, Germany
Tris base	Carl Roth, Germany
Triton X-100	Merck, Germany
Trypan blue solution	Sigma-Aldrich, USA
Tween20	Carl Roth, Germany
Trypsin-EDTA	Sigma-Aldrich, USA

3.1.2 Kits

Table 3-3: Kits

Kit	Company
Bicinchoninic Acid (BCA) protein assay kit	Thermo Fischer Scientific, USA
BrdU Staining Kit for Flow Cytometry APC	Affymetrix eBioscience, USA
CD34 Microbead Kit, human	Milteniy Biotec, Germany
CellTraceTM CFSE Cell Proliferation Kit	Thermo Fischer Scientific, USA
DreamTaq PCR Master Mix	Thermo Fischer Scientific, USA
DuoSet ELISA Development kit for SDF-1	R&D systems, USA
M-Per mammalian protein extraction reagent	Thermo Fischer Scientific, USA
Pierce Bicinchoninic Acid (BCA) protein assay kit	Thermo Fischer Scientific, USA
Plasmid Kit with QIAGEN-tip 500	QIAGEN, Netherlands
ReliaPrep RNA Cell Miniprep System	Promega, USA
RevertAid First Strand cDNA Synthesis kit	Thermo Fischer Scientific, USA

3.1.3 Media

Table 3-4: Media

Medium	Company
CellGro medium	CellGenix, Germany
Dulbecco´s Modified Eagle Medium (DMEM)	Thermo Fischer Scientific, Gibco, USA
HSC CFU complete with Epo	Milteniy Biotec, Germany
Human Stem MACS medium	Milteniy Biotec, Germany
Iscove's Modified Dulbecco's Media (IMDM)	Biochrome, USA

3.1.4 Antibodies

Table 3-5: FACS antibodies

Anti-human	Clone	Company	Catalogue No.
CD11b PE	ICRF44	Biolegend, USA	301306
CD29 PE	MAR4	BD Biosciences, USA	555443
CD34 APC	AC136	Milteniy Biotec, Germany	130-090-954
CD41 FITC	MAB4143	Immunotech, France	PN IM0649
CD44 FITC	G44-26	BD Biosciences, USA	555478
CD45 V500	HI30	BD Biosciences, USA	560777
CD49d APC	9F10	BD Biosciences, USA	559881
CD49e PE	IIA1	BD Biosciences, USA	555617
CD49f FITC	GoH3	BD Biosciences, USA	555735
CD51 PE	NKI-M9	BioLegend, USA	327909
CD61 PE	VI-PL2	BD Biosciences, USA	555754
CD73 PE	AD2	BD Biosciences, USA	550257
CD90 APC	5E10	Affymetrix eBioscience, USA	17-0909-73
CD105 FITC	SN6	AbD serotec, USA	MCA1557F
CD133/1 PE	AC133	Milteniy Biotec, Germany	130-080-801
CD146 APC	541-10B2	Milteniy Biotec, Germany	130-092-849
CD166 PE	3A6	BD Biosciences, USA	559263

Table 3-6: primary antibodies

Antibody	Clone	Company	Catalogue No.
Polyclonal rabbit-anti-human-CXCL12&/SDF-1	Polyclonal	Acris Antibodies, Germany	PP1067P1
Polyclonal rabbit-anti-human-CXCR4	Polyclonal	Abcam, UK	ab2090
Polyclonal rabbit-anti-human-Fibulin-1	Polyclonal	SantaCruz Biotechnology, USA	Sc-20818
Monoclonal mouse- anti-human-ITGαVβ3	VNR-1	Abcam, UK	ab78289
Polyclonal rabbit-anti-human-p-paxillin (Tyr118)	Polyclonal	CellSignaling, USA	2541S
Monoclonal mouse-anti-human-vinculin	hVIN1	Sigma-Aldrich, USA	V9131

Table 3-7: secondary Antibodies

Antibody	Clone	Company	Catalogue No.
Polyclonal goat-anti-mouse-Cy2	Polyclonal	Dianova, Germany	115-225-166
Polyclonal sheep-anti-rabbit-Cy3	Polyclonal	Sigma-Aldrich, USA	C2306
ECl-polyclonal-donky-anti-rabbit IgG-HRP	Polyclonal	GE Healthcare, UK	NA934-100UL

3.1.5 Primers, sh-RNA sequences, and vectors

Table 3-8: Primers

Primer	Sequence 5´-3´	Size	Accession No.
Fibulin-1 forward	CCT ACC GCT GCA TCA ACA T		
Fibulin-1A reverse	ATG CAG AGT TCC CTA CGA TCA	236	NM_006487
Fibulin-1B reverse	CCT TCC CTT CTT GGA TTT CTG	236	NM_006485
Fibulin-1C reverse	GAT TCT CAT GGC AAG GCA AG	246	NM_001996
Fibulin-1D reverse	GAG ATG ACG GTG TGG GAG AT	322	NM_006486
GAPDH forward	GCC AAA AGG GTC ATC ATC TC		
GAPDH reverse	GGT GCT AAG CAG TTG GTG GT	198	

Table 3-9: sh-RNA sequences

Clone	Target sequence 5´-3´	Clone ID
pLKO.1 puro shRNA vector 10	CCTCCAAGAAACGGATAAGAT	TRCN0000055675
pLKO.1 puro shRNA vector 11	CGAATGCAAGACGGGTTACTA	TRCN0000055676

Table 3-10: Vectors

Vector	Reference
pLKO.1 puro	Mission RNAi (Mission shRNA), Sigma-Aldrich, USA
psPAX	Trono Lab Packaging and Envelop Plasmids (Addgene#12259)
pVSVg	Stewart et al., 2003

3.1.6 Equipment

Table 3-11: Equipment

Equipment	Company
ACCellerator	Zellmechanik Dresden, Germany
Autoclave DE-23	Systec Sci, Germany
Biological Safety Cabinet HeraSafe	Thermo Fischer Scientific, USA
BD FACSAria III	BD Biosciences, USA
BD FACSCalibur	BD Biosciences, USA
BD LSRII	BD Biosciences, USA
Centrifuge Biofuge primoR	Thermo Fischer Scientific, Heraeus,USA
Centrifuge Rotixa 120RS	Hettich-Zentrifugen, Germany
CO_2-Incubator Heraeus HERAcell 240	Thermo Fischer Scientific, USA
G:Box.	Syngene, USA
Heraeus heating and drying oven	Thermo Fischer Scientific, USA
LAS-3000 imager	Fujifilm, Japan
Laser Scanning Microscope, Leica SP5	Leica Microsystems, Germany
Light microscope Axiovert 200M	Carl Zeiss, Germany
Light and fluorescence microscope Axiovert S100	Carl Zeiss, Germany
MACS Quant Analyzer	Milteniy Biotec, Germany
Microplate reader Anthos htII	Richmond Scientific, UK
Microwave Continent MW 800 G	GGV Exquisit, Germany
MilliQ Purification System for deionized water	Millipore, Germany
Molecular Imager Gel Doc	Bio-Rad Laboratories, USA
NanoDrop 200	Thermo Fischer Scientific, USA
Neubauer counting chamber	LO Laboroptik, UK
Page chamber	Bio-Rad Laboratories, USA
Pipetboy Easypet	Eppendorf, Gemany
Pipets 0.1 µl – 5000 ml	Eppendorf, Germany
PowerPac Universal	Bio-Rad Laboratories, USA
Quadro MACS Seperator	Milteniy Biotec, Germany
Spincoater RC5	Süss Microtec, Germany
Vacuubrand-CVC2000	Brand, Germany
Vacuum pump	VWR, Germany

3.1.7 Software

Table 3-12: Software

Software	License	Developer/ Company
Anaconda (Python)	Open Source	Continuum Analytics, USA
Chemotaxis and Migration Tool	Proprietary Freeware	Ibidi, Germany
Flowing Software	Proprietary Freeware	Perttu Terho, Turku Centre for Biotechnology
FlowJo Software 10.0	TreeStar License	TreeStar, USA
GraphPadPrism 5.0	GraphPadPrism License	GraphPad Software, USA
ImageJ / Fiji	Public Domain	Wayne Rasband (retired from NIH)
Inkscape	Open Source	Public development
MS Office	Microsoft License	Microsoft, USA
ShapeIn	Zellmechanik Dresden License	Zellmechanik Dresden, Germany
ShapeOut	Proprietary Freeware	Zellmechanik Dresden, Germany

3.2 Methods

3.2.1 Cell preparation and culture

3.2.1.1 Mesenchymal stromal cells

Bone marrow aspirates were collected from healthy donors at the Bone Marrow Transplantation Center of the University Hospital, TU Dresden, after obtaining verbal and written consent. The study was approved by the local ethics committee (ethical approval no. EK221102004, EK47022007). Briefly, bone marrow aspirates were diluted with PBS at a ratio of 1:5. A 20 ml aliquot was layered over a 1,073 g/ml Percoll solution and centrifuged at 200 x g for 15 min at room temperature (RT) with low acceleration and without deceleration. After centrifugation, mononuclear cells at the interphase were recovered and washed with 50 ml PBS. All cells were seeded onto a T-75 cell culture flask in low glucose DMEM supplemented with 10% FCS and cultured at 37°C, 5% CO_2 in a humidified incubator. After two days, hematopoietic and non-adherent dead cells were removed by washing with PBS. Medium was changed twice a week. MSCs were passaged using 0.25% Trypsin-EDTA. Cell viability was determined using the Trypan blue dye exclusion method and cell counting in a Neubauer hemocytometer.

Human MSC preparations from individual donors were not pooled. MSCs used in this study were chosen according to the minimal criteria for MSCs, according to the International Society for Cellular Therapy (ISCT) guidelines (Dominici et al., 2006) and prior characterization of osteogenic differentiation capacity, as measured by alkaline phosphatase-activity (AP-activity, Hempel et. al, 2012) at the Institute of Physiological Chemistry, TU Dresden).

3.2.1.2   Hematopoietic stem cells

G-CSF (granulocyte colony-stimulating factor)-mobilized peripheral blood was obtained from healthy donors at the Bone Marrow Transplantation Center of the University Hospital, TU Dresden, after obtaining verbal and written consent. The study was approved by the local ethics committee (ethical approval no. EK221102004, EK47022007). CD34$^+$ HSPCs were purified from leukapheresis samples using the human CD34 Microbead Kit. Briefly, a 2 ml aliquot of PB was washed in 23 ml washing buffer (50 ml PBS + 15 ml 4% sodium citrate, at 4°C). After centrifugation (200 x g, 5 min without deceleration, 4°C), the cell pellet was resuspended in 300 µl cold separation buffer (50 ml PBS + 15 ml 4% sodium citrate + 5 ml human serum albumin) at the rate of 1 x 10^8 total nucleated cells (TNCs), 100 µl blocking solution added, incubated for 5 min at RT, 100 µl CD34 antibody-conjugated magnetic beads added, and incubated for 15 min in the refrigerator. To ensure an optimal mixing of the cell suspension, the sample was agitated every 5 min, followed by washing in 25 ml separation buffer. After centrifugation (200 x g, 5 min without deceleration, 4°C), cells were resuspended in 2 ml separation buffer. For cell separation, LS Columns equilibrated with 2 ml separation buffer and Pre-Separation Filters (30 µm) were placed in a Quadro MACS Separator. The cell suspension was added and flow-through collected in a falcon tube. Bound cells were washed 4 times with 2 ml separation buffer, the LS column removed from the MACS separator, and the cells plunged out using 8 ml separation buffer. Cell were collected by centrifugation (200 x g, 5 min without deceleration, 4°C), followed by a second cell separation step to increase purity.

Purified CD34$^+$ HSPCs were seeded onto 6 well plates containing ECM scaffolds and grown in CellGro medium supplemented with 2.5 ng/ml SCF, IL-3, and Flt-3, for 5, 7, or 11 days without medium change. As controls, CD34$^+$ HSPCs were seeded onto 6 well plates without ECM scaffold slides (plastic culture dish, PCD-cells). For co-culture experiments, SCP-1 cells were seeded at a density of 1 x 10^5 cells per cm² and grown in DMEM supplemented with 10 % FCS for 48 h, before the addition of freshly isolated CD34$^+$ cells at 1 x 10^4 cells per cm². SCP-1/HSPC co-cultures were maintained in cytokine supplemented CellGro and were cultured at 37°C, 5% CO$_2$ in a humidified incubator.

3.2.1.3   Single cell picked clone 1 (SCP-1) cells

To produce uniform and highly reproducible ECM scaffolds, we predominantly used SCP-1 cells. This mesenchymal cell line originates from human MSCs overexpressing the human telomerase reverse transcriptase to facilitate immortalization. These cells are known to display key features of MSCs like CD73, CD90, and CD105 surface marker expression, and osteogenic, adipogenic, and chondrogenic differentiation potentials. The SCP-1 cell line was generously provided by

Matthias Schieker (Boeker et al., 2008). Cells were cultured in standard medium consisting of low-glucose DMEM supplemented with 10% FCS at 37°C and 5% CO_2 in a humidified incubator. Cells were passaged once a week using Trypsin-EDTA and the medium was changed twice a week

3.2.2 Generation of surface immobilized ECM preparations

Surface immobilization of ECMs and their subsequent characterization has been described in detail by Prewitz et al., 2013. Generation of ECM preparations is described in brief as follows.

3.2.2.1 Surface functionalization

Aminosilane chemistry was applied to round glass slide surfaces to allow covalent attachment of POMA and bioactive molecules like FN. Coverslips were oxidized in a 1:1:5 ratio of ammonia, H_2O_2 and H_2O at 70°C for 15 min, followed by two washing steps in Millipore-water, and a drying step using pressurized nitrogen. Surface modification of glass substrates were done by incubation in 1,16 ml aminosilan in 250 ml Isopropanol/ H_2O (1:9) for 1 h, followed by rinsing in isopropanol and drying at 120°C for 1 h. This step also ensures stable bonding of the copolymer solution (0.16% POMA in THF;Figure 1-9**Fehler! Verweisquelle konnte nicht gefunden werden.**). Using spin-coating, thin films of POMA were generated and covalently bound to glass surfaces. To activate the surface,slides were tempered for 2 h at 120°C and rinsed with acetone for 15 min. Slices were stored for up to 3 months, protected from light.

Using POMA coated glass slides, proteins can be covalently linked to glass surfaces that then serve as linkers to cell-derived ECM. After sterilization in an autoclave at 121°C and annealing in a hot-air oven at 120°C for 2 h, proteins bind to the anhydride moieties of the copolymer via free amino groups. FN was suspended in PBS (50 µg/ml) and incubated on annealed surfaces for 1 h at 37°C and 5% CO_2 in a humidified incubator to a final concentration of 5 µg/cm².

3.2.2.2 ECM preparation

To generate ECM scaffolds, SCP-1 cells were seeded at a density of 1 x 10^4 cells per cm² on functionalized glass slides and grown to confluency at 37°C and 5% CO_2 in a humidified incubator. The medium was changed every second day. To obtain cell-free ECM structures, cultures were decellularized at day 7 to 10 using double distilled water supplemented with 20 mM ammonium hydroxide, and the ECM acquired by gentle agitation for 10-min at room temperature. The resulting protein layers were washed thrice with deionized water and twice with PBS containing calcium and magnesium. These ECM scaffolds were used directly or stored in PBS containing calcium and magnesium for up to 4 weeks at 4°C.

3.2.3 Flow cytometry and fluorescent activated cell sorting

For flow cytometry and FACS sorting, cells needed to be harvested. PCD-cultured and SN-cells were harvested after three washes in FACS buffer (PBS + 5% FCS), and AT-cells were detached by vigorous pipetting in FACS buffer. SCP-1 cells were detached by incubation with Trypsin-EDTA for 5 min, after the cell layer was washed with PBS, and the trypsin-EDTA reaction was stopped by adding 5 times greater volume of a medium containing 10% FCS. After centrifugation (200 x g, 5 min, RT), cells were stained for surface markers using fluorescent-labeled antibodies listed in Table 3-5, and corresponding human immunoglobulin G controls were used. At least $10^5 – 10^6$ cells were resuspended in FACS buffer and incubated with antibodies in the dark for 20 min RT, according to the manufacture's protocol. Stained cells were washed twice with 5 ml FACS buffer and analyzed directly or fixed using 1% PFA. Cells were measured by flow cytometry using the FACScalibur or LSRII and were analyzed by FlowJo software (version 10.0, Tree Star). Fluorescent activated cell sorting for HSPCs was performed on a FACSAria machine according to the scheme provided in Figure 4-16. Dead cells were excluded by 4′,6-Diamidin-2-phenylindol (DAPI) staining, and sorted cells were harvested in ice-cold PBS.

3.2.4 Cell cycle analyses

The BrdU assay for HSPCs was carried out according to manufacturer's instructions for the BrdU Staining Kit for Flow Cytometry using 10 µM BrdU-staining solution. Briefly, BrdU was thawed on ice, diluted in PBS under sterile conditions to a working concentration of 1 mM, and 10 µl of this working solution added directly to 1 ml cell culture medium. Incubation was titrated to be most efficient at 2 h. SN-cells were harvested by collecting the cell culture supernatant, followed by washing of the ECM with 2 ml FACS buffer. AT-cells were detached by vigorous pipetting using 3 x 2 ml FACS buffer. Cells were centrifuged (200 x g, 5 min, RT) and resuspended at $1 – 2 \times 10^6$ cells in PBS by pulse-vortexing. Freshly prepared 1x BrdU Staining Buffer working solution (1 mL) was added, the cell suspension gently mixed, and incubated for 15 min at RT in the dark. After washing of cells twice with 2 ml FACS buffer, DNA was stained with 1 µg/ml propidium iodide for 30 min at RT in the dark. Cells were again washed twice with 2 ml FACS buffer. DNase I solution was thawed on ice and diluted by adding 700 µl FACS buffer to 300 µl DNase I solution. Cells were resuspended in 100 µl DNase I working solution and incubated for 1 h at 37°C in the dark. Cells were then washed twice with 2 ml FACS buffer, resuspended in 100 µl FACS buffer, 5 µl of anti-BrdU fluorochrome-conjugated antibody added, and incubated for 30 min at RT in the dark. Cells were washed twice with 2 ml FACS buffer, followed by fluorescence acquisition on a FACSLSRII.

3.2.5 Proliferation analyses

The CellTraceTM CFSE Cell Proliferation Kit was used to detect HSPC generations according to manufactures instruction. CellTrace CFSE staining solution was prepared by diluting 1 µl in 999 µl sterile PBS. Freshly isolated CD34$^+$ cells were centrifuged (200 x g, 5 min, RT), supernatant removed, cells resuspended in CellTrace CFSE staining solution at 10^5 cells per 100 µl, followed by 20 minutes incubation at 37°C in the dark. 1 ml DMEM + 10% FCS was added, followed by incubation for a further 5 min at 37°C in the dark. Cells were centrifuged (200 x g, 5 min, RT), resuspended in pre-warmed CellGro medium containing cytokines as described in 3.2.1.2, and prepared cells cultured for 5 d either on Matrix or PCD at 37°C and 5% CO_2 in a humidified incubator. After cells were collected, washed, and counterstained using CD34-APC as described in 3.2.3, the number of cell divisions was quantified according to the CFSE signal intensity on a LSRII flow cytometer and analyzed on FlowJo-software.

3.2.6 Colony forming unit cell assay (CFU-GEMM)

To investigate the clonogenicity of HSPCs, colony-forming unit cell assays were performed in semisolid human Stem MACS medium. Briefly, cells were washed, counted, and resuspended at a final volume of 1 x 10^5 cells in 1 ml PBS. Cells (n=500) were suspended in 3 ml human Stem MACS medium, 1 mL aliquots were seeded in 3 petri dishes (35x10 mm), and cultivated at 37 °C in a humidified 5% CO_2 atmosphere. This assay triggers differentiation towards myeloid lineages, i.e., granulocytes, erythrocytes, monocytes; and megakaryocytes, is mediated by multiple growth factors (Ogawa, 1989) and therefore, yields the number of HSCs and common myeloid progenitors (Carow et al., 1993). After 14 days, each well was scored for the number of burst-forming units–erythroid (BFU-E), colony forming units–erythrocytes, colony forming units–granulocyte (CFU-G), CFU–granulocyte macrophage (CFU-GM), and CFU–macrophage (CFU-M), according to standard criteria (Pereira et al., 2007).

3.2.7 Migration assays

3.2.7.1 Transwell migration

A transwell migration system was used to test HSPC migration towards a gradient of SDF-1, before and after ECM culture. This system uses a 96-well plate that is reversibly covered by a porous membrane (pore size = 5 µm). The cavities of the provided wellplate were filled with 30 µl medium containing 100 ng/ml SDF-1. Spontaneous migration rates were examined without adding SDF-1. After placing the membrane onto the plate, 60 µl of Cellgro medium containing 3x10^4 cells was added onto the membrane, the system placed in a humidified incubator at 37°C with 5% CO_2, and cells allowed to migrate for 3 h. Control wells used 30 µl medium containing 3x10^4 cells for analyses. The total number of migrated cells was counted by removing the porous

membrane and placing the 96-well plate on the MACS Quant Analyzer. Data were analyzed using FlowJo software.

3.2.7.2 Live cell migration

To analyze the spontaneous cell migratory behavior on ECM preparations, SN-cells were removed by washing 3 times with PBS. AT-cells were live-cell imaged for 40 min using an inverted microscope Axiovert S100 (Carl-Zeiss). An image was taken every 30 sec and cell migration was analyzed using Fiji software and the Chemotaxis and Migration Tool. For functional integrin blocking, AT-cells in 6 well plates were pre-incubated for 1 h before migration analysis with either 2 µg monoclonal mouse-anti-human-ITGαVβ3 antibody or appropriate IgG$_1$ control in serum-free CellGro medium.

3.2.8 Confocal laser scanning microscopy

PCD cultured, SN- and AT-cells on ECM preparations or SCP-1 cells alone or in co-culture with HSPCs were washed once with ice cold PBS. Cells were fixed with 4% paraformaldehyde for F-actin, CXCR4, and SDF-1 staining or with methanol/acetone (1:1) for integrin, vinculin, and p-paxillin staining. After a second washing step, cells were permeabilized using PBS containing 0.1% Triton X-100 (T-PBS) for 15 min, followed by blocking for 1 h with T-PBS containing 10% FCS and 1% HSA (IF buffer). Antibody dilutions were prepared in IF buffer as follows: monoclonal mouse-anti-human-ITGαVβ3 1:200, polyclonal rabbit-anti-human-CXCR4 1:500, polyclonal rabbit-anti-human-CXCL12/SDF-1 1:500, monoclonal mouse-anti-human-vinculin 1:500, and polyclonal rabbit-anti-human-p-paxillin (Tyr118) 1:50. Alexa Fluor 488 phalloidin for actin staining was prepared by dissolving one vial Alexa Fluor 488 phalloidin in 1 ml methanol and 5 µl added to 200 µl cell-IF buffer solution. Cells were incubated overnight at 4°C. After washing thrice for 10 min with T-PBS, secondary antibodies were incubated for 1 h RT in IF buffer as follows: polyclonal sheep-anti-rabbit-Cy3 1:200, or polyclonal goat-anti-mouse-Cy2 1:200. After washing thrice with T-PBS for 10 min, DNA was counter confocal laser scanning microscopy.

3.2.9 Real-time deformability cytometry (RT-DC)

RT-DC was performed as described in detail by Mietke et al., 2015; Otto et al. and 2015; Xavier et al., 2016. Freshly isolated PB and BM CD34$^+$ cells, SN- and AT-cells from ECM, SCP-1 co-cultures, and PCD-cultured HSPCs were harvested as described above. Centrifuged cells (200 x g, 5 min, RT) were washed with PBS and suspended in PBS containing 0.63% methylcellulose (MC-PBS) at a concentration of 1-2 x 10^6 cells/ml. The cell suspension was drawn in a syringe and connected to a microfluidic chip as depicted in Figure 3-1. The chip is made from Polydimethylsiloxane (PDMS) and is mounted on a glass slide. The chip consists of a

central channel separated by two reservoirs. A second syringe, filled with MC-PBS, was used to hydrodynamically focus the cells inside the constriction of the chip (Figure 3-1, middle plane), which was then mounted on an inverted microscope. A syringe pump flushes the cells through the channel at a constant flow rate of 0.06 µl/sec that results in the cells being deformed into a characteristic bullet-like shape. A high-speed CMOS camera images the cells at the end of the constriction and cell cross-sectional area (size [µm²]) and deformation are calculated in real-time..
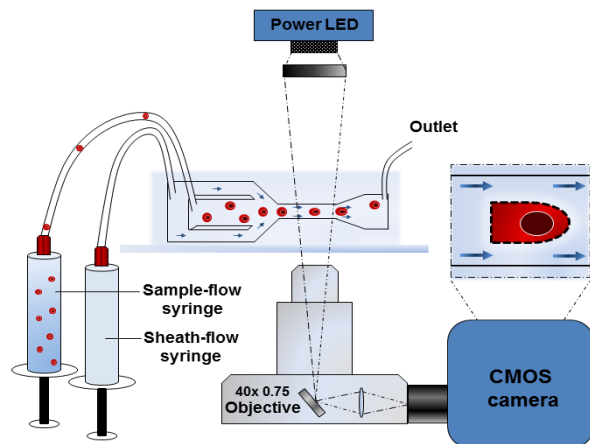

Figure 3-1: Real-time deformability cytometry
Schematic representation of RT-DC setup and measurement. Sample-flow contains cells and sheath-flow contains MC-PBS with same viscosity as the sampkle flow. A syringe pump flushes sample-flow and sheath-flow through the microfluidic chip at constant speed with a 1:3 ratio of sample- to sheath flow, which hydrodynamically focuses the cells in the middle of the channel constriction. Here cells are imaged, and the deformation and cell size is calculated in real-time.

Statistical comparison of deformation was carried out using 1-dimensional linear mixed model analysis. One fixed and one random effect were considered in order to analyze the difference between subsets of cells and to consider replicate variance, respectively. P-values were determined by a likelihood ratio test that compared the full model with a model lacking the fixed effect term.

3.2.10 Molecular biological methods

3.2.10.1 RNA isolation, reverse transcription, and PCR

For RNA isolation, SCP-1 cells were cultured in T-75 flasks with normal DMEM or osteogenic medium (DMEM + 10% FCS with 100 nM dexamethasone, 10 nM β-glycerol-phosphate, and 50 µM 2-phospho ascorbic acid) until confluence, followed by an additional 10 days of culture. RNA isolation was performed according to manufacturer's protocol for adherent cells using the ReliaPrep RNA Cell Miniprep System. Briefly, cells were detached by Trypsin-EDTA treatment as described in 3.2.1.1, collected by centrifugation (200 x g, 5 min, RT), cell pellet resuspended

in ice cold PBS, and again pelleted by centrifugation. The supernatant was discarded, 10^6 cells resuspended in 250 µl BL+TG (1,500 µl 1-Thioglycerol to 150 ml BL buffer) by vortexing, 85 µl Isopropanol added and mixed by vortexing for 5 sec. The lysate was transferred to a Minicolumn and centrifuged (12,000 x g, 30 sec, RT) with total RNA trapped in the Minicolumn. RNA Wash Solution (500 µl) was added and again centrifuged (12,000 x g, 30 sec, RT). DNase I working solution was prepared by mixing 2 µl Yellow Core Buffer, 3 µl $MnCl_2$, and 3 µl DNase I, and added to Minicolumn, followed by 30 min incubation at RT. To wash the column, 200 µl Column Wash Solution was added and centrifuged (12,000 x g, 15 sec, RT), followed by 500 µl RNA Wash Solution and centrifugation (12,000 x g, 30 sec, RT). The second washing step used 300 µl RNA Wash solution and 2 min centrifugation at maximum speed. RNA was eluted by centrifugation (12,000 x g, 1 min, RT) using Nuclease-Free Water. RNA concentration was determined on a NanoDrop 200 UV-Vis spectrophotometer and up to 5 µg total RNA was reverse transcribed using the RevertAid First Strand cDNA Synthesis kit. Briefly, an appropriate amount of RNA was mixed with 1 µl Oligo (dT)$_{18}$ primer and water to a volume of 12 µl. This mixture was incubated for 5 min at 65°C, chilled on ice, and 4 µl 5X Reaction Buffer, 1 µl RiboLock RNase Inhibitor (20 U/µl), 2 µl 10 nM dNTP Mix, and 2 µl RevertAid M-MuLV RT (200 U/µl) added to make a total volume of 20µl. The suspension was mixed and cDNA reverse transcribed by 60 min incubation at 60°C. The reaction was terminated by heating the mixture to 70°C for 5 min. PCR for fibulin-1 was done using the DreamTaq PCR Master Mix and primers were designed according to Hergeth et al., 2013 (Table 3-8). An initial denaturation step occurred at 96°C for 1 min, followed by 45 cycles of replication (denaturation at 96°C for 45 s, annealing at 57°C for 40 s, elongation at 72°C for 1 min) and was terminated with a final elongation at 72°C for 10 min, followed by cooling to 4°C. PCR products were directly analyzed in a 1.5% agarose gel stained with RedSafe or stored at -80°C till usage. Agarose gels were imaged using Syngene G:Boxsoftware and GAPDH was amplified using primers depicted in Table 3-8 as the housekeeping gene. The GeneRuler 100bp DNA ladder was used ot estimate product size.

3.2.10.2 Lentiviral shRNA transduction

Plasmid pLKO.1 vectors (Figure 3-2) encoding shRNAs targeting the human fibulin-1 gene (SHCLNV-NM_001996) were kindly provided by Frank Buchholz as *E.coli* glycerol stocks. To expand, plasmid DNA stocks were defrosted, 250 ml liquid LB-medium was infected and incubated at 37°C overnight under constant shaking. Plasmid DNA was isolated using the QIAGEN Plasmid Kit with QIAGEN-tip 500 according to manufactures instruction. Plasmid quality and amount were determined on a NanoDrop 200 UV-Vis spectrophotometer.
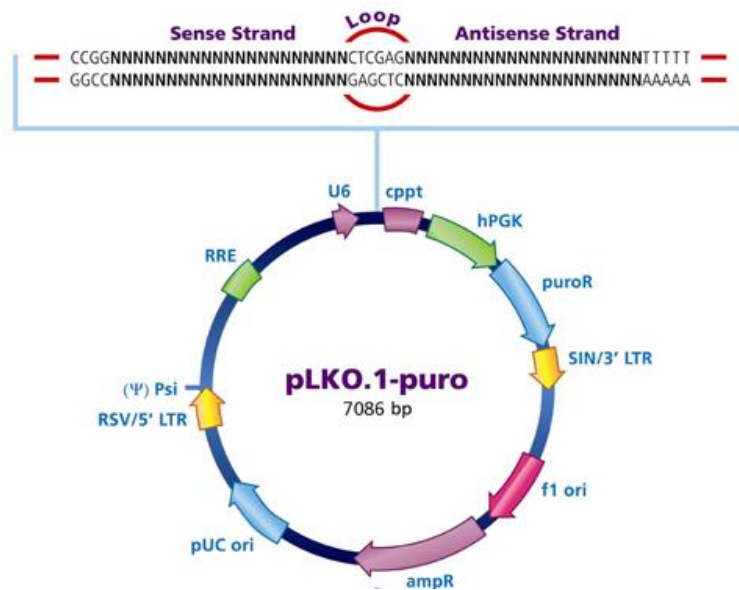
Figure 3-2: pLKO.1-puro vector map
Vector map shows the schematic construction of the pLKO.1-puro vector, including the cloning site for shRNA constructs as well as regions for puromycin and ampicillin resistance. In combination with an origin of replication (ori), it is possible to expand the vector and effectively select only transfected bacteria. Puromycin resistance mediates selection of transduced eukaryotic cells. Additionally, vector structure allows for lentiviral particle production (vector map adapted from: sigmaaldrich.com).

To produce lentiviral vector particles, HEK293T cells were transfected with pLKO.1 plasmid that were either empty or contained shRNA 10 or shRNA 11 in combination with the packaging plasmids psPAX and pVSVg using PEI. After 48 h of growth in IMDM medium, the lentiviral vector containing media supernatants were collected, and SCP-1 wildtype (WT) cells were infected twice by adding the supernatant to previously PBS washed cells. The medium containing the lentivirus vector was supplemented with 1 µg/ml protamine and incubated for 1 h and fresh DMEM medium with 10% FCS was added in at a ratio of 1:1. This procedure was repeated after 12 h. Sequences of the shRNAs 10 and 11 are shown in Table 3-9.

3.2.10.3 Western blot

After washing the decellularised ECM twice with ice-cold PBS, the protein layer was detached using 100 µl/cm^2 M-Per mammalian protein extraction reagent and the Halt protease inhibitor cocktail at a ratio of 10:1 (v/v). Using a cell scraper, the ECM was sheared, transferred into reaction tubes, and centrifuged at 14,000 g for 7 min. Supernatant was collected and protein concentration determined using the Pierce Bicinchoninic Acid (BCA) protein assay kit according to the manufacturer's instructions. A standard curve was prepared using BSA (0, 0.2, 0.4, 0.6, 0.8, 1 and 1.5 mg/ml) as standard, provided in the kit. Working reagent and samples were added into microplate wells at a ratio of 20:1 (v/v) and incubated for 45 min at 37°C. The absorbance of

bicinchoninic acid-Cu+ chelate complex was measured at 570 nm using a plate reader. A representative standard curve and linear regression curve are shown in Figure 3-3.
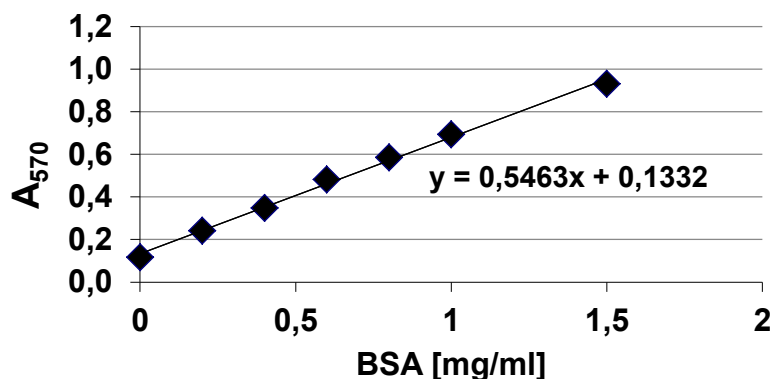

$$y = 0{,}5463x + 0{,}1332$$

Figure 3-3: BSA assay standard curve
Representative image of a standard curve estimation for BCA assay.

Isolated proteins (7 μg) were separated by SDS-PAGE on 7.5% acrylamide gels in duplicate. As loading control, one gel was stained with Coomassie blue solution (0.25% Coomassie blue dissolved in 45% methanol and 10% acetic acid) for 10 min. Destaining was performed by incubating the gels in a solution containing 45% methanol and 10% acetic acid for 1 h, and in distilled water overnight. The gel was imaged using Syngene G:Box and the Prestain Protein Ladder PAGE Ruler was used as the marker.

Protein transfer onto 0.45 μm nitrocellulose membranes was performed for 1h at 15 V and 3 A. Membranes were blocked for 1 h in blocking solution consisting of 5% milk powder (Carl Roth, Germany) dissolved in 10% Tris-buffered saline (1.5M NaCl, 30mM KCl, 250mM Tris, pH 7.4, all Carl Roth, Germany) containing 0.05% Tween 20 (TBST, Carl Roth, Germany). Incubation with fibulin-1 antibody (rabbit anti-human IgG, 1:800 in blocking solution, Santa Cruz Biotechnology, USA) occurred overnight at 4°C. Anti-rabbit IgG conjugated to horseradish peroxidase (1:5000 in blocking solution, GE Healthcare, UK) was applied as secondary antibody for 1h. Visualization of antigen-antibody complexes was performed with ECL plus western blotting detection reagents (Amersham, UK) and chemiluminescence was analyzed on a LAS-3000 imager (FUJIFILM, Japan). Semi-quantification was performed using the ImageJ software (1.47v, National Institutes of Health, USA) using SCP-1 WT signal as reference.

3.2.10.4 ELISA

To assess SDF-1 secretion levels, cells were seeded in 6-well plates at a density of 15,000 cells/well and medium changed after 24 h. Cells were cultured in standard or osteogenic medium, the supernatant collected after different time points (1 d, 2 d, 5 d, 7 d), and frozen at -

80°C before analysis. The ELISA assay was performed using reagents from the DuoSet ELISA Development kit for SDF-1 according to the manufacturer's protocol. Absorbance was measured on a microplate reader (Anthos htII) at 405 nm with reference wavelength at 570 nm. SDF-1 concentrations were calculated from optical density values using a calibration curve. All assays were performed in duplicate.

3.2.11 Statistical analysis

All results are presented as mean ± standard error of the mean (SEM) or standard deviation (SD). All experiments were performed independently at least thrice with the exception of SDF-1 ELISA, which was performed in duplicate. Means were compared using the Students two-tailed unpaired t-test and variance was analyzed using ANOVA, both in GraphPad prism software (ver.5.0). A p-value ≤ 0.05 was considered statistically significant.

4 Results

We adapted and applied a technique, published by Prewitz et al. 2013, to mimic the HSPC niche with respect to the extracellular compartment of the human BM. We used decellularized ECM scaffolds derived from SCP-1 cells, a human MSC cell line. We found that these ECMs are supportive substrates for HSPC proliferation and cell expansion. Moreover, CD34^{+} HSPCs were found to be a heterogeneous population of adherent and non-adherent cells. After cells adhere via the ITGβ3, ITGαIIb, and ITGαV (RGD-receptors), they adapt to the biochemical and biomechanical properties of the ECM and show cell stiffening and migratory morphology.

4.1 Extracellular matrix scaffolds for HSPCs

ECM scaffolds are cell-free protein layers secreted by growing cells and covalently bind to specialized glass surfaces. To produce ECM scaffolds for HSPCs, SCP-1 cells were seeded onto glass surfaces at a density of 1×10^4 cells/cm². After reaching confluency, cells were cultured for another 5 to 7 days before decellularization by osmotic shock. The quality of the remaining macromolecular protein structure was visualized and assessed for ECM delamination using inverted microscopy (Figure 4-1).
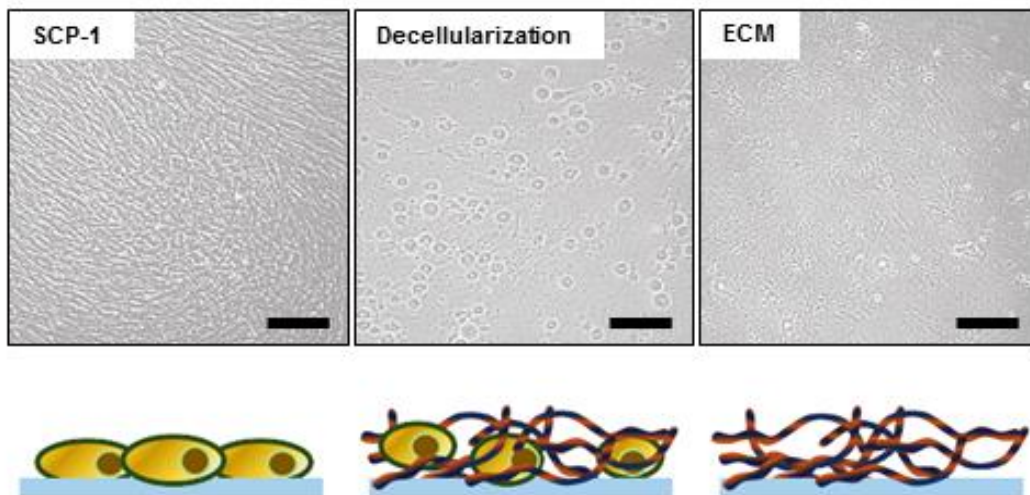
Figure 4-1: Decellularization process for ECM generation
Phase contrast images and corresponding cartoons show the process of decellularization. SCP-1 cells were grown to confluency on a glass substrate. After an additional culture period of up to 7 days, cells were decellularized using ddH2O treatment for up to 15 min under slight and continuous shaking (Decellularization). The macromolecular protein meshwork (cell-free ECM) remains covalently bound on the surface of the glass slide (ECM). Bars = 200 µm.

4.1.1 ECM properties

Prewitz et al. (2013) reported that ECMs derived from BM isolated MSCs were approximately 1 µm in height when cells were cultured in standard DMEM supplemented with 10% FCS for 10 days after confluency. These ECMs showed soft material properties with an elastic modulus of approximately 10 to 10^3 Pa, which is in the range of human BM measured by AFM indentation (Jansen et al., 2015). Surface distribution of the ECM was approximately 10% when cells were cultured on PCD without surface coating but was up to 95% when POMA-coated glass surface were used. Using mass spectroscopy, Prewitz et al. (2013) detected more than 500 proteins, including, structural constituents in the ECMs, such as fibronectin, collagen, and GAGs,. Moreover, they also found that classical MSCs secreted and released cytokines like HGF, FGF, VGF, and IL-8; all of these molecules participate in regulating the HSPC niche (Prewitz et al., 2013, 2015).

In this study, using the same anchoring method but with a different decellularization technique, ECM preparations derived from SCP-1 cells remained covalently bound to the copolymer-(POMA) and FN-coated glass surfaces (Figure 4-2A), indicating, applicability to multiple cells and cell lines. Contrarily, when uncoated surfaces like conventional PCDs were used, we observed delamination of ECM proteins upon decellularization (Figure 4-2B). The scaffolds generated by us were found to be approximately 1 µm in height, as measured by z-scan confocal microscopy. However, by probing different areas on a single ECM layer, enormous differences in ECM height could be detected ranging from 100 nm to 5 µm. Thus, ECM scaffolds derived from SCP-1 cells possess similar features to those derived from MSCs, as described by Prewitz et al. (2013).
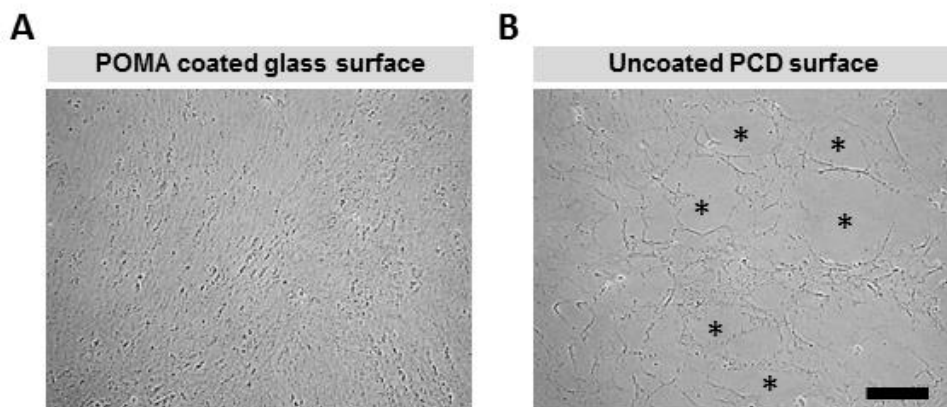

Figure 4-2: ECM lateral distribution after decellularization
(A) Phase contrast images of ECM structure on POMA-coated glass surfaces show up to 100% lateral ECM distribution. (B) Phase contrast images of ECM structure on uncoated PCD surfaces shows ECM delamination (asterisks = areas of ECM delamination from surface). Bar = 200 µm.

4.1.2 HSPC survival in ECM and PCD cultures

Human G-CSF mobilized peripheral blood was used to obtain useable numbers of HSPCs. Healthy volunteer donors were treated with G-CSF and apheresis was performed to concentrate HSPCs. However, for cultivation, cells needed to be further enriched due to excessive leukocyte contamination (Figure 4-3A). HSPCs were isolated using the immuno-magnetic bead separation technique where antibodies against the surface antigen CD34, bound to a magnetic bead, were used to label HSPCs. Cells were then trapped in a strong magnetic field, washed, and eluted. The CD34$^+$-cell proportion was regularly tested using flow cytometry and cells were used when purity was above 95%. CD133, an additional HSPC marker, was counterstained to visualize stem cell heterogeneity (Figure 4-3B).
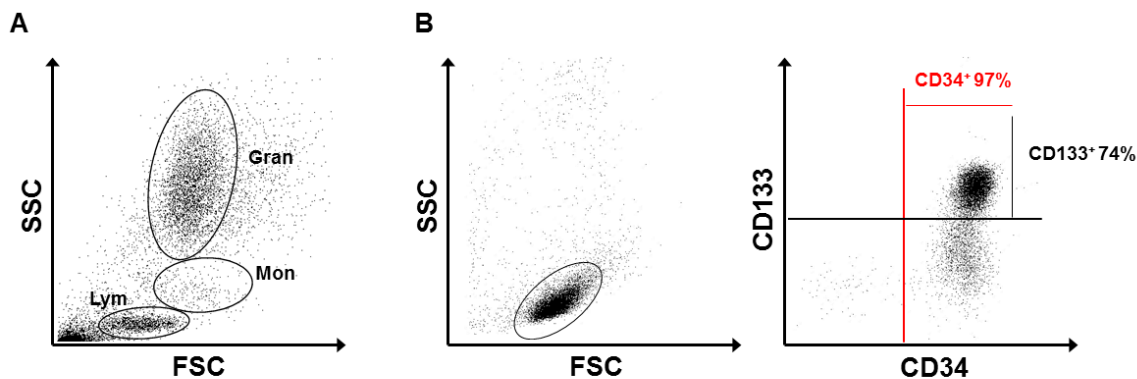

Figure 4-3: Stem cell marker expression on freshly isolated HSPCs
(A) Separation of PB leukocytes by flow cytometry. Scatter light forward scatter (FSC) and side scatter (SSC). Lym = lymphocytes including HSPCs (~40%), Mon = monocytes (~5%) and Gran = granulocytes (~55%). (B) Freshly isolated CD34$^+$ HSPCs in scatter showed an enriched population of cells. Cells were stained for stem cell surface markers CD34 and CD133 using antibodies. Approximately 97% of freshly isolated HSPCs were found CD34$^+$ and approximately 74% showed CD133 expression.

Isolated HSPCs were seeded at a density of 1 x 10^4/cm² on ECM scaffolds in serum-free CellGro culture media. At less than 12 h after seeding, we observed clustered adhesion of HSPCs to the underlying substrate using bright field microscopy (Figure 4-4A). Remarkably, only about 20% of CD34$^+$ HSPCs adhered (AT-cells) to the ECM proteins, indicating a strong heterogeneity in the HSPC pool of PB-derived cells. The remaining cells remained in the supernatant (SN-cells). In parallel, we performed classic expansion cultures using PCDs where cells were cultured in suspension and no adhesion to plastic surfaces could be detected.

To quantitate cell survival in both these conditions, cells were stained with DAPI at different time points and detected by flow cytometry (Figure 4-4B). Freshly isolated HSPCs were found to show highest DAPI fluorescence with approximately 1.1% dead cells due to intensive handling

during their isolation. After 5 days in ECM culture or PCD culture, we detected decreased amounts of DAPI$^+$ cells (Figure 4-4C). This was true at days 7 and 11compared to freshly isolated cells (Figure 4-4C). In PCD cultures, a DAPI signal was obtained in less than 1% of cells. In general, we found very low numbers of dead cells, indicating cell survival consistent with proliferation.
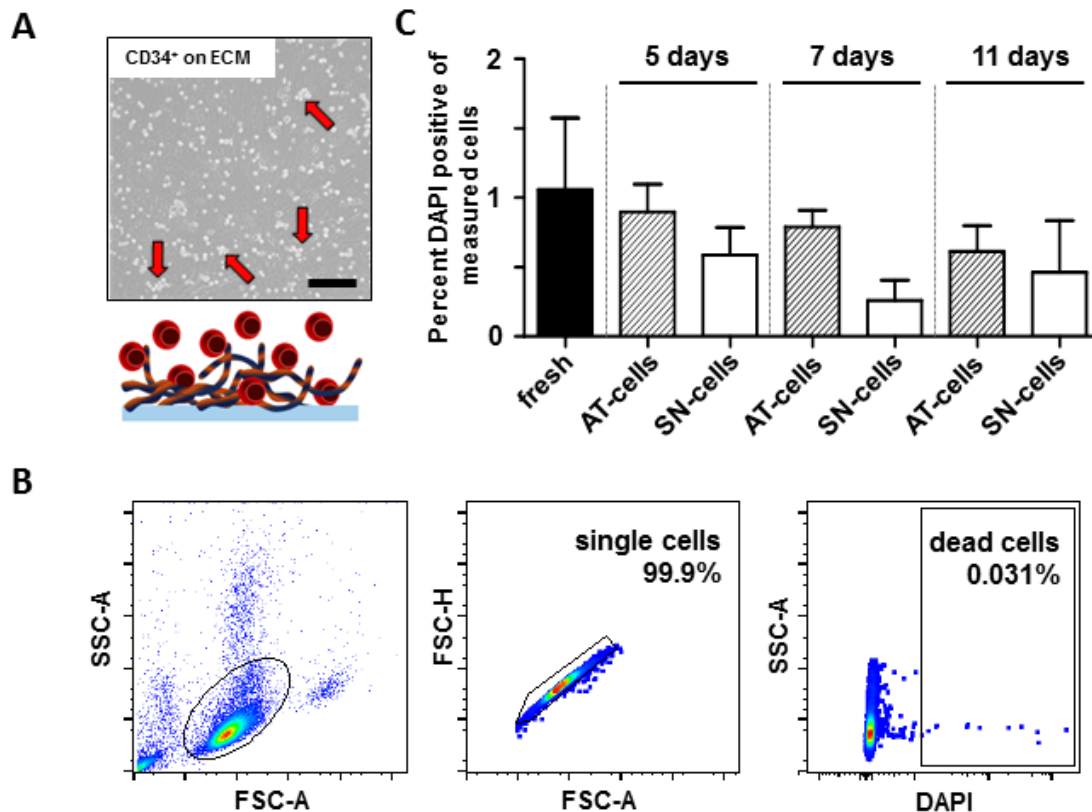

Figure 4-4: HSPC survival cultured on ECM scaffolds
(A) Representative phase contrast images and corresponding cartoon of CD34$^+$ HSPCs seeded onto ECM for 12 h (red arrows indicating clustered accumulation). Bar = 200 μm. (B) Representative flow cytometry panel for DAPI staining for detecting dead cells. Scatter light indicates enriched cell population in the lymphocyte and single cell gates. DAPI$^+$ cells are dead cells. (C) Quantification of percent DAPI$^+$ cells; n = 4, two-tailed t-test, no significant differences between groups. Error bars denote SEM.

4.1.3 HSPC expansion in ECM and PCD cultures

As mentioned before, HSPC were classified as either AT-cells or SN-cells after less than 12 h in ECM culture. As enumerated by absolute cell counts, we found both populations to be actively proliferating. After 5 days in culture, TNCs expanded by 3-fold, which represented a significantly higher expansion compared to PCD cultures (1.5 fold, $p < 0.05$). By increasing the culture period to 7 or 11 days, TNC numbers cultured on ECM increased by respectively 7.2-fold and 13-fold, on average. Notably, the number of AT-cells did not further increase after 7 days (Figure 4-5A). In contrast, PCD-cells expanded remarkably less during the same time. After a culture period of

7 or 11 days, expansion of TNCs in PCD cultures was 4.8-fold (p < 0.01) and 7.5-fold (p < 0.01), respectively (Figure 4-5A). In addition, using flow cytometry, we found that after 5 days, ECM scaffolds significantly expand CD34$^+$ HSPCs (by 1.8 fold) compared to only maintenance of CD34$^+$ HSPCs in PCD cultures (p < 0.05). Similarly, at 7 and 11 days, CD34$^+$ cells expanded by up to 4.5-fold in ECM culture but only up to 1.9-fold in PCD cultures (p < 0.01). Interestingly, expansion of CD34$^+$ cells stagnated after 7 days, indicating this time point as the limit of HSPC expansion culture due to nutritional turnover (Figure 4-5B). After removing SN-cells, we monitored the proliferation of AT-cells and the repopulation of the supernatant fraction by bright field microscopy, which showed only further division but no increase in adhesion. Similar findings have been reported by by Jing et al. (2010) using a MSC-HSC co-culture *in vitro* model. From these findings, we conclude that our ECM scaffolds provide additional pro-expansive factors during HSPC culture.
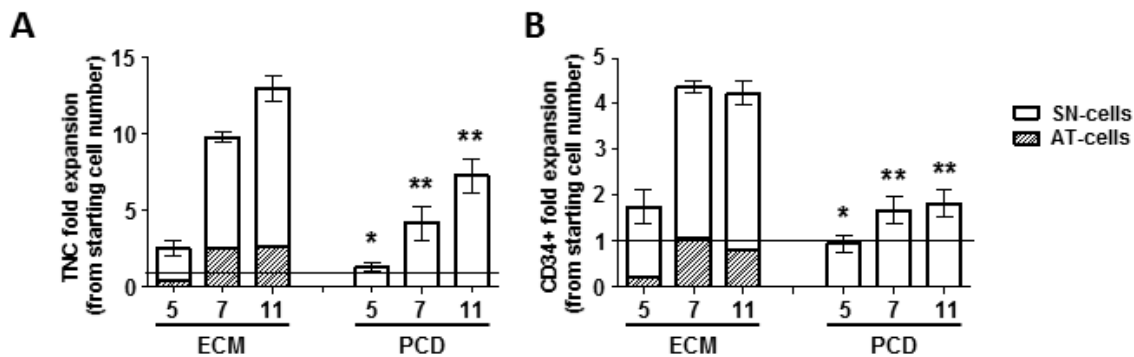

Figure 4-5: HSPC expansion on ECM substrates and PCD
(A) In vitro TNC expansion on ECM or PCD culture for 5, 7, and 11 days. Histogram bars represent fold change in relation to starting cell number (black line). AT-cells are shown as percentage share of total counted cells; n = 5, two-tailed t-test, significance in comparison to ECM culture. (B) CD34+ cell expansion on ECM or PCD culture for 5, 7, and 11 days. Histogram bars represent fold change in relation to starting cell number (black line). AT-cells are shown as percentage share of counted cells; n = 5, two-tailed t-test, significance in comparison to ECM culture. Error bars represent SD; *p < 0.05, **p < 0.01, ***p < 0.001.

To gain further understanding of the impact of culture conditions (PCD or ECM) and the state of division of AT-cells or SN-cells, we performed CFSE generation tracking using flow cytometry. Figure 4-6A shows representative CFSE intensity histograms of AT-, SN- and PCD-cells after 5 days of culture. Freshly isolated CD34$^+$ HSPCs that were labeled with CFSE served as control (generation 0). We found up to 6 generations in both culture conditions. However, PCD-cells had undergone lesser number of cell divisions compared to ECM-cells, as observed by the heterogeneous peak distribution.

To further quantify the cell divisions, 3 independent experiments were performed. AT- and SN-cells had predominantly undergone 5-6 divisions in around 80% of all AT-cells and in 70% of all SN-cells. Surprisingly, AT-cells showed greatest proliferation as 55% of AT-cells divided 6 times compared to only 30% of SN-cells (Figure 4-6B). Contrarily, only approximately 10% of PCD-cells divided 6 times, which is in line with the aforementioned lower expansion rate. Accordingly, significantly lower numbers of AT- and SN-cells were found in generations 1-3 ($p < 0.05$) compared to PCD-cells (Figure 4-6B). Furthermore, flow cytometry was used to separate CD34$^+$ HSPC from differentiated cells in every generation and remarkably, no significant differences could be detected between the classical PCD expanded HSPCs and ECM expanded HSPCs (Figure 4-6B), further strengthening evidence for the ECM as a HSPC-supportive culture substrate.
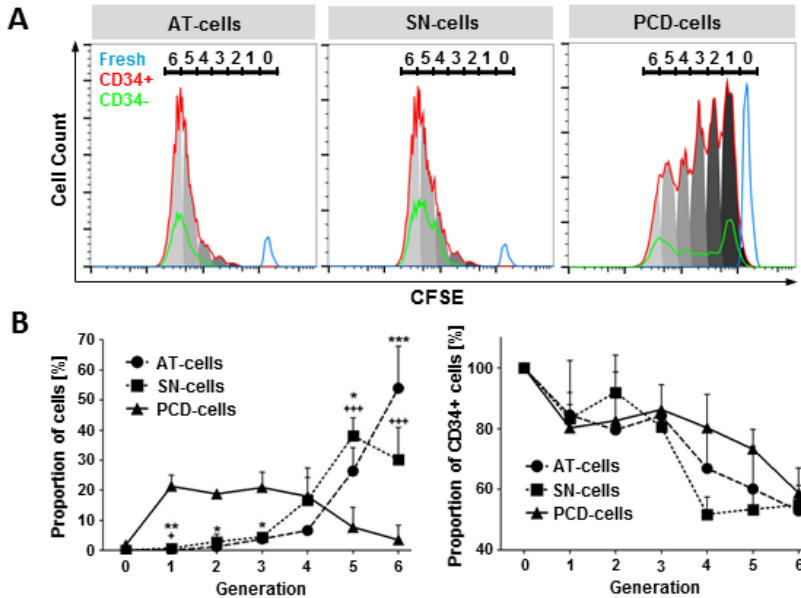
Figure 4-6: CFSE generation tracking of HSPCs cultured on ECM or PCD after 5 days
(A) Representative CFSE-intensity histogram showing distribution of cell generations of CD34$^+$ (red) and CD34$^-$ (green) cells after 5 days in ECM (AT-cells and SN-cells) or PCD (PCD-cells) culture. Freshly isolated cells (blue) served as control (generation 0). (B) Proportion of TNCs (left) and CD34$^+$ cells (right) detected in cell generations (0 - 6) after 5 days in ECM or PCD; n = 3, two-tailed t-test; * = AT-cell and + = SN-cell significance in comparison to PCD. Error bars represent SD.; *$p < 0.05$, **$p < 0.01$, ***$p < 0.001$.

As AT-cells divided most, we aimed to identify cell cycle phases in AT- and SN-cells using flow cytometry. Figure 4-7A shows a representative flow cytometry experiment of BrdU/PI incorporation. Cells with low PI and BrdU intensity are defined as G0/G1 cells. Through DNA synthesis in the S phase, cells incorporate BrdU and appear BrdU positive. G2/M phase cells do not incorporate BrdU as DNA was synthesized in S phase but increase PI intensity. According to

the BrdU incorporation assay after 5 days of culture, AT-cells were predominantly in the cycling G0/G1 phase (79.3% ± 5.4%), followed by S-phase (18.5% ± 3.9%), and significantly lower number of cells were detected in G2/M phase (1.9% ± 1.4%). Comparatively, SN-cells were 63.4 ± 3.4% in G0/G1, ($p < 0.01$); 11.8% ± 2.9%, ($p < 0.05$) in S phase, 25.4% ± 6.8%, ($p < 0.01$) in G2/M phase (Figure 4-7B). As PB mobilized HSPCs were all found in G1/G0 phase (Uchida et al., 1997), it is possible that ECM contact supports synchronized proliferation of AT-cells.
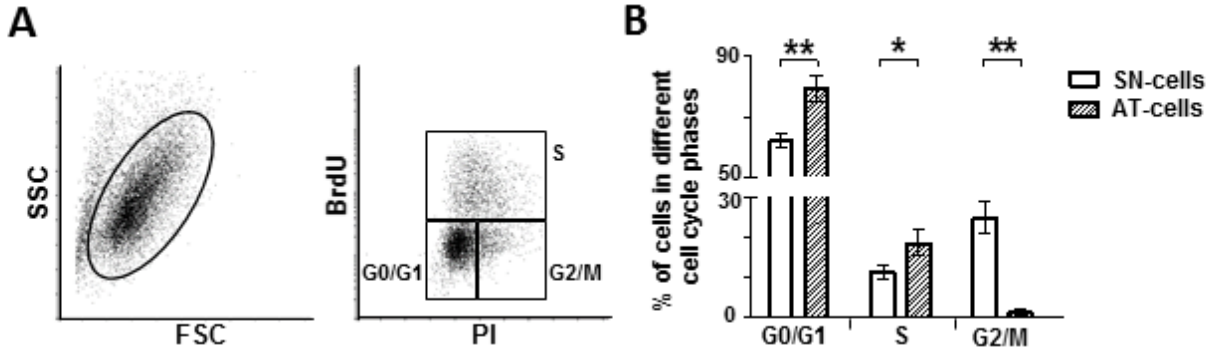
Figure 4-7: BrdU incorporation assay of 5 days ECM expanded HSPCs
(A) Representative flow cytometry dot-plots of 5 day expanded HSPCs on ECM scaffolds. Scatter light plot represent heterogeneous population of cells. BrdU- and PI-staining represent cells in G0/G1, S, and G2/M cell cycle phases, respectively. (B) Quantification of cell cycle phases in SN- and AT-cells after 5-day ECM culture; n = 3, two-tailed t-test. Error bars denote SD; *$p < 0.05$, **$p < 0.01$, ***$p < 0.001$.

4.2 HSPC morphological and mechanical adaptation to ECM

As contact with ECM scaffolds or MSC feeder-layers strongly influence HSPC shape (Freund et al., 2006b; Fonseca et al., 2010; Reichert et al., 2015) we investigated how SN- and AT-cells differ in terms of morphology. AT-cells displayed a heterogeneous phenotype with regard to cell shape (Figure 4-8A). Specifically, some cells showed an elongated morphology forming a magnupodium or lamellipodium at their front pole and an uropod at their rear pole, while others displayed a spherical shape with either a smooth surface or developed numerous protrusions on their surface (Figure 4-8B). Interestingly, some cells were flattened such that they appeared with one face in the ECM upon bright field microscopy; no uropods could be detected in these cells (Figure 4-8A). Contrarily, SN-cells remained spherical during the culture period, similar to those found in PCD cultures (Figure 4-8C).

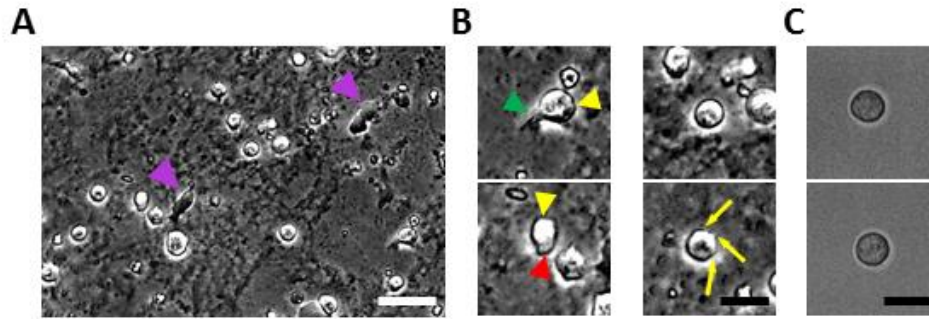**Figure 4-8: AT- and SN-cell morphology in ECM culture**
(A) Representative phase contrast image of AT-cells on ECM showing different morphologies (purple arrowheads indicating flat cells). Bar = 40 μm. (B) Representative phase contrast images of AT-cells on ECM showing elongated cells forming a magnupodium (green arrowhead) or lamellipodium (red arrowhead) at their front pole and an uropod (yellow arrowhead) at the rear pole. Spherical adhered cells displayed either a smooth surface or developed numerous protrusions (yellow arrow). Bar = 10 μm. (C) Representative phase contrast images of SN-cells (upper image) or PCD cultured cells (lower image) showing spherical shape. Bar = 10 μm.

4.2.1 Actin polymerization and polarization

Morphological adaptation towards a polarized phenotype, as detected in AT-cells, mostly depends on cytoskeletal rearrangement. As polarization indicates migration, we focused on the actin cytoskeleton as it contributes to cell motility and adhesion. To analyze actin cytoskeletal arrangement, we performed immunofluorescence staining of the filamentous actin (F-actin) and found stress fiber formation along AT-cells. This was true in ECM as well as MSC co-cultured AT-cells (Figure 4-9A-B). Interestingly, on ECM, these fibers were mostly polarized towards the front end of the cells, indicating migration in this direction (Figure 4-9A). In SN-cells, we detected F-actin only around the cell membrane as a cortical actin belt (Figure 4-9A).
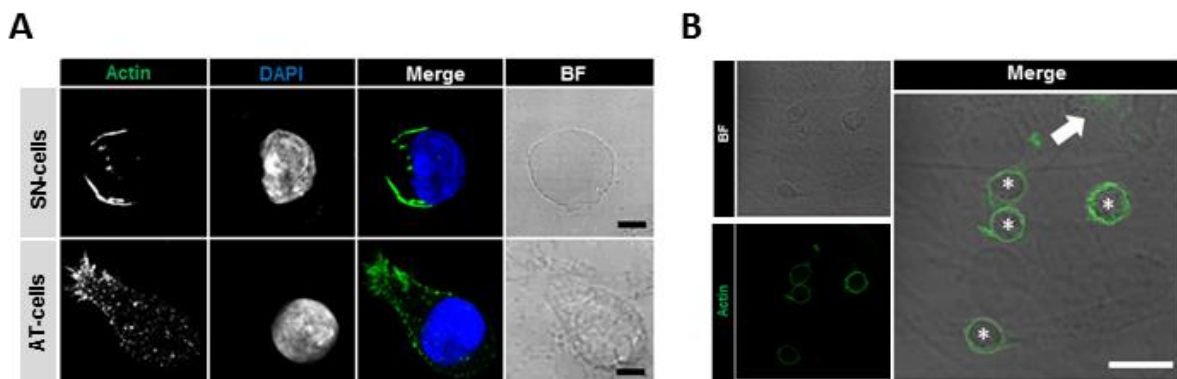
Figure 4-9: F-actin polarization on AT- and SN-cells
(A) Representative confocal microscopy images of the f-actin cytoskeleton using phalloidin-488 (green) and nuclear DAPI (blue) staining. AT-cells show a polarized phenotype and stress fiber formation towards a lamellipodium. SN-cells show cortical localization of f-actin fibers. Bars = 5 μm. (B) Representative confocal microscopy images of the f-actin cytoskeleton using phalloidin-488 (green) and nuclear DAPI

(blue) staining. Freshly isolated HSPCs (10^4 cells per cm²) were seeded to a confluent layer of SCP-1 cells. After 5 days in culture, AT-cells show stress fiber formation (asterisks). Arrow indicates actin staining of one SCP-1 cell. Bar = 10 μm.

4.2.2 Biomechanical phenotype

During stem cell mobilization, HSPCs undergo multiple steps of mechanical rearrangement. Further, as G-CSF stimulation leads to proliferation of BM HSPCs, the cytoskeleton needs to be remodeled in preparation for cell division. Furthermore, the intravasation of HSPCs into the blood stream requires cell softening so that these cells can pass through the basal membrane and the endothelial cell spaces. Once in the blood stream, HSPCs are exposed to blood pressure that also requires cytoskeletal adaptation. Thus, to analyze the mechanical phenotype of PB HSPCs and BM HSPCs, we used real-time deformability cytometry where shear stress was applied to cells in a microfluidic channel constriction and resulting deformation and cell size recorded in real-time. This technique is based on image processing and allows the optical validation of cell shape and morphology (Otto et al., 2015). In Figure 4-10A, representative images of freshly isolated CD34$^+$ HSPCs from PB are displayed while passing through the channel constriction. Freshly isolated cells, either from the PB or the BM, were found to be homogeneous in cell-size (range: 50-60 μm²) and shape. Importantly, they remained nearly un-deformed, reflecting a stiff phenotype. However, BM HSPCs showed heterogeneity in cell size and deformability (Figure 4-10B), which reflects the aforementioned mechanical remodeling processes.
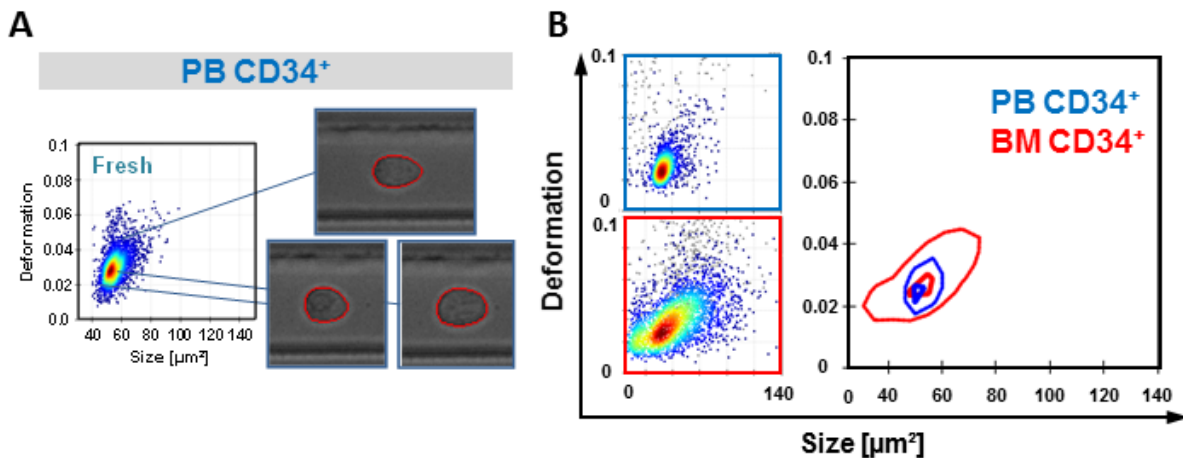
Figure 4-10: Freshly isolated PB and BM CD34$^+$ HSPCs measured in RT-DC
(A) Heat-plot of cell size and deformation of freshly isolated PB CD34$^+$ HSPCs in RT-DC. Cells appear as a homogenous population. Phase contrast images represent cells passing through the channel constriction. (B) Representative heat-plots of cell-size and cell-deformation in CD34$^+$ HSPCs from PB or BM. Contour plot shows direct comparison of both populations by highlighting 95% (outer line) and 50% (inner line) density.

Furthermore, we investigated how SN- and AT-cells differ from each other and PCD-cells in terms of physical parameters. Next, to validate our results, we also tested the same with SCP-1-co-cultured HSPCs. Interestingly, ECM-cultured and SCP-1 co-cultured AT-cells exhibited macroscopically denser intracellular packaging and accumulation of granular structures compared to SN-cells, which might be associated with the aforementioned F-actin structure (Figure 4-11A). Upon culture on ECM scaffolds, cells became larger with an average cell size of approximately 104.1 $\pm$ 7.3 µm². In contrast, SCP-1 co-cultured cells were smaller with an average cell-size of 80.8 $\pm$ 1.4 µm² (p < 0.001; Figure 4-11B and C). However, cell-size of ECM-cultured (p < 0.001) and SCP-1 co-cultured (p < 0.001) cells significantly differed from freshly isolated CD34$^+$ HSPCs (Figure 4-11B and C). For active proliferation in ECM culture and SCP-1 co-culture, cells had to initially grow before subsequent cell division. A comparison of deformability of ECM-cultured AT-cells and SN-cells showed that AT-cells had a significantly less deformable phenotype (d = 0.041 $\pm$ 0.006 vs. 0.056 $\pm$ 0.003; p < 0.01). This was also true for SCP-1 co-cultured HSPCs (AT-cells, d = 0.034 $\pm$ 0.005; SN-cells, d = 0.055 $\pm$ 0.007; p < 0.05) (Figure 4-11B and C). Interestingly, deformation in AT-cells did not significantly differ from freshly isolated CD34$^+$ cells (d = 0.034 $\pm$ 0.006; p > 0.05) while that of SN-cells was remarkably higher than freshly isolated cells (p < 0.001; Figure 4-11B and C). Nevertheless, SN-cells were comparable to classical suspension cultured PCD-cells with regard to cell size and deformation (Figure 4-11D).

Taken together, our data indicate that adhesion to ECM-proteins remodels HSPCs towards a more naïve morphological and mechanical phenotype, pointing perhaps to functional equality.
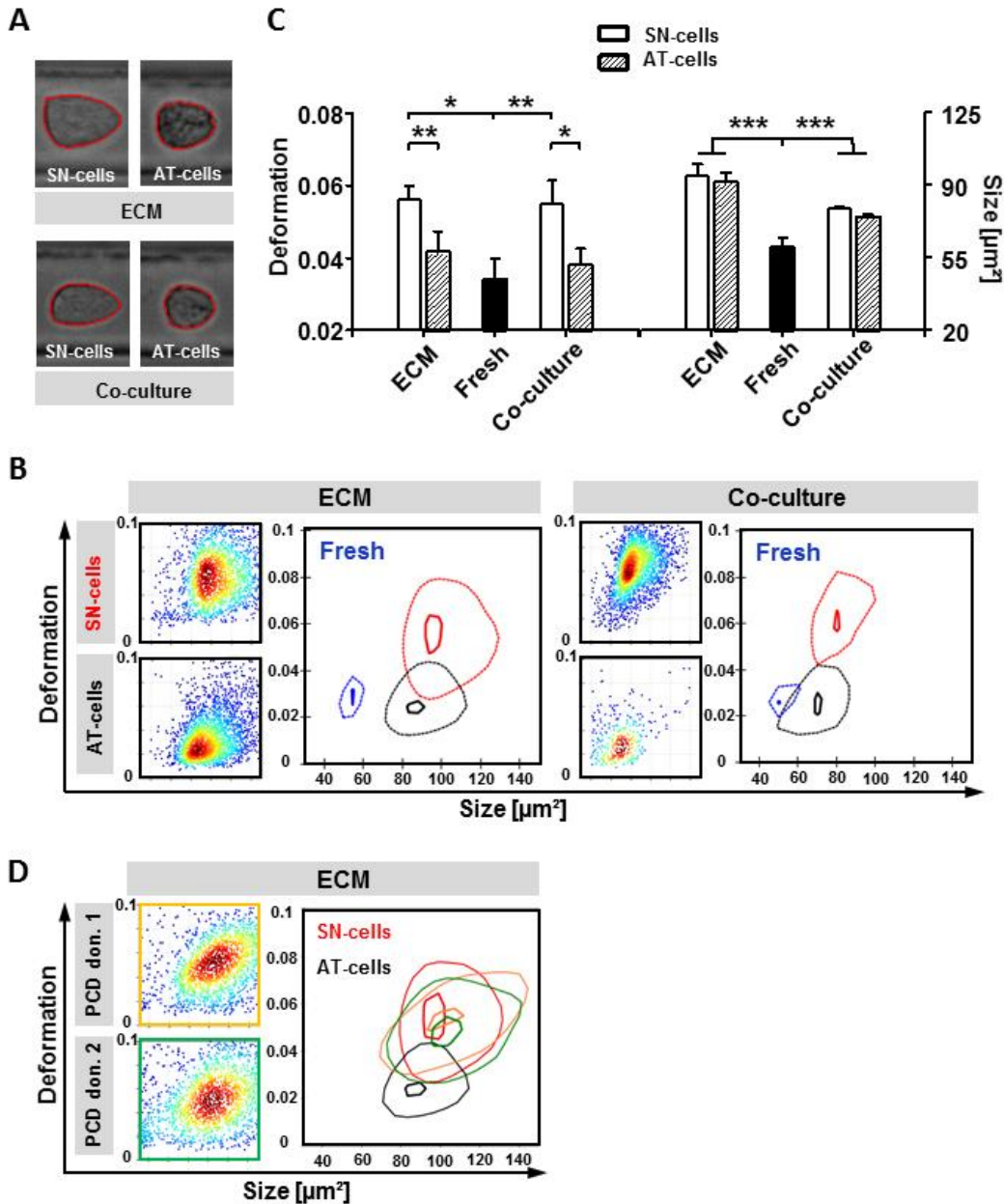
Figure 4-11: HSPC biophysical properties in ECM, SCP-1 co-culture, and PCD culture
HSPCs were cultured in ECM, as SCP-1 co-cultures, or PCD cultures. After 5 days, cell size and deformation were analyzed using RT-DC. (A) Representative images of ECM- and MSC co-cultured cells deformed through microfluidic channel constriction. (B) Representative heat-plots of cell-size and cell-deformation of ECM- and SCP-1 co-cultured AT- and SN-cells. Contour plots highlight 95%- (inner line) and 50%- (outer line) density of freshly isolated (Fresh), AT- and SN-cells. (C) Histogram bars representing RT-DC analyses of deformation and cell-size of freshly isolated cells (Fresh) and ECM- or SCP-1 co-cultured cells; n = 5, linear mixed model analysis, Error bars denote SD; *p < 0.05, **p < 0.01, ***p < 0.001. (D) Representative RT-DC scatter plot of PCD-cells (PCD donor 1 (orange) and PCD donor 2 (green)). Contour plot overlay highlights 95%- (inner line) and 50%- (outer line) density of PCD cells, SN-cells (red) and AT-cells (black).

4.3 **Bioactive SDF-1 is incorporated in ECM scaffolds**

The SDF1/CXCR4 axis is the most commonly investigated chemokine axis in hematology and is known to be essential for homing and retention of HSPCs in the BM (Peled et al., 1999; Petit et al., 2002). SDF-1 is largely secreted by BM MSCs and incorporated into the ECM. Additionally, an SDF-1 gradient is established upon its transport through endothelial cells into the blood stream and it serves to orient and direct HSPCs into the BM. CXCR4 serves is a major receptor expressed by HSPCs during this process. Therefore, we asked whether SDF-1 is involved in the adhesion of HSPCs to ECM scaffolds.

Prewitz et al. (2013, 2015) have previously demonstrated that amongst various morphogens, SDF-1 can be retrieved from decellularized ECMs derived from human BM-MSCs. To test whether SCP-1 cells secrete bioactive SDF-1 and if this is anchored to the ECM proteins, we performed immunostainings for SDF-1 and CXCR4 after 5 days of culture on ECM. Using confocal microscopy, we detected CXCR4 expression in AT- and SN-cells. Specifically, while SN-cells showed a predominantly membranous expression pattern, AT-cells exhibited both cytosolic and membranous CXCR4 expression. Further, we detected AT-cells with intracellular SDF-1 using identical experimental settings for SDF-1, which points towards SDF-1 internalization by active recognition and uptake from the ECM scaffold (Figure 4-12, upper panel). Contrarily, SN-cells did not stain for SDF-1. In Figure 4-12, the schematic illustrations portray a hypothesized situation for AT- and SN cells cultured on ECM. Nevertheless, as SN-cells express CXCR4, they must be able to recognize SDF1 within the supernatant. In order to assess SDF-1 processing within SN-cells, we added exogenous SDF-1 at varying concentrations to the medium. The lower panel of Figure 4-12 illustrates the expected uptake of SDF-1 from the supernatant. Upon exogenous addition of SDF-1, we found CXCR4 and SDF-1 to be localized in the cytosol of SN-cells, indicating internalization of ligand-receptor-complex by active recognition of recombinant SDF-1 by CXCR4 (Figure 4-12, lower panel).
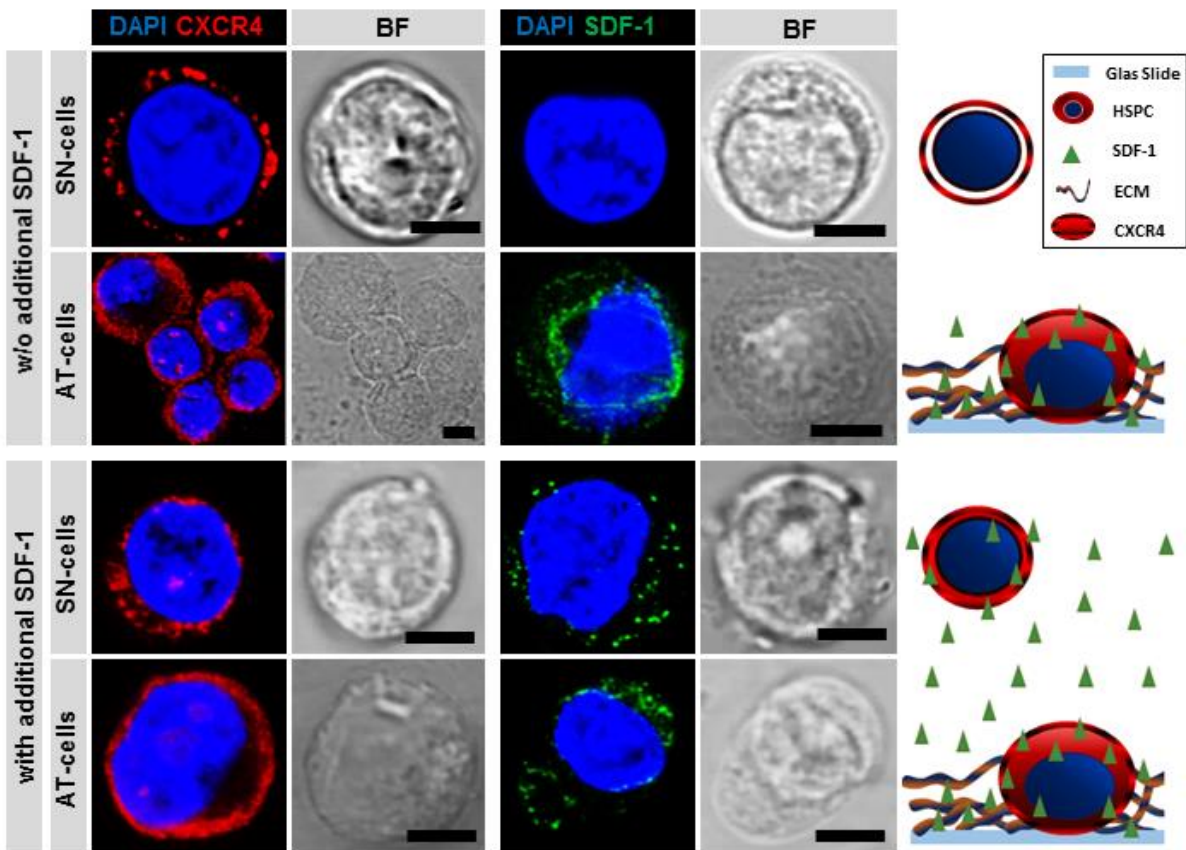
Figure 4-12: Bioactive SDF-1 is incorporated into ECM scaffolds and is recognized by AT-cells
Representative confocal microscopy images of CXCR4 (red) or SDF-1 (green) staining and nuclear DAPI (blue) staining. Cells were cultured for 5 days on ECM scaffolds and treated either without (w/o) or with exogenous SDF-1 in the culture medium. Schema illustrates experimental settings. Bars = 5 µm.

Interestingly, increased adhesion of HSPCs was not induced via additional SDF-1 treatment (Figure 4-25B). Our results show that SDF-1 is incorporated in the SCP-1 cell-derived ECM scaffolds and that it can be actively recognized and internalized by HSPCs.

4.3.1 CXCR4 polarization towards ECM

To further determine SDF-1 function in ECM scaffolds, we analyzed the distribution of CXCR4 on AT-cells using Z-stack imaging in confocal microscopy. CXCR4 is described to be polarized to the leading edge of CD34$^+$ HSPC when cultured in media containing serum on PCD (Giebel et al., 2004). These authors also reported polarized distribution of several CD markers like CD43, CD44, CD50, and CD54 in the uropod of plastic adherent HSPCs, similar to findings in peripheral leukocytes (Sánchez-Madrid and Del Pozo, 1999). Therefore, we asked whether recognition of SDF-1 within the ECM scaffolds by CXCR4 expressed on the cell surface is associated with cell polarization.

In our experiments, AT-cells were stained for CXCR4 and DNA was counterstained using DAPI. In z-stack microscopy, HSPCs were virtually divided into three planes, namely, top = I, middle = II, and bottom = III planes (Figure 4-13). Using ECM scaffolds during culture, we detected the greatest amount of CXCR4 at the bottom of cells when in contact with ECM, as the fluorescence signal steadily increased from planes I to III (Figure 4-13A). We also observed an intensive intracellular CXCR4 localization. However, we also detected a vertical but not a lateral polarization, as described by Giebel et al. (2004). To test whether this phenotype represents SDF-1 localization, we added an additional 10 ng/ml recombinant SDF-1 to the supernatant. Interestingly, this resulted in the suppression of CXCR4 polarization, which indicates that polarization of CXCR4 is triggered by the local concentration of SDF-1 within the ECM scaffolds. To further confirm this, we analyzed CXCR4 polarization after adhesion of HSPCs to SCP-1 cells. SCP-1 cells were found to both produce and secrete SDF-1 (Figure 4-30) into the supernatant at a concentration that was 50-fold lower than that of the exogenously added SDF-1. Remarkably, under these conditions, we also found identical polarization of CXCR4 towards the SCP-1 cell layer (Figure 4-13). This shows that SDF-1 released by the SCP-1 cells is incorporated into the ECM scaffold and stored during the 5 days of culture, and that AT-cells polarize CXCR4 towards the prevalent SDF-1 gradient.
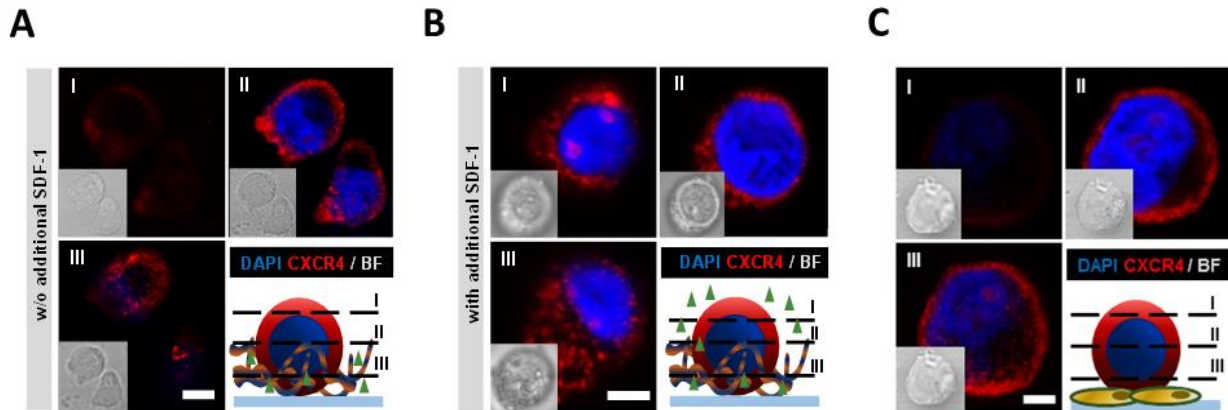
Figure 4-13: CXCR4 is polarized towards the ECM on AT-cells
Representative confocal microscopy z-stack images of α-CXCR4 (red) and nuclear DAPI (blue) staining. I = top, II = middle, and III = bottom planes of cells. (A) Cells were cultured in medium without (w/o) additional SDF-1. Scheme shows cutting planes and SDF-1 (green arrowheads) incorporation in the ECM. (B) Cells were cultured in medium supplemented with additional exogenous SDF-1 (10 ng/ml). Scheme shows cutting planes and SDF-1 (green arrowheads) suspended in supernatant and incorporated into ECM scaffolds. (C) Cells were co-cultured with a layer of SCP-1 cells in medium without (w/o) additional SDF-1. Schema shows cutting planes and SCP-1 cell layer. Bars = 5 µm.

4.4 **HSPC integrin expression and migration**

The interaction of cells with the surrounding ECM components is primarily mediated through integrin signaling through formation of focal contacts (Hynes, 2002). However, to recognize adhesive sides on ECM proteins, the alpha and beta subunits of the integrins need to hetero-dimerize and be activated. Several integrins are known to be activated via the CXCR4/SDF-1 signaling axis, e.g. LFA-1 (CD11a), VLA-4 (CD49d), and VLA-5 (heterodimer of CD49d and CD29). Such integrins then mediate endothelial adhesion and trans-endothelial migration (Peled et al., 2000) while others retain HSPCs in the BM (Wagers et al., 2002) and are associated with quiescent and long-term repopulating cells (Table 4-1).

Table 4-1: Integrins described as being HSPC-related.

Integrin	CD	Gene Name	Ligands (in heterodimeres)	HSPC Function
α4	CD49d	ITGA4	Fibronectin VCAM-1	BM homing, BM engraftment, maintenance, blocking leads to mobilization (Prosper et al., 1998; Wagers et al., 2002)
α5	CD49e	ITGA5	Fibronectin Osteopontin	BM lodging via osteopontin binding (Barry et al., 2000; Nilsson et al., 2005)
α6	CD49f	ITGA6	Laminin	Blocking leads to reduced BM homing (Qian et al., 2006)
αIIb	CD41	ITGAIIb	Fibronectin	Early hematopoiesis, BM lodging, regulation of progenitor number (Berridge et al., 1985; Corbel and Salauen, 2002; Emambokus and Frampton, 2003)
αV	CD51	ITGAV	Fibronectin Vitronectin Tenascin	HSPC maintenance (Umemoto et al., 2012)
β1	CD29	ITGB1	Collagen Laminin Fibronectin Osteopontin	BM lodging, differentiation (Williams et al., 1991; Teixido et al., 1992)
β3	CD61	ITGB3	Fibronectin	Maintenance (Umemoto et al., 2006, 2008, 2012)

4.4.1 **Integrin surface expression on HSPC subsets**

We asked whether integrin expression differed among freshly isolated PB HSPCs, AT- and SN-cells derived from ECM or SCP-1 co-cultures. We used flow cytometry to identify surface expression of HSPC-related integrins, namely CD29, CD41, CD49d, CD49e, CD49f, CD51, and

CD61 (Table 4-1). Expression screening was done using the panel represented in Figure 4-16, upper row. No significant differences could be identified between these groups of cells in terms of CD29, CD49d, CD49e, and CD49f surface expression. However, remarkably, 22.9% $\pm$ 6.3% of AT-cells expressed ITGαIIb, whereas only 6.7% $\pm$ 5.2% of SN-cells and 3.4% $\pm$ 2.8% of freshly isolated cells were ITGαIIb-positive. Moreover, 22.7% $\pm$ 6.6% of AT-cells showed ITGαV expression and 41.5% $\pm$ 14.7% were positive for ITGβ3. In contrast, 6.7% $\pm$ 3.4% and 16.1% $\pm$ 9.4% of SN-cells were positive for ITGαV and ITGβ3, respectively. Accordingly, a minority of freshly isolated cells, 5.8% $\pm$ 4.2% and 3.9% $\pm$ 2.6%, were positive for ITGαV and ITGβ3, respectively (Figure 4-14A). Slightly different results were obtained in SCP-1co-cultured HSPCs as greater numbers of ITGαV-positive cells were encountered; however, the effect was the same as on ECM-cells (Figure 4-14B).
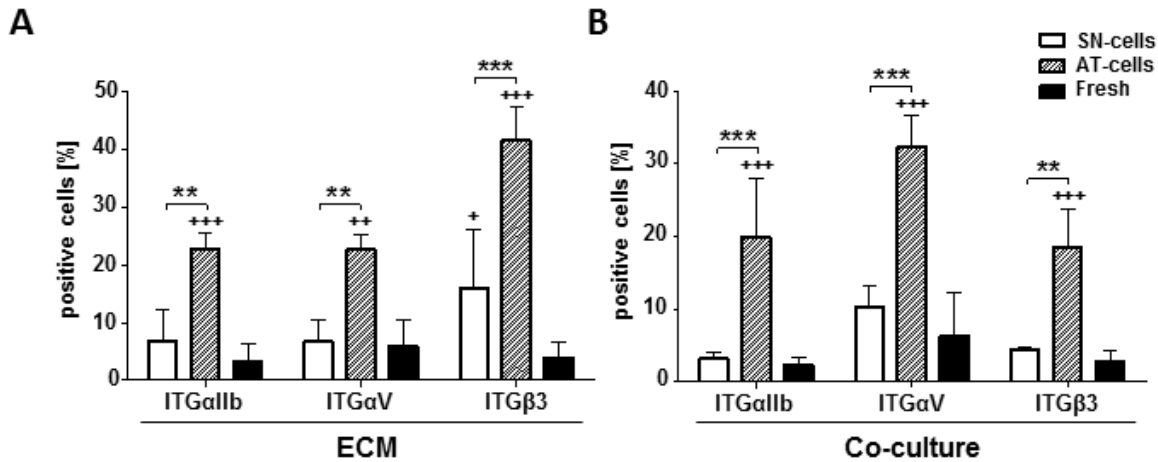
Figure 4-14: Integrin surface marker expression on cultured and freshly isolated CD34^{+} cells
Flow cytometry analyses of integrin surface marker expression of (A) freshly isolated CD34^{+} cells and 5-days ECM cultured SN- or AT-cells, or (B) freshly isolated CD34^{+} cells or 5-day SCP-1 co-cultured SN- and AT-cells; n = 4, two-way ANOVA with Bonferroni post-hoc test; + = significant when compared to freshly isolated cells. Error bars denote SEM; *p < 0.05, **p < 0.01, ***p < 0.001.

4.4.2 Focal contact formation

Interestingly, these integrins are known to form RGD-motive recognition dimers (Hynes, 2002). Therefore, we checked if a heterodimere of ITGαV and ITGβ3 is expressed on AT-cells, as it regulates HSPC engraftment and maintenance by forming focal contacts and promoting outside-in (ECM to cell) signaling (Umemoto et al., 2012). Using confocal microscopy, we identified ITGαVβ3 as being membrane-associated in AT-cells (Figure 4-15A), but ITGαVβ3 could not be detected in SN-cells. To prove active focal adhesion formation, we performed further immunostainings for vinculin and phosphorylated paxillin. Vinculin was found to be highly expressed in AT-cells and localized to the cytosol as well as membrane-associated (Figure

4-15A). As AT- and SN-cells expanded rapidly in ECM culture and vinculin is indispensable for HSPC repopulation (Ohmori et al., 2010), we also found vinculin expression in SN-cells (Figure 4-15B). Paxillin, in contrast, was found to be phosphorylated at Tyr118 when membrane associated (Figure 4-15A and C) and was localized near the ITGαVβ3 heteromer exclusively in AT-cells (Figure 4-15C, arrowheads). This indicates formation of activated signaling focal contacts through integrin mediated adhesion to the ECM proteins.
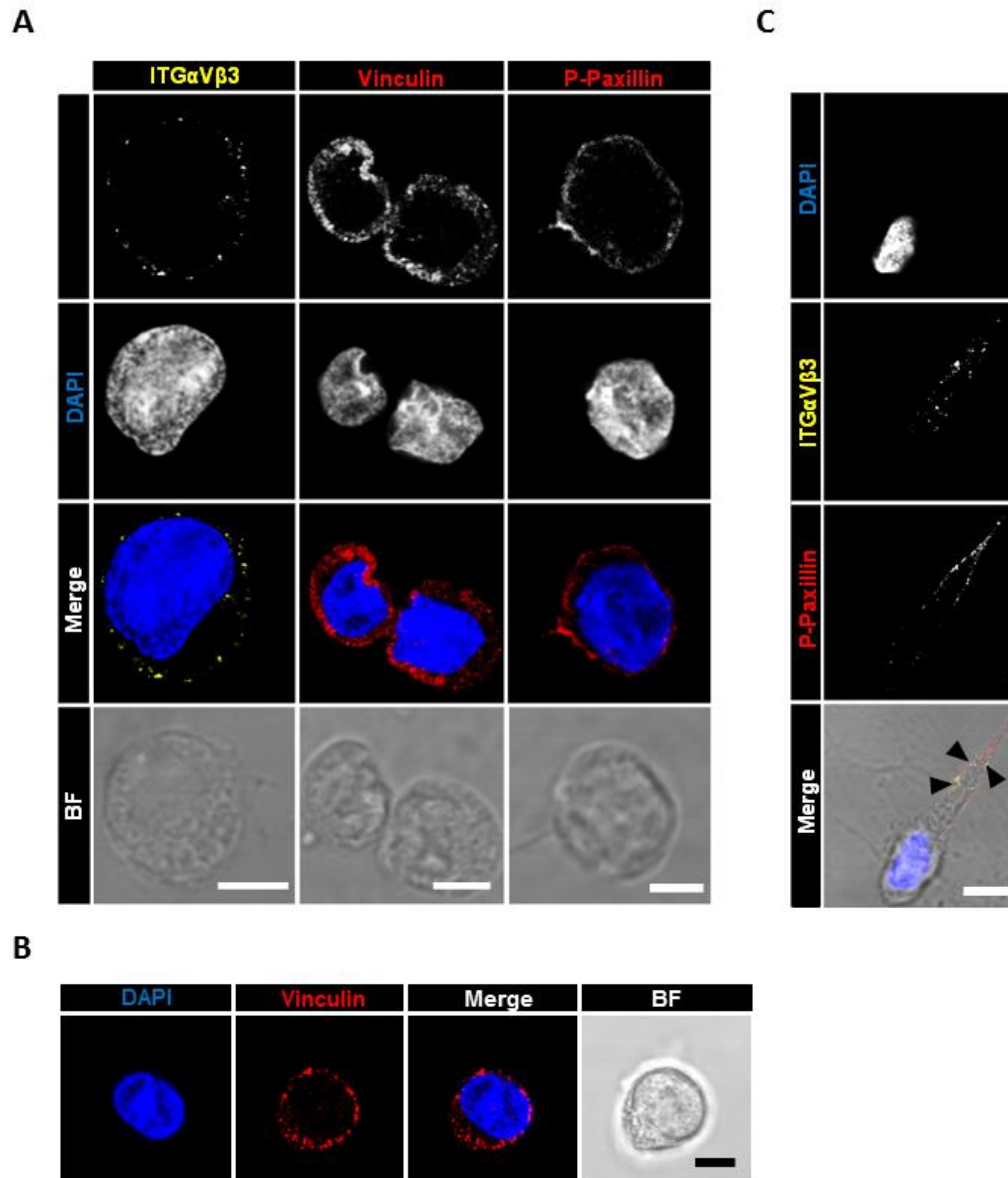
Figure 4-15: Integrins recognize RGD-motives and promote active focal contact formation
(A) Representative confocal microscopy images of α-ITGαVβ3 (left panel, yellow), α-vinculin (mid panel, red), α-p-paxillin (right panel, red), nuclear DAPI (blue) staining, merged and corresponding bright field images of 5 days cultured AT-cells, showing cortical localization of ITGαVβ3. Activated paxillin and vinculin are distributed throughout the cytosol. Bars = 5 µm. (B) Representative confocal microscopy images of α-vinculin (red), nuclear DAPI (blue) staining, merged and corresponding bright field image of 5-

day cultured SN-cells showing cytosolic distribution of vinculin. Bar = 5µm (C) Representative confocal microscopy images of α-ITGαVβ3 (yellow), α-p-paxillin (right panel, red), nuclear DAPI (blue) staining, and merged and corresponding bright field images of 5-day cultured AT-cells. Arrowheads represent proximitry of ITGαVβ3 and p-paxillin in a cellular protrusion. Bar = 5 µm

4.4.3 Integrin activation via ECM adhesion

Our findings prompted us to investigate whether ECM scaffolds induce ITGβ3 expression within CD34$^+$ cells or only enrich ITGβ3$^+$ cells. FACS was used to sort CD34$^+$ITGβ3$^-$ or CD34$^+$ITGβ3$^+$ cells from mobilized PB (Figure 4-16).
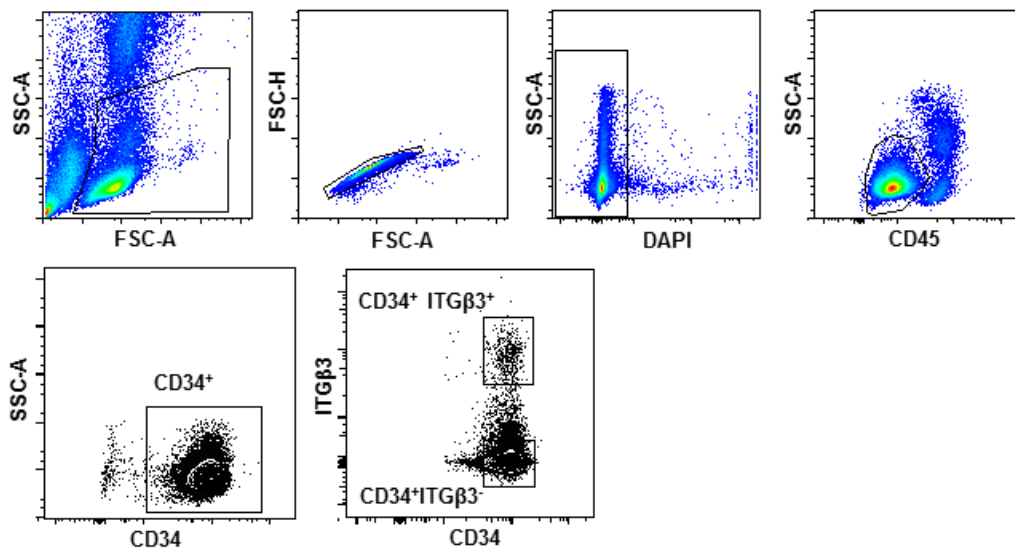
Figure 4-16: FACS sorting panel for CD34$^+$ ITGβ positive and negative cells
Representative gating strategy for fluorescence activated cell sorting experiments for cells derived from PB. Lymphocytes and single cells were enriched using light-scatter. Dead cell exclusion was done by DAPI staining. Progenitor enrichment was done using the SSC-A^{low}/CD45^{dim} and CD34$^+$ gate. Sorting gates were CD34$^+$ITGβ3$^-$ and CD34$^+$ ITGβ3$^+$.

After culture for 5 days on ECM scaffolds, previously sorted CD34$^+$ITGβ3$^+$ or CD34$^+$ITGβ3$^-$ HSPCs were analyzed for CD34 and ITGβ3 expression (Figure 4-17A). As expected, the sorted CD34$^+$ITGβ3$^+$ cells continued to exhibit strong ITGβ3 surface expression (55.4% ± 1.8%) when attached to ECM. However, only 31.2% ± 1.7% of previously sorted CD34$^+$ITGβ3$^+$ SN-cells were positive for ITGβ3. Interestingly, previously sorted CD34$^+$ITGβ3$^-$ AT- and SN-cells showed upregulated ITGβ3 surface expression at 29.9% ± 11.9% and 19.8% ± 7.35%, respectively (Figure 4-17B and C). Along this line, CD34$^+$ITGβ3$^+$ sorted cells showed an increased adhesion capacity, compared to CD34$^+$ITGβ3$^-$ cells. Up to 90 % of CD34$^+$ITGβ3$^+$ cells were found to adhere to ECM proteins after 12 h, as identified by phase contrast microscopy. However, sorted CD34$^+$ITGβ3$^+$ showed reduced proliferation and expansion from starting cell numbers (1.2 ± 0.1 fold) when cultured for 5 days on ECM-scaffolds (Figure 4-17D). On the other hand,

CD34$^+$ITGβ3$^-$ cells proliferated significantly more, with 2.9 ± 0.04 fold expansion (p < 0.0001), which is comparable to unsorted CD34$^+$ cells cultured on ECM scaffolds for 5 days (Figure 4-5C). Thus, our data suggest that ITGβ3 expression is induced by ECM preparations and that this is essential for effective adhesion. Interestingly, freshly isolated BM CD34$^+$ HSPCs displayed the same ratio of ITGβ3$^+$ cells as AT-cells (Figure 4-17E), which further strengthens our hypothesis that the ECM remodels the BM stroma with ITGβ3 as a major player in BM-ECM interactions.
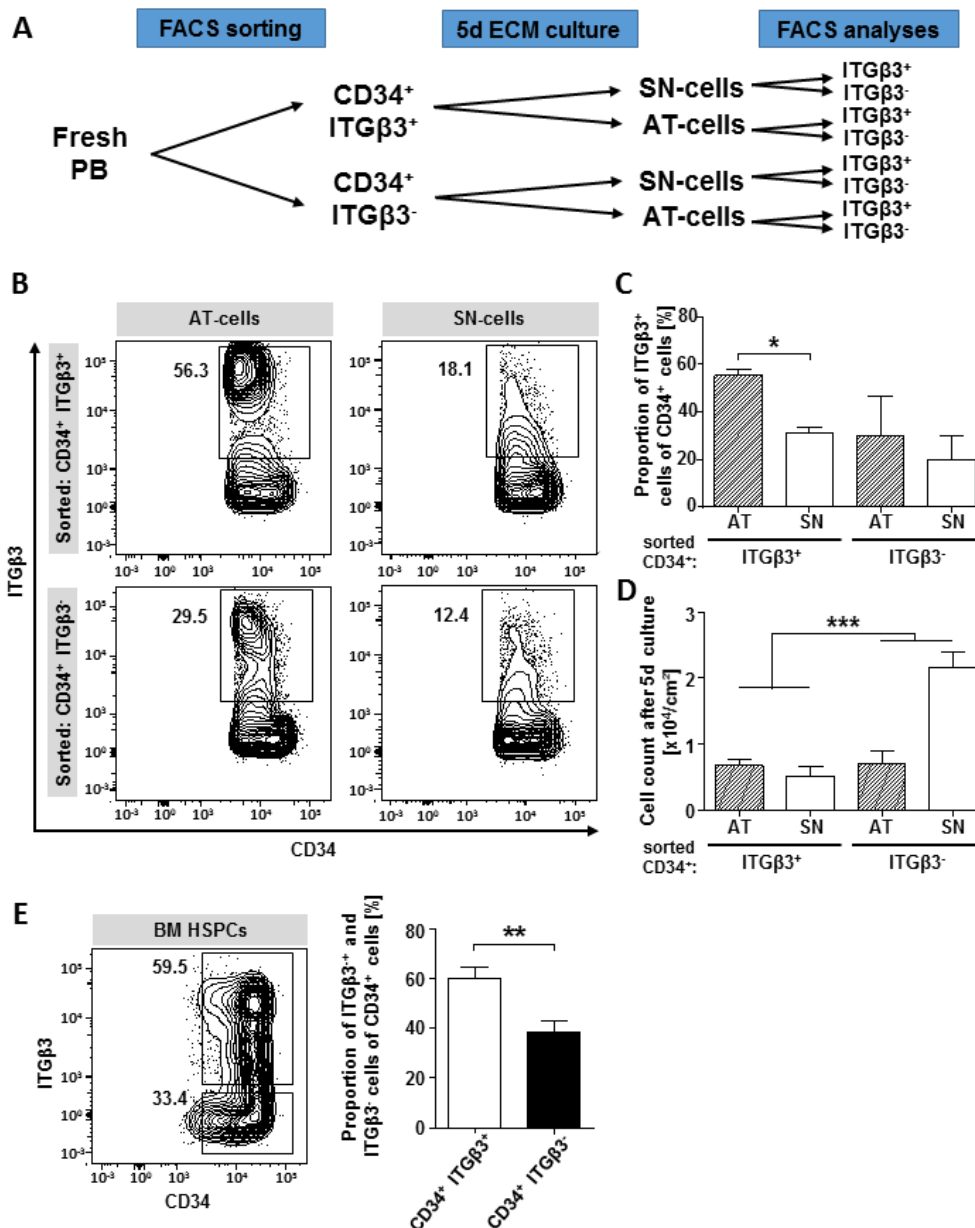

Figure 4-17: ECM scaffolds induce ITGβ3 surface expression
(A) Schema represents work flow. CD34$^+$ITGβ3$^+$ and CD34$^+$ITGβ3$^-$ HSPCs were FACS sorted from PB and cultured for 5 days separately on ECM scaffolds. SN- and AT-cells were found in both cultures and were analyzed for ITGβ3 expression by FACS. (B) Representative FACS plots for primarily sorted

CD34$^+$ITGβ3$^+$ and CD34$^+$ITGβ3$^-$ cells after 5 days of culture on ECM scaffolds. AT- and SN-cells are shown according to CD34 and ITGβ3 surface expression. (C) Flow cytometry analyses of ITGβ3 surface expression in primarily sorted CD34$^+$ITGβ3$^+$ and CD34$^+$ ITGβ3$^-$ cells after 5 days of culture on ECM scaffolds; n = 2, error bars denote SD; *p < 0.05, **p < 0.01, ***p < 0.001. (D) Fold-expansion in cell numbers from starting cell numbers of AT- and SN-cells of primarily sorted CD34$^+$ ITGβ3$^+$ and CD34$^+$ ITGβ3$^-$ cells after 5 days of culture on ECM scaffolds; n = 2, two-tailed t-test; error bars denote SD; *p < 0.05, **p < 0.01, ***p < 0.001. (E) BM aspirates of healthy donors were stained for CD34 and ITGβ3. Histogram bars represent proportion of ITGβ3$^+$ cells in the total CD34$^+$ HSPC population; n = 3, two-tailed t-test; error bars denote SD; *p < 0.05, **p < 0.01, ***p < 0.001.

4.4.4 Clonogenicity of ECM cultured HSPCs

Beside maintenance in early hematopoiesis, ITGβ3 expression is a known differentiation marker and predominantly expressed during megakaryopoiesis (Naik and Parise, 1997; Ficko, 2008) and erythropoiesis (Ferkowicz et al., 2003). Additionally, ITGβ3 was found to be essential for acute myeloid leukemia progression in mice (Miller et al., 2013). Therefore, ITGβ3 surface expression on the CD34$^+$ HSPCs could also imply HSPC commitment. To verify clonogenicity of ECM cultured CD34$^+$ HSPCs, we performed CFU-GEMM assays and compared them to those from freshly isolated CD34$^+$ cells obtained from PB and BM using FACS (sorting panel presented in Figure 4-16). Interestingly, overall, BM CD34$^+$ cells were found to form significantly fewer colonies compared to CD34$^+$ PB-, CD34$^+$ AT-, and CD34$^+$ SN-cells (p < 0.01; Figure 4-18A). However, CD34$^+$AT-cells showed significantly more erythroid colonies with a mean of 125 ± 19 colonies, including BFU-E and CFU-E, compared to 58 ± 12 colonies formed by CD34$^+$ BM cells and 70 ± 14 colonies formed by CD34$^+$ PB cells. No differences were found when compared to CD34$^+$ SN-cells (114 ± 15 colonies; Figure 4-18B). These findings indicate a differentiation bias of CD34$^+$ITGβ3$^+$ cells towards the megakaryocyte-erythroid lineage.
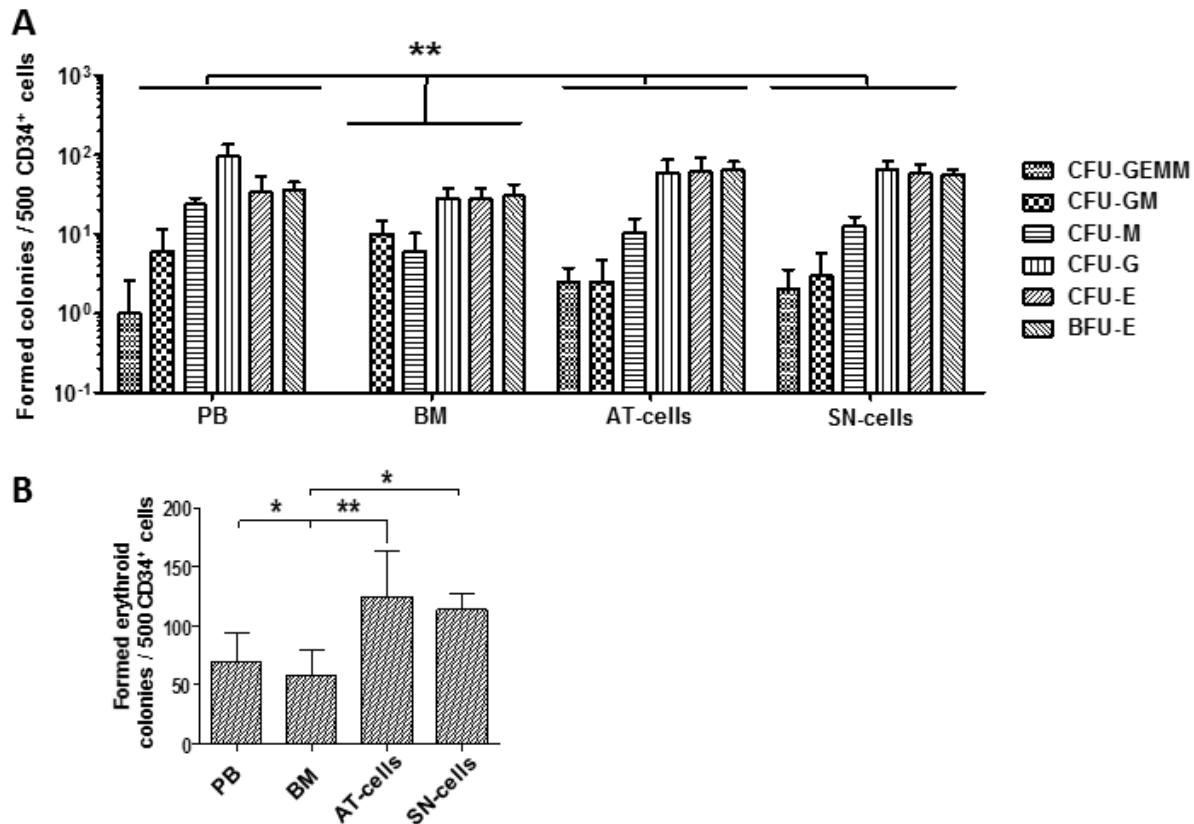
Figure 4-18: CFU-GEMM colony formation of CD34⁺ cells

(A) Histogram bars represent formation of colonies per 500 cells of CD34$^+$ PB, BM, AT, and SN-cells. (B) Histogram bars represent formation of erythroid colonies (including CFU-E and BFU-E); n = 3 (including 3 technical replicates), two-tailed t-test; error bars denote SD; *p < 0.05, **p < 0.01, ***p < 0.001.

To clarify whether this lineage differentiation bias is due to ITGβ3 surface expression, we performed clonogenicity assays with FACS-sorted CD34$^+$ITGβ3$^+$ (Figure 4-19A) and CD34$^+$ITGβ3$^-$ (Figure 4-19B) cells derived from freshly isolated PB and 5 days ECM scaffold cultured AT- and SN-cells (Figure 4-19A and B). We identified that CD34$^+$ITGβ3$^+$ cells from ECM culture form predominantly erythroid colonies. Surprisingly, AT-cells formed remarkably fewer erythroid colonies compared to SN-cells and freshly isolated PB-cells (Figure 4-19A). CD34$^+$ITGβ3$^-$ cells showed equal colony formation from all cell sources including all colony types (Figure 4-19B).
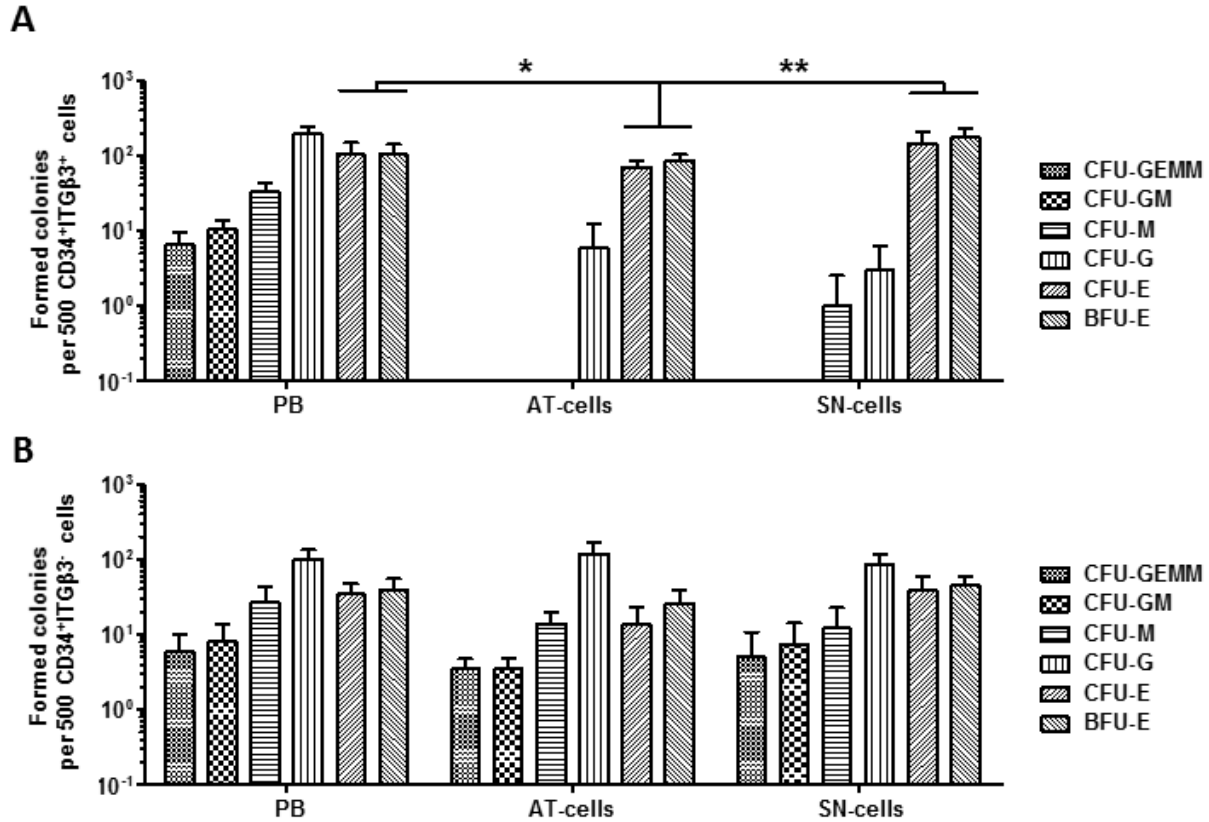
Figure 4-19: CFU-GEMM colony formation of PB-derived and ECM-cultured CD34$^+$ITGβ3$^+$ and CD34$^+$ITGβ3$^-$ cells

Histogram bars summarize colony formation after seeding 500 CD34$^+$ITGβ3$^+$ cells (A) and CD34$^+$ITGβ3$^-$ (B) onto semi-solid CFU-GEMM medium; n = 3 (including 3 technical replicates), two-tailed t-test; error bars denote SD; *p < 0.05, **p < 0.01, ***p < 0.001.

Moreover, PB-derived CD34$^+$ITGβ3$^+$ cells formed significantly more colonies than PB-derived CD34$^+$ITGβ3$^-$ cells, indicating that these cells have an increased self-renewal and differentiation potential. However, overall colony formation by CD34$^+$ITGβ3$^+$ cells cultured on ECM did not reflect this potential (Figure 4-20A and B). Interestingly, CD34$^+$ITGβ3$^+$ SN-cells were found to be remarkably enriched in erythroid progenitors, as they formed the greatest number of colonies (Figure 4-20C). Additionally, between CD34$^+$ITGβ3$^+$ and CD34$^+$ITGβ3$^-$ sorted cells, erythroid-colony formation was significantly increased in all cell sources(Figure 4-20C).
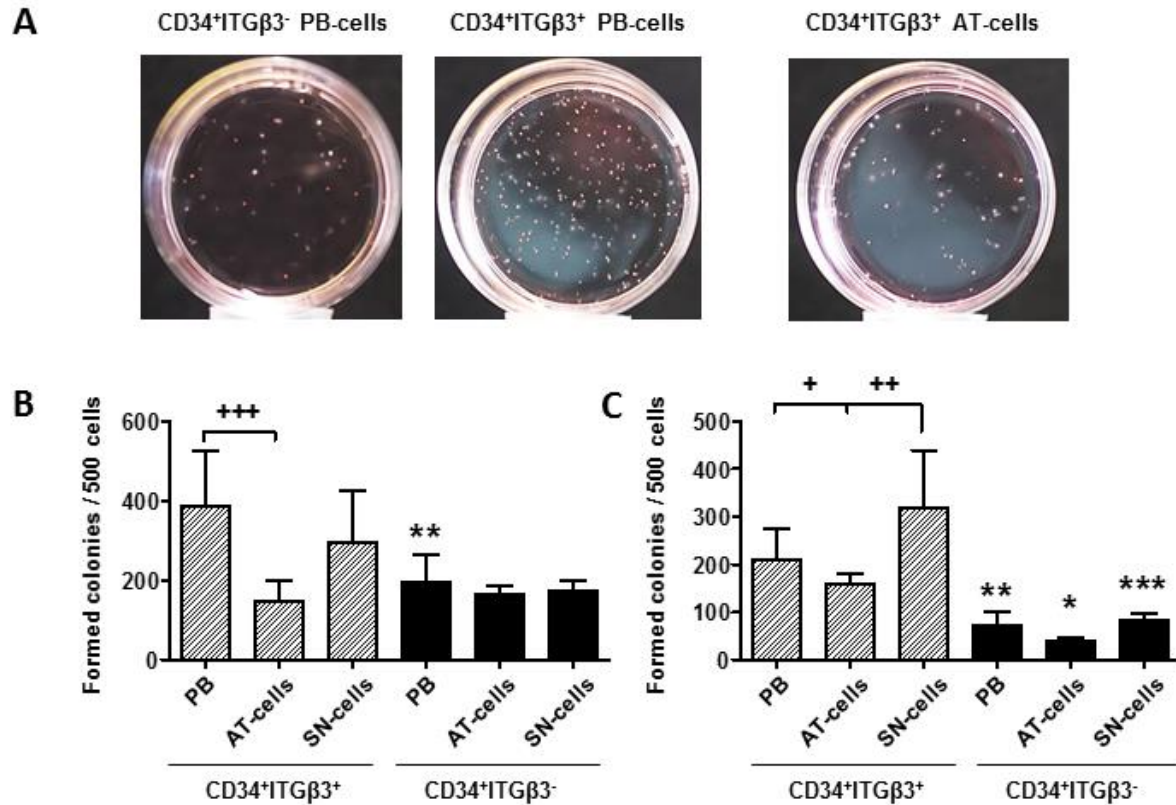
Figure 4-20: CFU-GEMM colony formation by CD34$^+$ ITGβ3$^+$/ ITGβ3$^-$ cells
(A) Representative images of colonies formed by the CFU-GEMM assay (166 cells seeded in semi-solid CFU-GEMM medium). (B) Histogram bars represent formation of all colonies (including CFU-E and BFU-E, CFU-G, CFU-M, CFU-GM and CFU-GEMM) when 500 CD34$^+$ITGβ3$^+$ cells or CD34$^+$ITGβ3$^-$ cells were seeded onto semi-solid CFU-GEMM medium. (C) Histogram bars represent formation of erythroid colonies (including CFU-E and BFU-E) when 500 CD34$^+$ITGβ3$^+$ or CD34$^+$ITGβ3$^-$ cells were seeded onto semi-solid CFU-GEMM medium; n = 3 (including 3 technical replicates), two-tailed t-test; Error bars denote SD; * = significance when compared to corresponding CD34$^+$ITGβ3$^+$ cells, *p < 0.05, **p < 0.01, ***p < 0.001.

These findings indicate that CD34$^+$ITGβ3$^+$ cells cultured on ECM have a differentiation bias towards erythroid progenitors. The same cells, when freshly sorted from PB, also showed increased erythroid differentiation; however, colonies for other differentiation lineages were also increased compared to CD34$^+$ITGβ3$^-$ cells. Thus, it is possible that ITGβ3$^+$ surface expression is a marker for megakaryocyte-erythroid lineage commitment.

4.4.5 HSPC migration when attached to ECM scaffolds

As described above, ECM contact leads to morphological adaptations of AT-cells towards a polarized phenotype. Sánchez-Madrid and Del Pozo (1999) described this morphological adaptation as a migrative phenotype of PB leukocytes. In line with this description, HSPCs in contact with stromal cell feeder layers were described as a heterogeneous population of migrating and non-migrating cells (Reichert et al., 2015). Additionally, we have identified HSPCs to be highly interactive with each other, forming and abandoning cell-cell contacts (Figure

4-21A). Similar to previous findings, we also show that AT-cells need to be elongated or polarized to migrate, but are spherical when resting or not migrating on ECM (Figure 4-21A and B, Figure 4-8). However, AT-cells appear to be highly dynamic and vary between these two states. Using time-lapse microscopy, we found that dynamic plasticity of individual AT-cells such that they changed between the migratory and non-migratory phenotypes during an observation period of just 25 minutes. These dynamics were characterized as migration (migratory phenotype), resting (non-migratory phenotype) and continued migration (Figure 4-21B).
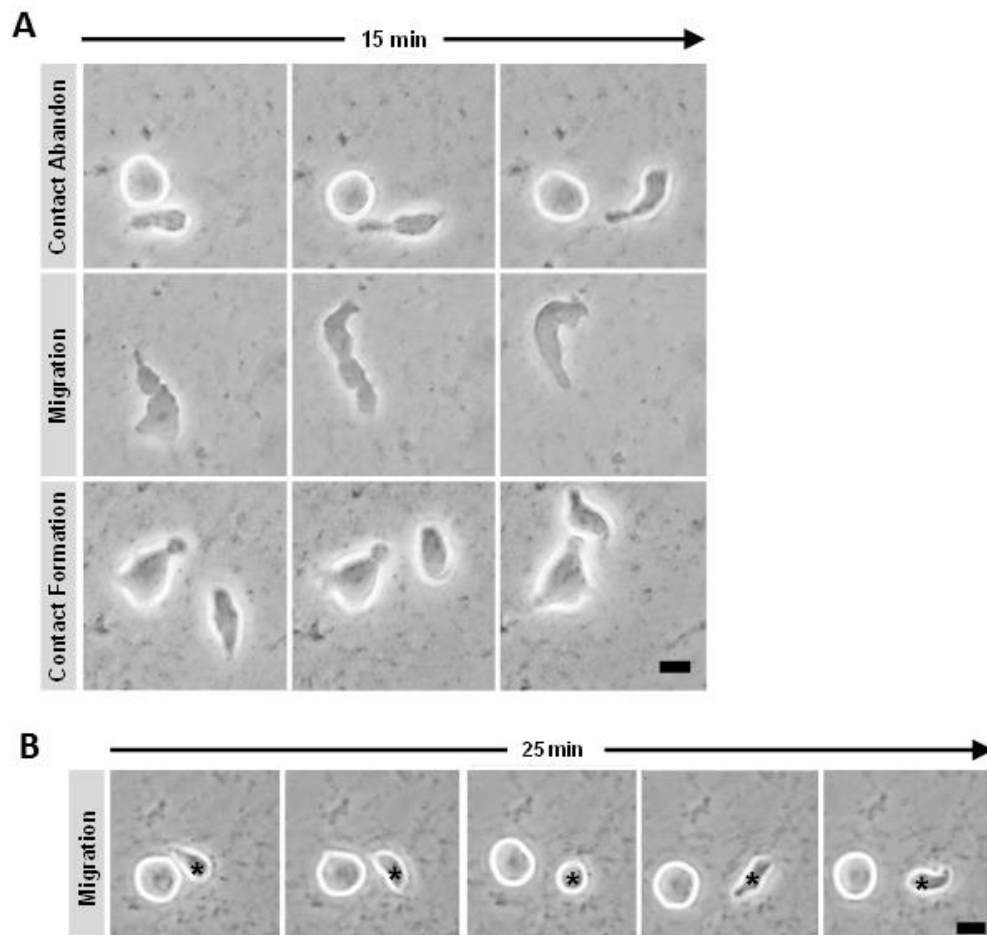
Figure 4-21: AT-cell migration
(A) Individual frames from 15 min time-lapse microscopy studies of migrating and interacting cells on ECM. Bar = 5 μm. (B) Individual frames from 25 minutes of time-lapse microscopy of a non-migrating cell and a migrating cell forming a non-migrating phenotype (asterisk). Bar = 5 μm.

4.4.5.1 Reduced migratory behavior via ITGαVβ3 inhibition

As we found that the ITGαVβ3 heterodimer was most predominantly expressed and used for forming focal contacts on AT-cells, we asked whether this integrin heterodimer promotes migration. Using a blocking antibody for ITGαVβ3 with an appropriate IgG control, we monitored

both migrating and non-migrating cells. Under both conditions the ratio of cells displaying the migratory or the non-migratory phenotype remained unchanged (Figure 4-22A and B).
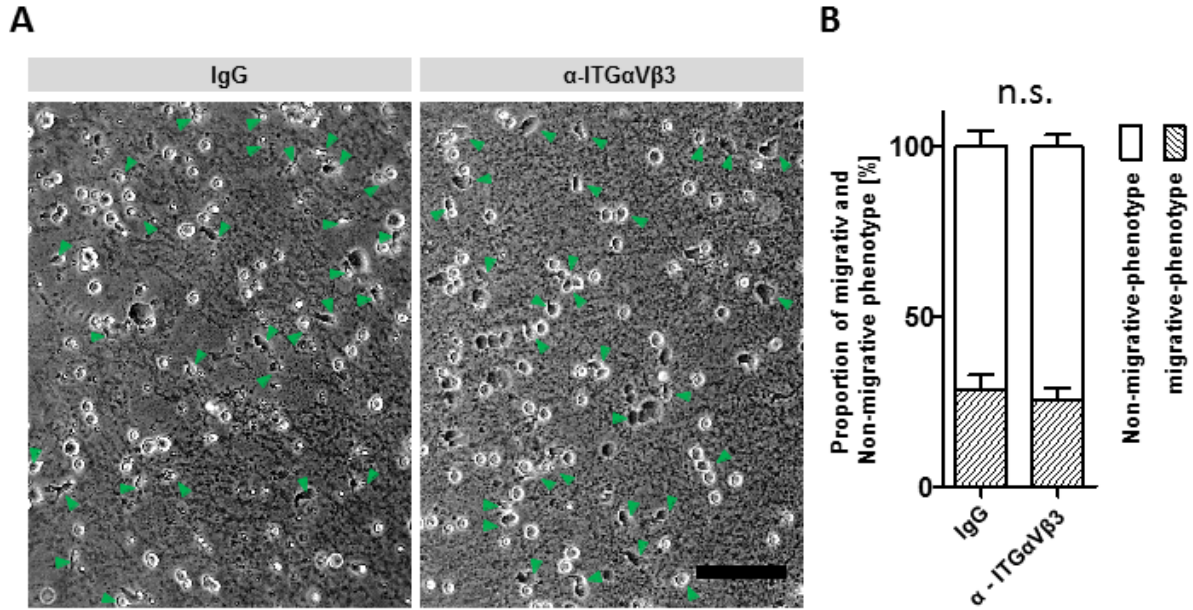
Figure 4-22: Ratio of migrating and non-migrating AT-cells
Freshly isolated HSPCs (10^4 cells per cm²) were seeded onto an ECM scaffold. After 5 days in culture, cells were incubated for one hour with a blocking antibody directed against ITGαVβ3 or a corresponding control IgG and imaged using bright field microscopy. Elongated migratory cell shapes (green arrowheads) or spherical non-migratory cell shapes (unmarked) were detected and counted. (A) Representative images of AT-cells treated with IgG or α-ITGαVβ3 are shown. Bar = 50 µm (B) Proportion of migratory and non-migratory phenotypes of AT-cells treated with IgG or α-ITGαVβ3; n = 5, two-tailed t-test, n.s. = non-significant.

In a second experiment, we monitored AT-cells for 45 minutes after incubating them with IgG or α-ITGαVβ3 for 1 h. The average migration distance and velocity were calculated from all cells in a section. AT-cells incubated with the blocking antibody migrated significantly slowly with an average velocity of 0.026 µm/s ± 0.02 µm/s compared to control cells with an average velocity of 0.038 µm/s ± 0.03 µm/s (p < 0.01;Figure 4-23B). The accumulated distance also decreased when AT-cells were incubated with ITGαVβ3 blocking antibody (60.6 µm ± 49.3 µm) compared to IgG treated cells (86.8 µm ± 65.5 µm; p < 0.01; Figure 4-23A and B).

Figure 4-23: ITGαVβ3 promotes migration of AT-cells in 5 days ECM culture
Cells were cultured for 5 days on ECM and incubated for one hour with α-ITGαVβ3 or IgG. (A) Trajectory plots depict migration of 25 HSPCs for 45 minutes. (B) Box-and-whisker plots present accumulated distance and velocity of 77 HSPC migration tracks monitored for 45 minutes when pre-incubated for 1 h with α-ITGαVβ3 or IgG. Lines show the $25^{th} – 75^{th}$ percentiles; horizontal line represents median and plus indicates mean value. Cells treated with blocking AB showed less migration distance and velocity; two-tailed t-test.; *p < 0.05, **p < 0.01, ***p < 0.001.

To identify whether the ITGαVβ3 heterodimer also mediates migration of freshly isolated CD34^{+} cells, we performed the same experiment after a shorter period of ECM culture (24 hours). Interestingly, an effective inhibition of cell migration using the blocking antibody could still be achieved (Figure 4-24). Nevertheless, short term ECM cultured HSPC migrated less compared to 5 days cultured cells, which points towards ITGαVβ3 as being an essential contact and migration mediating integrin in HSPCs.
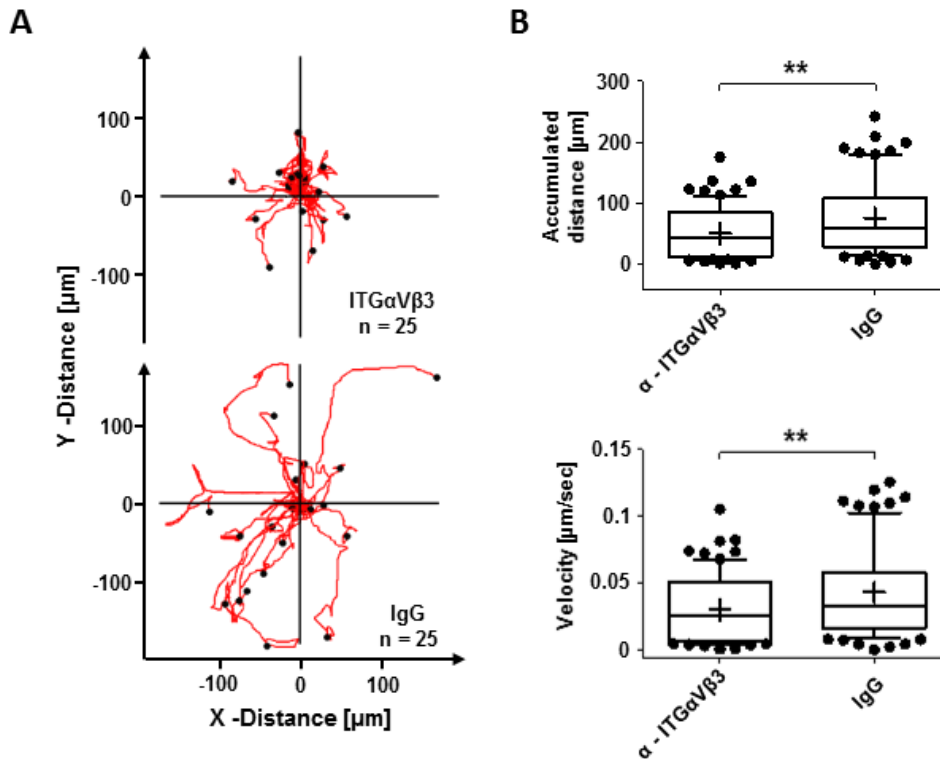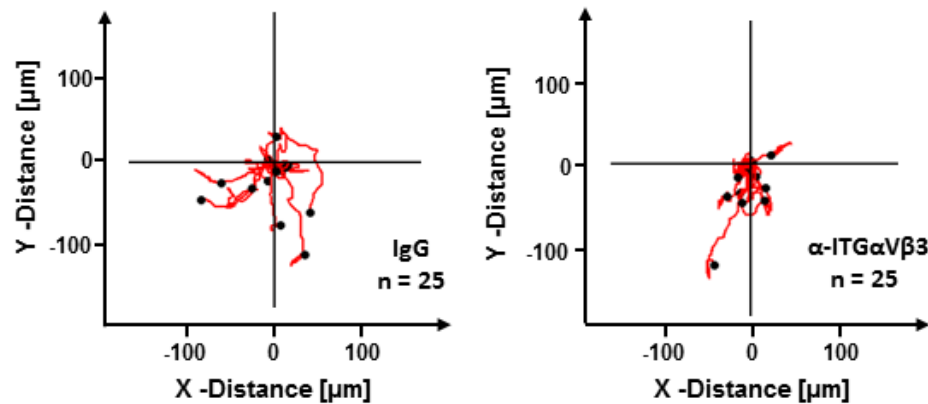
Figure 4-24: Integrin αVβ3 promotes migration of AT-cells on 24 h ECM culture
Cells were cultured for 24 hours on ECM and incubated for one hour with α-ITGαVβ3 or IgG. Trajectory plots depict migration of 25 HSPCs for 45 minutes. Migration was reduced when cells were incubated for one hour with α-ITGαVβ3, compared to IgG.

4.4.5.2 SDF-1 induces migration but not adhesion

To identify whether SDF-1 leads to migration of AT-cells as described by Lee-Thedieck et al. (2012), we performed trans-well migration assays with freshly isolated CD34^{+} cells, AT-cells, and SN-cells. We found that $20.1 \pm 3.4\%$ of freshly isolated cells actively migrated towards SDF-1 containing medium while the spontaneous migration rate was $3.6\% \pm 1.8\%$ (Figure 4-25A); these observations are in line with previously reported findings (Jacobi et al., 2010). AT- and SN-cells, however, significantly differed in their potential to migrate towards SDF-1: while $16.9 \pm 1.1\%$ of AT-cells were found to migrate within 3 h, only $9.9 \pm 1.1\%$ of SN-cells reached the bottom chamber ($p < 0.01$). Spontaneous migration was measured to be less than 3.5% in AT- and SN-cells (Figure 4-25A). Therefore, we conclude that CXCR4 polarization and receptor/ligand internalization, as presented above, are associated with AT-cell migration along the ECM scaffold. Further, the cells maintain and translate this capacity to follow a chemokine gradient as effective as freshly isolated cells. However, SDF-1 is not directly associated with adhesion to our ECM scaffolds, as seen upon the exogenous addition of recombinant SDF-1 (Figure 4-25B).
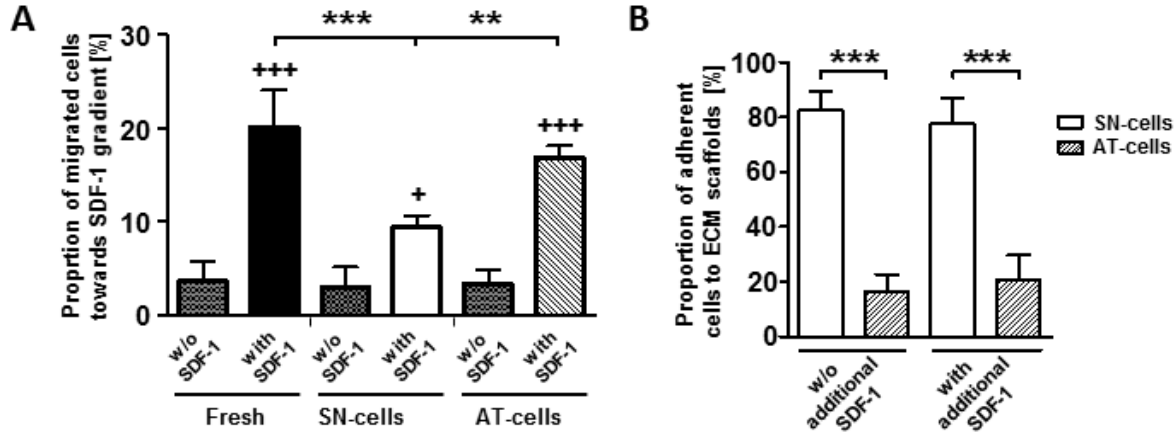
Figure 4-25: Trans-well migration along a SDF-1 gradient and cell-matrix adhesion
(A) Proportion of migrated freshly isolated-, SN- or AT-cells in a trans-well migration assay towards SDF-1 containing medium (with SDF-1) or towards SDF-1 free medium (spontaneous migration, w/o SDF-1); n = 4, two-tailed t-test; + = significant when compared to corresponding w/o SDF-1. (B) Proportion of cells adhering to ECMs in medium alone or medium containing additional exogenous SDF-1; n = 3, two-tailed t-test. Error bars denote SD; *p < 0.05, **p < 0.01, ***p < 0.001.

4.5 **Targeted modulation of ECM scaffolds**

Multiple proteins incorporated into the BM-ECM regulate HSPC maintenance, proliferation, and maturation (Hergeth et al., 2008). However, the degree of influence of distinct ECM components still remain unclear. Cell-free ECMs derived from SCP-1 cells provide a suitable model system to identify the effect of individual protein components on HSPCs. To investigate cell-specific crosstalk, we aimed to reduce specific proteins of the ECM scaffolds derived from SCP-1 cells using RNA interference. The modified scaffolds were then used to culture HSPCs to identify cellular alterations in terms of proliferation and adhesion capacity.

The extracellular matrix protein fibulin-1 is known to reduce adhesive structures for HSPCs on FN and to regulate HSPC proliferation and differentiation in the BM (Hergeth et al., 2008). Therefore, fibulin-1 expression was initially analyzed. Using immunofluorescence staining, we identified fibulin-1 in the perinuclear region of SCP-1 cells (Figure 4-26A, white arrowhead) and in the intercellular space (Figure 4-26A, yellow arrowheads), indicating its incorporation into the ECM. Interestingly, osteogenic differentiation of SCP-1 cells increased the expression of fibulin-1 (Figure 4-26A upper panel compared to Figure 4-26B), as reported by Zachos et al. (2006) for primary MSCs.
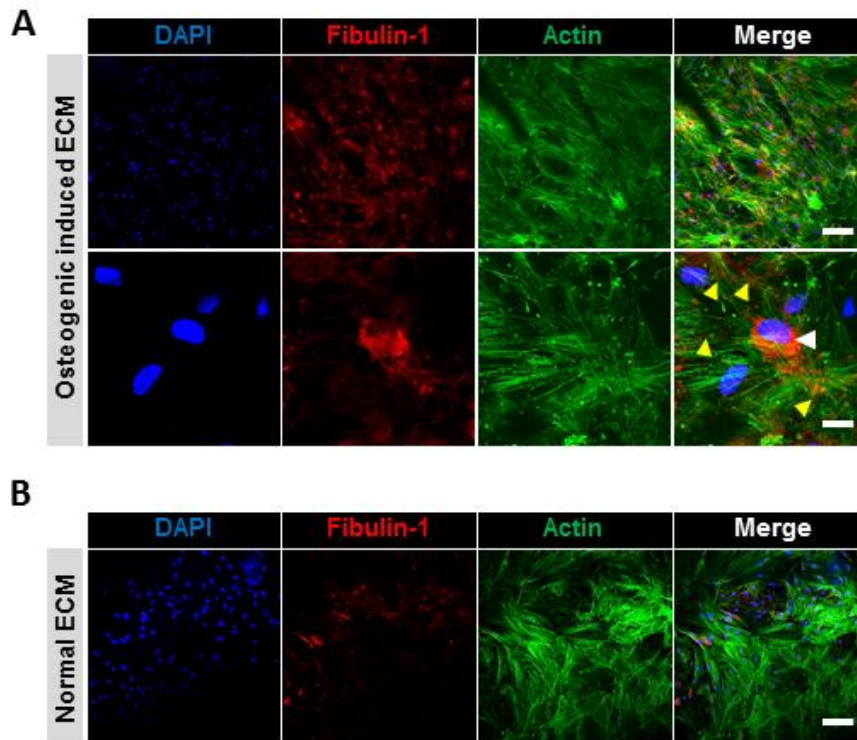
Figure 4-26: Fibulin-1 in SCP-1 cells cultured in osteogenic differentiation medium and DMEM alone
SCP-1 cells were grown to confluency and incubated for 7 days in osteogenic differentiation medium or DMEM alone. Immunostaining for α-fibulin-1 (red), f-actin (green), and nuclear counterstaining using DAPI (blue) were performed. (A) Representative confocal microscopy images of osteogenic medium SCP-1 cells showed intra- (perinuclear; white arrowhead) and extracellular (yellow arrowheads) fibulin-1 expression. Bar = 100 μm (upper panel), 25 μm (lower panel). (B) Representative confocal microscopy images of DMEM treated SCP-1 cells showed intra- and extracellular fibulin-1 expression but to a lower extend compared to osteogenic medium cells. Bar = 100 μm.

Due to the formation of anti-adhesive sites in the ECM, we hypothesized that lower expression of fibulin-1 in the decellularised ECM-scaffolds might enhance AT-cell number and HSPC lodging.

4.5.1 Fibulin-1 knock down in SCP-1 cells

To prove our hypothesis, SCP-1 cells were transduced with lentivirus-based shRNA vectors targeting fibulin-1 with puromycin resistance as the selection marker. An empty vector (Ke) was used as control, while shRNA vectors 10 (K10) and 11 (K11), which differ in target sequence identity, were transduced into SCP-1 cells to generate Fibulin-1 knock down clones. As osteogenic differentiation increases the expression of fibulin-1 in SCP-1 cells, we used osteogenic differentiation medium or DMEM alone to verify knockdown efficiency. As shown by semi-quantitative PCR, fibulin-1 expression was not affected when cells were transduced with control vector (Ke) or when cells were untransduced (WT). Contrarily, SCP-1 cells transduced

with shRNA vectors K10 and K11 showed reduced expression of all fibulin-1 splice variants. In WT and Ke transduced SCP-1 cells, fibulin-1A expression was the lowest, fibulin-1B and -1D showed similar expression levels, while fibulin-1C expression was the highest. Identical expression ratios were observed in osteogenically-induced SCP-1 cells, but as indicated above WT and Ke transduced SCP-1 cells showed stronger band intensity and therefore increased expression (Figure 4-27A and B). Thisclearly demonstrats that shRNA vectors used (K10 and K11) were capable of downregulating fibulin-1 mRNA expression across all splice variants in both undifferentiated and osteogenically- differentiated SCP-1 cells.
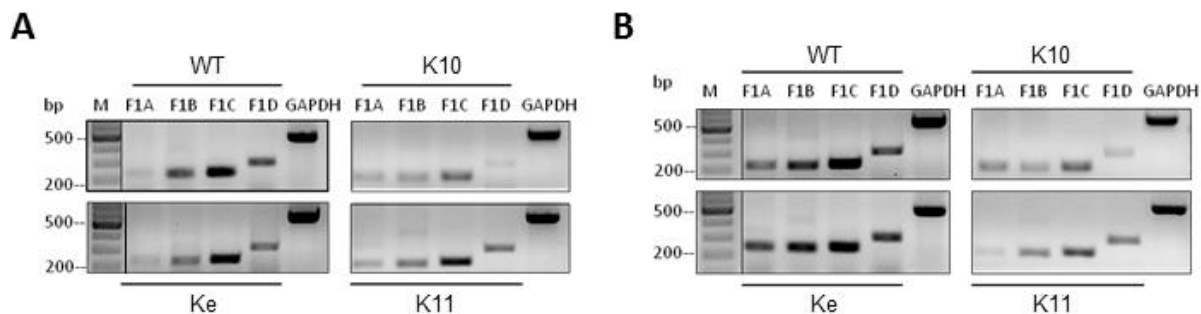
Figure 4-27: Fibulin-1 mRNA knockdown in SCP-1 cells
Representative agarose gel electrophoresis of PCR products derived from amplification of all fibulin-1 splice variants, fibulin-1A (F1A), -B (F1B), -C (F1C), and -D (F1D) using (A) DMEM alone and (B) osteogenic differentiation medium. GAPDH was used as reference gene for normalization of DNA content. M: GeneRuler.

As RNA expression does not necessarily correlate with protein expression, the effective knockdown of fibulin-1 protein in ECM scaffolds derived from SCP-1 cells was quantified by Western Blot analyses. Before decellularization, SCP-1 cells were cultured in osteogenic differentiation medium to ensure high fibulin-1 expression in SCP-1 cells. Human primary MSCs served as control cells. Decellularized ECM proteins were separated on SDS-PAGE and immunoblotted with anti-fibulin-1 antibody that can recognize all splice variants. To date, no housekeeping protein has been reported for Western Blot analyses of proteins from ECM scaffolds as ECM composition is continuously altered by deposition time, differentiation stimuli, and media additives (Prewitz et al., 2013, 2015). Thus, as a suitable method to verfiy equal protein loading, we performed coomassie blue staining after SDS PAGE in parallel with the gels for the immunoblot. Figure 4-28A shows a representative coomassie gel staining that shows similar band intensities in each lane implying comparable protein loading for each sample.

Fibulin-1 (approx. 90 kDa; Argraves et al., 1990) was incorporated into ECMs as detected by Western Blot analyses of proteins from ECM scaffolds derived from osteogenically differentiated SCP-1 cells and primary human MSCs (Figure 4-28B). Fibulin-1 band intensity was weaker in

K10 and K11 transduced samples, whereas bands from WT, SCP-1 Ke, and MSC samples were similar in intensity (Figure 4-28B). Semi-quantitative image analysis with ImageJ confirmed significant reduction in band intensities for K10 and K11 compared to WT, implying successful knockdown of fibulin-1 expression. Further, the shRNA vector K10 was more efficient than K11 in downregulating fibulin-1 in osteogenic induced SCP-1 cells (Figure 4-28C).
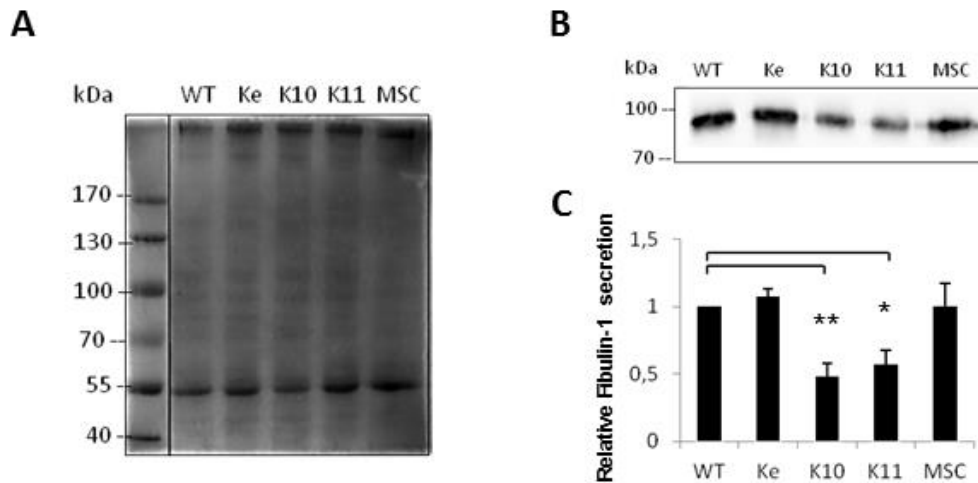
Figure 4-28: Fibulin-1 protein secretion in knockdown SCP-1 cells
(A) Representative Coomassie-stained SDS PAGE gel pcture to illiustrate equal protein loading of decellularized ECM. WT: wildtype, MSC: mesenchymal stromal cells, first lane: Prestain Protein Ladder PageRuler. (B) Western blot analyses of decellularized ECM proteins derived from SCP-1 WT, -Ke, -K10, -K11 and primary human MSCs using anti fibulin-1 antibody. All cells were cultured in osteogenic differentiation medium. Decellularized ECM proteins show reduced band intensities for K10 and K11, while band intensities were similar among wildtype (WT), Ke, and MSC samples. (C) Semi-quantitative analysis of Western Blot band intensities using ImageJ; n = 3, two-tailed t-test. Error bars denote SD; *p < 0.05, **p < 0.01, ***p < 0.001.

To verify that the knock down (KD) procedure did not lead to alterations in cell character, including due to selection medium treatment, we analyzed surface marker expression and SDF-1 secretion in SCP-1 cells under WT and KD conditions.

The maintenance of surface markers suggests unaltered cell identity (Lv et al., 2014), and we initially analyzed SCP-1 cells for the presence of characteristic cell surface molecules: CD29, CD44, CD73, CD90, CD105, CD146, and CD166, as well as CD45 in intervals of one month for a period of three months by flow cytometry. The applied gating strategy is shown in Figure 4-29A. Figure 4-29B provides a representative analysis of SCP-1 cells stably transduced with the shRNA vectors Ke, K10 and K11, and WT cells after a three-month selection culture. CD29, CD44, CD73, CD90, CD105, CD146, and CD166 were found to be consistently expressed on upto 100% of all SCP-1 cells, while CD45 was stably absent. Slightly different expression levels among the three cell clones, namely, SCP-1 Ke, SCP-1 K10, and SCP-1 K11 were observed but

was comparable to expression levels found on SCP-1 WT cells (Figure 4-29B). These findings indicate that shRNA transduction did not alter expression of characteristic cell surface molecules and therefore, did not alter cellular characteristics.
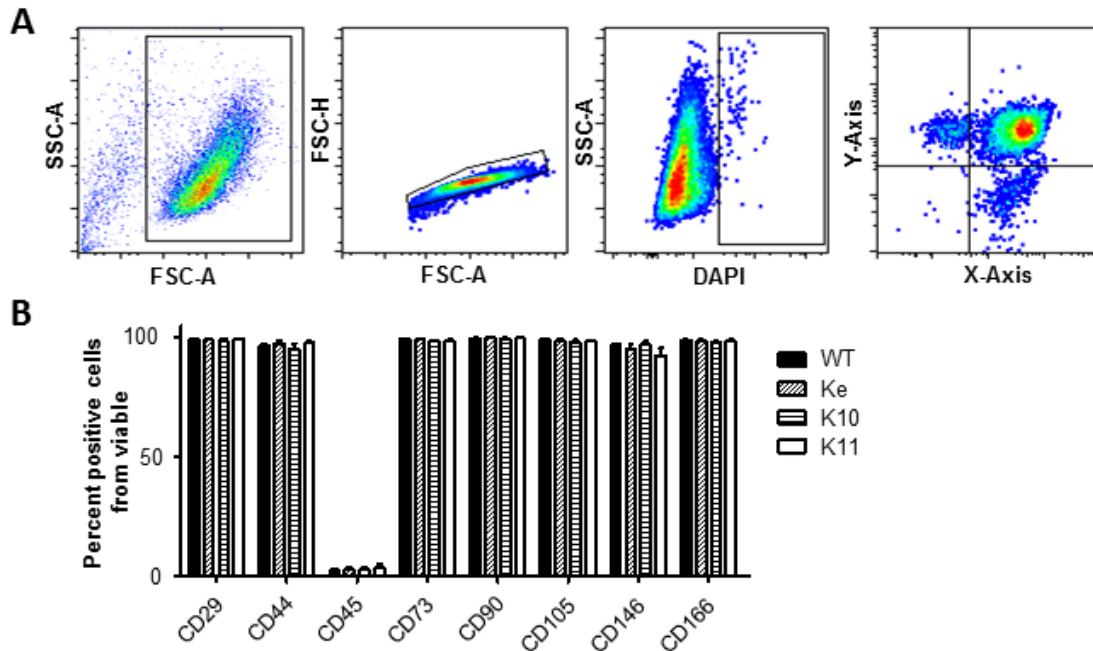
Figure 4-29: Maintenance of surface molecule expression in Fibulin-1 knockdown SCP-1 cells
(A) Representative flow cytometry gating strategy to analyze SCP-1 cell surface marker expression. Scatter light indicates cell population and single cells. Dead cells were excluded by DAPI staining. Right-most plot indicates fluorescence intensity of applied fluorophores. (B) Flow cytometry analysis of indicated mesenchymal cell surface markers in SCP-1 cells cultured in selection medium at the three-month time point. No differences in surface marker expression after fibulin-1 knockdown were observed. Data are mean ± SEM; n=3.

To further characterize SCP-1 cell function, we quantified the amount of secreted SDF-1. As mentioned above, SDF-1 was found to be incorporated into the ECM scaffolds derived from WT SCP-1 cells and could be recognized by HSPCs. To exclude alterations in HSPC-ECM interaction mediated by changes in SDF-1 levels rather than fibulin-1 knock down, the amount of SDF-1 secreted into the culture medium supernatant was measured using ELISA. SCP-1 WT, Ke, K10, K11, and human primary MSCs (as controls) were seeded in 6-well plates and the supernatant collected at indicated time points for up to 7 days. Both normal and osteogenic differentiation media were tested (Figure 4-30). SDF-1 accumulated in the supernatant over time and the highest concentrations were measured on day 7. Overall, supernatants from Ke, K10, K11, and WT cultures showed similar levels, regardless of fibulin-1 knockdown, implying that the shRNA vector transduction did not interfere with SDF-1 secretion. Furthermore, MSCs showed lower SDF-1 concentrations than the SCP-1 cells, and osteogenic differentiation reduced SDF-1 secretion. Highest SDF-1 concentration in the supernatant of osteogenic differentiated SCP-1

cells was found after 7 days of culture and represented only one-tenth of the SDF-1 secreted into the supernatant of undifferentiated SCP-1 cells. In general, SDF-1 levels were found to be highly variable between cells and over time. However, there were no differences in SDF-1 secretion by SCP-1 Ke, K10, and K11 cells compared to SCP-1 WT and MSCs neither in osteogenic nor in DMEM (Figure 4-30). These results indicate that viral transduction of SCP-1 cells did not affect SDF-1 secretion compared to WT cells or primary MSCs
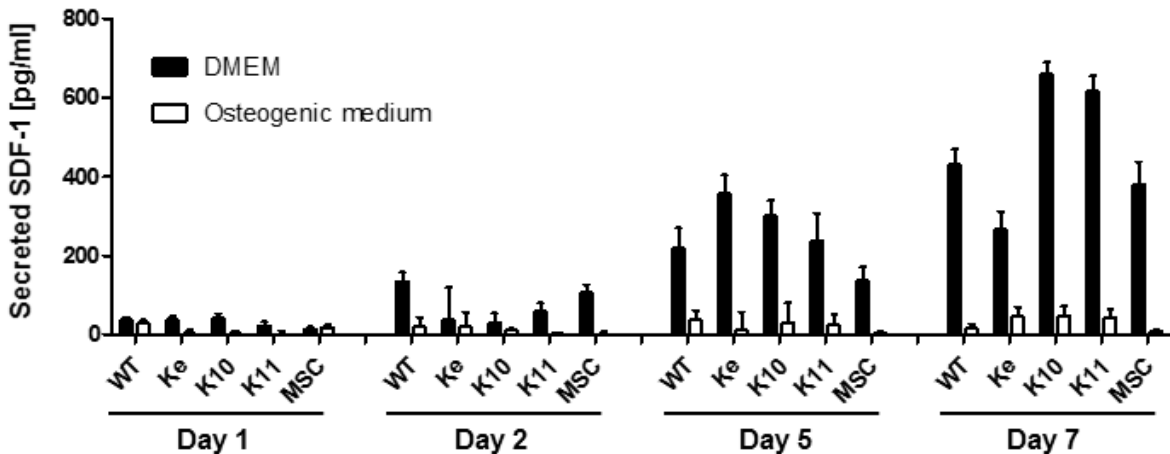
Figure 4-30: SDF-1 secretion by fibulin-1 knockdown SCP-1 cells cultured in DMEM or orosteogenic differentiation medium.
Cells were cultured in DMEM or osteogenic medium over a period of 7 days. Supernatant was collected at indicated time points and SDF-1 concentration determined using ELISA. SDF-1 secretion remained unaltered upon transduction with fibulin-1 KD in Ke, K10 and K11 vectors compared to WT and MSCs. Data are mean ± SD; n = 2 (with 3 technical replicates).

4.5.2 HSPC support of fibulin-1 reduced ECM scaffolds

To test our hypothesis that ECM with lower levels of fibulin-1 should provide enriched adhesion sites and thereby increase the number of AT-cells, we seeded freshly isolated CD34$^+$ cells onto ECM scaffolds derived from fibulin-1 knock down SCP-1 clones. Additionally, we also hypothesized that HSPCs should show increased proliferation as fibulin-1 negatively regulates HSPC proliferation. In our preliminary experiments, we tested these premises by preparing ECMs from fibulin-1 KD SCP-1 cells cultured in DMEM or osteogenic differentiation media but we could neither detect increased cell adhesion nor increased expansion of HSPCs in either of these ECMs. Contrarily, on ECMs derived from SCP-1 cells under selection conditions (SCP-1 Ke, -K10 and –K11), we found slightly decreased expansion rates of HSPCs compared to corresponding WTs (Figure 4-31). Most interestingly, the ECM derived from osteogenic differentiated SCP-1 WT cells was able to more efficiently and signfincatly expand HSPCs compared to all other conditions while ECMs derived from osteogenic differentiated SCP-1 cells,

under selection conditions, showed least HSPC expansion (Figure 4-31). Nevertheless, under all conditions tested, we observed better HSPC expansion compared to classical PCD expansion culture (Figure 4-31).
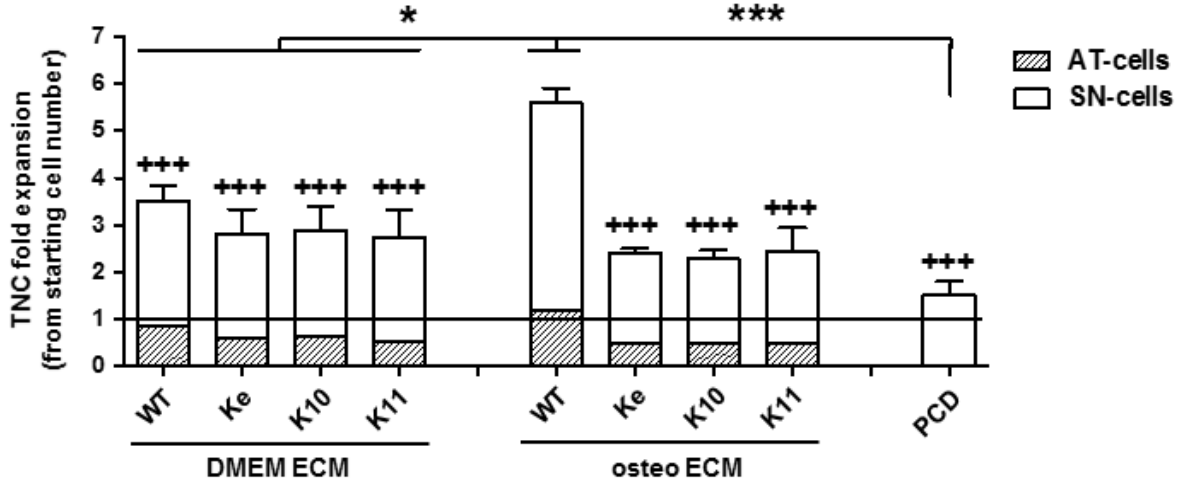
Figure 4-31: HSPC expansion on fibulin-1 KD ECM
HSPCs were seeded onto ECMs derived from DMEM or osteogenic differentiated SCP-1 cells under conditions required for fibulin-1 KD selection (SCP-1 Ke, -K10 and –K11) or WT conditions. Ke served as empty shRNA-vector transduction control. WT corresponds to untransduced SCP-1 cells. Expansion, either on ECM or PCD culture, was monitored for 5 days. Fold change in relation to starting cell numbers (black line) is displayed. AT-cells are shown as percentage share of counted cells; n = 3, error Bars denote S.D, two-tailed t-test, + = significant compared to WT osteo ECM, $*p < 0.05$, $**p < 0.01$, $***p < 0.001$.

Taken together, our findings suggest that a small proportion of approximately 20% freshly isolated PB CD34^{+} HSPCs are capable of adhering (AT-cells) to SCP-1 derived BM mimetic ECM scaffolds while 80% of these freshly isolated HSPCs remain in the supernatant (SN-cells). ECM scaffolds show native macromolecular structure, can store SDF-1 secreted by SCP-1 cells, and release it as required. This naïve phenotype promoted signficant HSPC expansion and permitted greater AT-cell proliferation compared to SN-cells or classical PCD cultures. Further, cellular adhesion leads to morphological and mechanical adaptation of HSPCs towards a migrative phenotype that is predominantly mediated through surface expression of ITGαIIb, ITGαV and ITGβ3, common RGD receptors. Random migration along the scaffold fibers was induced by SDF-1 recognition through the CXCR4 receptor on HSPCs and inhibition of a single RGD receptor (ITGαVβ3) reduced HSPC random migration. These observations show that ECM scaffolds provide a naïve environment for HSPCs, and that adhesion to these structures promotes morphological, and functional adaptation mediated by ITGβ3 signaling. Nevertheless, we failed to decipher the role of fibulin-1, an ECM molecule covering adhesion sides on FN within the ECM scaffolds. Fibulin-1-reduced ECM scaffolds, generated by shRNA knock down in

SCP-1 cells, should have exhibited more adhesion sides and, therefore, should have lead to increased cellular adhesion.

5 Discussion

The extracellular matrix is inarguably the most important cell-derived protein network for maintaing tissue stability. Every cell is surrounded by a tissue- and organ-intrinsic ECM, and is therefore, literally, connected to all other cells. Within the BM, HSPCs reside in close association with different cell types that are tightly anchored to an ECM scaffold which is a highly crosslinked, insoluble fibrillary structure composed of multiple proteins including fibronectins, collagens, proteoglycans, and laminins (Klein, 1995; Lee-Thedieck et al., 2012; Hynes, 2014). Besides structural integrity and biomechanical cues, the ECM can store and release growth factors and cytokines to generate morphogen gradients, which then regulate HSPC fate and determine tissue specificity. Moreover, the ECM composition provides certain unique biomechanical features that are sensed by adhesion receptors on HSPCs, transduced into intracellular signaling, and are thought to regulate stem cell function. As the ECM is synthesized and secreted by all cells in the BM niche, this regulation occurs in a bi-linear fashion, i.e., both from the ECM to the cells and vice versa, resulting in a highly dynamic ECM network. Furthermore, cell-secreted proteinases degrade ECM proteins in a highly specific manner to facilitate cell migration, structural remodeling, and growth factor release (Daley et al., 2008). These specific ECM properties enable and guide regulatory cell-cell and cell-matrix communications and highlight the role of the ECM as a key player in the functional regulation of hematopoietic stem and progenitor cells (HPCs) in BM tissue homeostasis.

However, the state-of-the-art HSPC ex vivo culture techniques use serum-free media and conventional plastic culture dishes wherein the cells are kept in suspension without contact with each other or other protein structures. Additionally, cytokine cocktails are used to control HSPC expansion and cell fate. These unnatural culture condtions can result in undefined cell phenotypes and do not allow investigation of naïve HSPC regulation, as occuring *in vivo*. To gain a better understanding of how the BM-niche ECM regulates HSPC expansion and cell fate, this thesis aimed to study the interaction between HSPCs and the extracellular compartment of the BM niche. We adapted a protocol published by Prewitz, et al. (2013) where BM-derived human MSCs were used to produce native ECM scaffolds. In this approach, the macromolecular protein networks were covalently anchored to culture glass-slide surfaces. Using a decellularization approach ensured that the ECM scaffold retained its native constitution and remained bioactive, for further use as HSPC expansion culture scaffold. However, as the primary MSC secretome is known to considerably differ from source to source and donor to donor (Amable et al., 2014; Kalinina et al., 2015), we used the immortalized MSC cell line, SCP-1 cells, to obtain highly reproducible ECM scaffolds.

The focus of this study was to characterize the morphological and mechanical adaptation of HSPCs upon their culture on BM-mimetic ECM scaffolds. Furthermore, we wanted to clearly understand the functional changes in HSPCs due to adhesion to ECM proteins.

5.1 SCP-1 cells as a source for ECM scaffold production

We used ECM scaffolds derived from decellularized SCP-1 cells to mimic the hematopoietic stem cell niche *in vitro*. This mesenchymal cell line was generated from human MSCs by overexpressing human telomerase reverse transcriptase to facilitate immortalization. These cells are known to display key features of MSCs, like plastic adherence, CD73, CD90 and CD105 surface marker expression, lack of expression of CD34, CD45, CD11b, CD19, and HLA-DR, as well as osteogenic, adipogenic, and chondrogenic differentiation potential (Boeker et al., 2008). Consequently, SCP-1 cells match the minimal criteria that define multipotent mesenchymal stromal cells (Dominici et al., 2006). Additionally, we found that SCP-1 monolayers support HSPC proliferation. Similar to Prewitz et al. (2013, 2015) we detected constant ECM production and successful anchorage of these ECMs to poly-octadecene-alt-maleic anhydride (POMA) and human fibronectin coated glass slides. In contrast, when SCP-1 cells were cultured on standard adherent PCD or uncoated glass slides, the ECM was not covalently anchored and it delaminated during decellularization. As SCP-1 cells are contact-inhibited and do not produce 3-D structures, the corresponding ECM layers ranged between 0.1 and 5 µm in height, as measured by confocal microscopy. Comparable covalently linked ECMs derived from human MSCs were demonstrated to have an average height of 1 µm, and compliance of these scaffolds was tested to be approximately 100 Pa (Prewitz et al., 2013, 2015), which matches BM stromal properties (Jansen et al., 2015). Importantly, these ECMs were able to support expansion, multilineage differentiation, and cytokine secretion in re-plated primary human MSCs (Seib et al., 2009b; Prewitz et al., 2013). Furthermore, ECM scaffolds were also able to maintain and enhance the expansion and engraftment potential of HSPCs upon transplantation into immunodeficient NSG mice (Prewitz et al., 2013). To exclusively elucidate the role of niche-mimetic ECM scaffolds in HSPC regulation, it is necessary to exclude donor-dependent variations in the MSC secretome (Kalinina et al., 2015). As SCP-1 cells derive from a single mesenchymal stromal cell, it is reasonable to assume that the secretome remains constant over time in culture and from passage to passage. Therefore, SCP-1 cells represent a powerful tool to produce standardized and highly reproducible ECMs.

After seeding 1×10^4 HSPCs/cm² on SCP-1-derived ECM, we found that a majority of HSPCs remained suspended in the culture medium while the other HSPCs adhered to the provided ECM scaffolds. The non-adherent cells were labelled as the supernatant fraction (SN-cells) and

the adherent cells were identified as the attached fraction (AT-cells). After a culture period of 12 h, an equilibrium between these two feactions was established wherein 20% of HSPCs were able to primarily adhere to the ECM preparations and 80% remained suspended. This finding might reflect an induced loss of adhesion molecules due to G-CSF mobilization as the HSPCs were collected from G-CSF mobilized PB (Mohle et al., 1995; Hall and Antonio, 2001). Total nucleated cell (TNC) and CD34^{+} HSPC expansion in the SN- and AT- fraction was enhanced by ECM scaffolds and is probably due to the presentation and release of growth factors. Interestingly, AT-cells proliferated the most; indicating that adhesion related signaling could be a mediator of cell expansion. Using the BrdU assay, we found that up to 80% of the AT-cells were within the G0/G1 cell cycle phase. It is important to note here that HSPCs harvested from G-CSF-mobilized PB have been previously reported to be synchronized to this cell cycle phase (Uchida et al., 1997). Taken together, these two facts indicate that ECM scaffolds are probabaly highly supportive of HSPC proliferation and have the capacity to manintain AT-cells synchronized in the G0/G1 phase. In addition, AT-cells showed morphological adaptations such as elongated cell shape and a migratory phenotype. Reichert et al. (2015) have reported similar findings after 7 days of HSPC co-culture with either human or murine MSCs. Thus, these observations point to the ECM as preliminary site of HSPC adhesion and migration in the BM niche.

5.2 Cell adhesion and focal contact formation

Cellular homing to the BM and its retention that are mainly promoted the chemokine by SDF-1 released by MSCs (Broxmeyer et al., 2003) necessitate morphological adaptations towards a migratory phenotype. Circulating HSPCs recognize SDF-1 via the CXC-receptors (CXCR). These receptors are known to activate integrins such as LFA-1 (ITGαL), VLA-4 (ITGα4), and VLA-5 (heterodimer of ITGα4 and ITGβ1), which lead to endothelial adhesion and trans-endothelial migration (Peled et al., 2000). We found that CXCR4, the most common of CXCR, was expressed on both SN- and AT-cells. However, in AT-cells, the CXCR4 seemed tobe localized within the entire cell cytoplasm, suggesting active SDF-1 turn-over with internalization of the receptor/ligand complex (Broxmeyer et al., 2003). We tested this internalization by immunostaining and demonstrate that SDF-1 was exclusively incorporated into AT-cells and not into SN-cells. Additionally, in AT-cells, CXCR4 was polarized towards ECM scaffolds, similar to findings in HSPCs and SCP-1 cell co-culture, where CXCR4 was polarized towards the confluent SCP-1 cell layer. These findings have been previously demonstrated only in primary MSCs (Giebel et al., 2004) and may indicate that SDF-1 is released by SCP-1 cells during ECM production, is bound by ECM proteins, and remains bio-active within the ECM scaffold after

decellularization. However, paradoxically, after addition of recombinant SDF-1 to the cell culture medium, AT-cells lost their CXCR4 polarity, and SN-cells showed internalization of the receptor/ligand complex, suggesting SDF-1 recognition capacity in these cells when SDF-1 was accessible as a solute in the medium rather than incorporated in to the ECM scaffold. Additional recombinant SDF-1 did not lead to adhesion of SN-cells, and therefore, did not influence the number of AT-cells. These observations suggest that SDF-1 induces adhesion molecule expression in HSPCs *in vivo* that leads to BM homing but not necessarily to adhesion to the BM stroma. However, its gradient activity still retains HSPCs in their niche. Which strengthen previously findings, that the adhesion capacity of HSPCs to human MSC monolayers is not altered when CXCR4 is blocked using a CXCR-4 antagonist AMD3100 (Jing et al., 2010). However, CXCR-4 blocking reduced migration in response to SDF-1 gradients in transwell assays. These results suggest that HSPCs recognize SDF-1 which facilitates their retention and migration, but does not actively regulate adhesion to BM stroma; similar observations have been made by others (Alakel et al., 2009). Nevertheless, incorporation of bioactive SDF-1 into the ECM scaffolds closely mimics the chemokine gradient present in the physiological BM niche. Sun et al. (2007) and Lai et al. (2009) have described that SDF-1 induces ITGαVβ3 expression in prostate cancer and chondrosarcoma cells, respectively, and that this induction is dependent on CXCR4 signaling. In line with these observations, HSPC culture on ECM scaffolds induced the surface expression of ITGβ3 on subsets of AT-cells to levels equivalent to those observed in the BM and led to the subsequent enrichment of ITGαVβ3$^+$ cells. However, freshly isolated cells were predominantly ITGβ3-negative and this probabaly implies that ITGβ3 expression occurs via SDF-1 when HSPCs adhere to ECM proteins and come into contact with the incorporated SDF-1. This subsequently retained HSPCs in the BM niche.

ITGβ3 exclusively heterodimerizes with either integrin αV or αIIb to form RGD recognizing focal contacts (Hynes, 2002). We found that both these integrins were upregulated in AT-cells. In HSPCs, dimers of these ITGs have been described as markers of long-term repopulating cells (Umemoto et al., 2008), mediators of HSPC maintenance (Umemoto et al., 2012; Boisset et al., 2013), and are correlated to properties of quiescent cells (Umemoto et al., 2006). By using an ITGαVβ3 blocking antibody, we show a reduction in the migratory capacity of AT-cells after a 5 day culture period, which is a key requisite for homing to or retention of HSPCs in the BM (Giordano and Lichtman, 1972). Within the observed time range of 5 days, ECM adhesion induced the surface expression of ITGβ3 and subsequently of the heterodimer ITGαVβ3. However, we asked whether ITGαVβ3 is indispensable for freshly isolated HSPC migration and whether ITGαVβ3 promotes migratory behavior during the early stages of HSPC-ECM contact.

Interestingly, when cells were incubated with the anti ITGαVβ3 antibody after a 24 h culture period, we detected a reduction in the migration of AT cells. This suggests that direct surface expression of ITGβ3 and establishment of migration occur when HSPCs come into contact with ECM scaffolds, despite the fact that ITGβ3 surface expression was almost absent on freshly isolated cells.

Morphological and mechanical adaptation of HSPCs

Studies on integrins in the last few decades show that they are able to sense physical parameters and transduce mechanical cues into cells to regulate fundamental functions such as migration, proliferation, and differentiation (Peyton et al., 2007). In HSPCs, their maintenance and stem cell fate decisions were found to be controlled through this contact-signaling machinery (Prosper and Verfaillie, 2001). ECM culture induced focal contacts, necessitated filamentous actin association, and thereby, outside-in signaling (Zamir and Geiger, 2001) that is further indicated by tyr[118] phosphorylation of paxillin (Nayal et al., 2006). These structures transduce physical cues from the substrate into cells by recruiting other signaling molecules and therefore directing lineage specification (Lee-Thedieck and Spatz 2014). However, most of these studies were performed using single or combined protein coating on rigid substrates like glass or plastic or on hydrogels with different elastic moduli in the range of several kPa to GPa. Which is not comparable to BM stroma mechanical properties ranging from 0.24 to 25 kPa (Jansen et al., 2015). Contrarily, the elastic modulus of our ECM scafoldds ranged between 0.05 to 0.3 kPa and are very similar to those of the BM (Prewitz et al., 2013). Additionally, as these ECMs consist of complex protein mixtures they provide various interaction partners for HSPCs. Several ITGs have been described as mechanosensors on HSPCs (Lee et al., 2013), however, none of these were found to be differentially expressed in the SN- or AT-cells. Interestingly, AT-cells adapt to the ECM scaffold and display a stiffer phenotype compared to SN-cells, as measured by RT-DC. This was also true in SCP-1 HSPC co-cultures. However, ECM-cultured and SCP-1-co-cultured HSPCs differed in cell size, which can be partially explained by an increase in compeitition for available nutrition. Thus, that extracellular stiffness transduction into intracellular tension might be facilitated via combinations of ITGβ3, ITGαIIb and ITGαV. Bae et al. (2014) using mouse embryo fibroblasts, showed that cells recognized stiff substrates (20 to 25 kPa) via focal adhesion kinase-cas-rac-signaling and tyr[118] phosphorylation of paxillin. Moreover, this particular signaling cascade increased cell cycling, whereas cultivation on soft substrates (2 to 4 kPa) prevented cells from mitogen-stimulated cycling. Additionally, Lee-Thedieck et al. (2012) have demonstrated that the adhesion of HSPCs to fibronectin is greater on hard hydrogels (E > 38 kPa) compared to soft scaffolds (*E* ≤ 20 kPa). They also showed that primary HSPCs

increased random migration in the presence of SDF-1 when cultured on hard hydrogels. Similarly, we demonstrate increased cycling, fast migration of up to 0.1 µm per second, and membrane associated paxillin tyr[118] phosphorylation. However, ECM scaffolds are more compliant, as ultra-soft scaffolds like tropoelastin coatings on plastic dishes were shown to induce stem cell proliferation (Holst et al., 2010). Therefore, our ECM approach represents a more complex set-up and more closely resembles the *in vivo* situation. This hypothesis is supported by the detection of incorporated chemokines like SDF-1 with the ECM scaffold and the provision of an extremely soft environment with its associated consequences on mechanotransduction. In contrast, thin ECM layers (1 µm in height) might not prevent the recognition of the stiff underlying glass slides and this stiffness can induce differentiation and migration. Therefore, a combination of hydrogels with different elastic moduli coated with decellularized ECMs could provide detailed insights into mechanosensing of HSPCs in a native BM ECM environment, complete with storage of growth factors and other signaling molecules.

5.3 HSPC multilineage potential

Arguably, ITGβ3 expression could be a marker for commitment as it is predominantly expressed during megakaryopoiesis (Naik and Parise, 1997; Ficko, 2008) and erythropoiesis (Ferkowicz et al., 2003). Moreover, ITGβ3 is essential for acute myeloid leukemia (AML) progression in mice (Miller et al., 2013). Due to increased HSPC proliferation after adhesion to ECM scaffolds, malignant transformation could not be excluded and needs to be carefully elucidated in detail.

We tested potential lineage bias by comparing freshly isolated HSPCs from the BM and PB with HSPCs (AT-cells and SN-cells) after 5 days of culture on ECM scaffolds. Using CFU-GEMM assay, we found that freshly isolated BM HSPCs form significant less colonies compared to all other tested cell types. This is surprising as adult BM CD34+ cells were found to be the most potent HSPC population in terms of colony formation in all HSPC lineages compared to PB or cord blood cells (Wu et al., 1999); though we only tested myeloid colony formation. Most interestingly, ECM-cultured cells, and especially AT-cells, were found to form increased amounts of erythroid colonies while the formation of other myeloid lineages was not altered. A possible explanation for the observed increase in erythroid differentiation potential is the fact that several soluble and ECM incorporated factors are known to induce erythropoiesis (Lodish et al. 2010). Moreover, Prewitz et al. (2013) showed that pro-erythroid growth factors like IL-3 and BMP4 (Hattangadi et al., 2011) are incorporated into primary MSC-derived ECM scaffolds.

To identify the role of ITGβ3 surface expression in erythroid lineage commitment, FACS was used to separate CD34+ITGβ3+ and CD34+ITGβ3- cells before performing CFU-GEMM assay.

The number of CFUs was equal among the CD34$^+$ITGβ3$^-$ PB, AT- and SN-cell populations, indicating that these cells are enriched in common myeloid progenitors and HSCs. Moreover, all cell types formed predominantly erythroid colonies, followed by CFU-Gs, CFU-Ms, CFU-GMs, and CFU-GEMMs; a well known phenomenon during CD34$^+$ HSPC (Lemoli et al., 1998). Most interestingly, we found that sorted CD34$^+$ITGβ3$^+$ cells from ECM culture formed only erythroid and granulocyte colonies; however, CFU-G capacity was lower compared to CD34$^+$ITGβ3$^-$ cells. Contrary, fresh PB derived CD34$^+$ITGβ3$^+$ cells were able to differentiate into all myeloid lineages but CFU-Es were also increased. Interstingly, both findings suggest that ITGβ3 surface expression on CD34$^+$ cells is a mediator or marker of erythroid lineage commitment. However, HSPC adhesion via ITGβ3 to ECM scaffolds (AT-cells) does induce an erythroid lineage bias and is of significant interest in regenerative medicine, as effective *in vitro* erythrocyte differentiation from induced pluripotent stem cells or isolated HSCs is still limited (Chang et al., 2011). Red blood cells (RBCs) are inarguably the most important blood cells not only because of their number per volume of blood (10% - 45% of total blood volume), but also because of their physiological roles, e.g. in oxygen delivery (Kimbrel and Lu, 2011). In the US, more than 16 million units of RBCs are collected and transfused annually into patients (Whitaker and Hinkins, 2011) suffering mostly from anemia or trauma-induced massive blood loss. As donated RBCs have to match host blood group phenotype, hospitals need units of all the blood groups readily available for use in emergencies. This represents a logistical challenge and requires time and money by necessitating the storage of thousands of blood units. In this context, ECM scaffolds used in this study can be used to gain insights into the regulatory mechanisms of HSC erythroid commitment, which can further lead to translational approaches on *in vitro* erythrocyte production (Dias et al., 2011). Further, the mature "universal" type (0)Rh-negative RBCs could be produced in therapeutic quantities that could counter shortages in RBC supplies or even replace state-of-the-art RBC donation (Nakamura, 2008; Ebihara et al., 2012; Xie et al., 2014).

5.4 ECM scaffold modulation

In translational medicine, engineered culture substrates for efficient HSPC expansion in the context of tissue transplantation represent a powerful tool to overcome current limitations in source tissue availability. Great research efforts have been spent in generating HSPC expansion culture techniques including cytokine or small molecule-based approaches (Dexter et al., 1977a, 1977b; North et al., 2007; Delaney et al., 2010; Csaszar et al., 2012; Arulmozhivarman et al., 2016). However, *in vitro* HSPC suspension cultures lead to heterogeneous cell populations with more or less undefined phenotypes (Blank et al. 2008). This might be due to our limited understanding of HSPC cytokine regulation but could also be partially explained by our neglect

of the biophysical and structural signals that HSPCs receive within the BM niche. As discussed before, these signals induce cellular biochemical and biomechanical remodeling of HSPCs that result in functional adaptation like HSPC maintenance or commitment. Targeted modulation of ECM culture carriers can be used to identify cell regulation within the context of ECM signaling.

Therefore, we induced osteogenic differentiation of SCP-1 cells during ECM production. Osteoblasts are MSC-derived cells that form the bone and reside mainly in the endosteal HSPC niche. These cells and their secreted proteins, which also facilitate ECM mineralization (Yamaguchi, 2014) signifcantly contribute to HSPC regulation (Taichman and Emerson, 1998; Visnjic et al., 2001; Calvi et al., 2003; Visnjic, 2004; Calvi, 2006). We assumed that osteogenic differentiated SCP-1 cells synthesize and secrete more endosteal niche related ECMs, which differ in amount of proteins and composition from those secreted by untreated SCP-1 cells. We found that osteogenic differentiated SCP-1 cells release lower amounts of SDF-1 into culture media, as measured by ELISA. Contrarily, SDF-1 is mainly produced by osteoblasts *in vivo*. This discrepancy can be explained by effective SDF-1 anchoring to the osteogenic ECM components (Jung et al., 2006; Greenbaum et al., 2013) and suggests that higher SDF-1 levels are incorporated into the osteogenic ECM. Interestingly, it has been shown that elevated SDF-1 levels near the endosteal niche direct megakaryocyte relocation (Thon, 2014); thus, osteogenic ECMs could act as a model system for megakaryopeiesis.

We identified increased fibulin-1 expression in osteogenic differentiated SCP-1 cells. Fibulin-1 is an important ECM component that regulates the adhesion of HSPCs to FN (Hergeth et al., 2008). These findings strengthen the perception that the osteogenic ECM is variable in protein composition compared to other ECM scaffolds. When HSPCs were cultured in presence of ECM derived from osteogenic differentiated SCP-1 cells, we found increased HSPC proliferation and remarkably elevated amounts of TNCs after 5 days, compared to ECM derived from undifferentiated SCP-1 cells. However, the different ECMs did not alter the ratio of AT-cells to SN-cells. Thus, as the ratio is the same but the number of HSPCs was increased on osteogenic ECM, we found a slight but insignificant increase in the number of AT-cells per unit area, compared to normal ECM.

As adhesion of HSPCs to ECM scaffolds induces morphological and biomechanical, and therefore, functional adaptions, we aimed to increase the number of HSPCs directly anchored to ECM scaffolds. Fibulin-1 is known to interfere with HSPC adhesion to FN and was, therefore, selected for targeted modulation experiments. We established lentiviral shRNA transduction using two clones (K10, K11) that targeted all four splice variants of fibulin-1. As controls, we used primary human MSCs, wild-type SCP-1 cells (WT), and an empty vector control (Ke) that

also transduced SCP-1 cells. Semi-quantitative PCR analyses of undifferentiated and osteogenic differentiated SCP-1 cells revealed efficient fibulin-1 knockdown and highlighted K10 as the most efficient fibulin-1 silencing vector in this study. This knock down was confirmed by Western Blot analysis of decellularized osteogenic ECM proteins. These observations confirm shRNA knock down of ECM proteins in SCP-1 cells as possible targets for ECM scaffold modulation. However, as no housekeeping protein for decellularized ECMs is described, we used a second coomassie blue stained gel, treated under identical conditions, to verify equal loading of samples. A more efficient method would be a transfer of the coomassie stained proteins to a nitrocellulose membrane, as reported by Ranganathan and De 1996, but our attempt to repeat their protocol failed. Interestingly, we found similar levels of fibulin-1 in ECMs of primary human MSCs, SCP-1 cells (WT), and SCP-1 cells transduced with Ke, indicating similar ECM composition of MSCs and SCP-1 cells. These results demonstrate the feasibility of using primary MSCs to produce ECM scaffolds to obtain allegedly more 'naïve scaffolds'; however, our data shows that SCP-1 cells have natural ECM composition.

In order to strengthen this notion, MSC-like characteristics of SCP-1 cells were verified by the analysis of surface marker expression, as described for minimal criteria (Dominici et al., 2006). Stable surface marker expression indicates stable cell identity and unaltered cell phenotype (Lv et al., 2014). We could not detect significant differences in surface marker expression between WT and lentiviral transduced SCP-1 cells, all of which exhibited stable expression of MSC surface markers. Specifically, the high percentage of CD146- and CD166-positive cells was remarkable because CD146 expression is considered an indicator for multipotency (Covas et al., 2008), while CD166 correlates with stromal cell character (Oswald et al., 2004).

Unfortunately, we could not detect increased adhesion of HSPCs, either to ECM scaffolds derived from undifferentiated WT and lentivirusl transduced SCP-1 cells or to ECM scaffolds derived from osteogenic differentiated WT and lentivirus transduced SCP-1 cells. Contrarily, cell expansion decreased when HSPCs were cultured on ECMs generated by lentivirus transduced SCP-1 cells and shows that we cannot exclude the fact that HSPC growth and adhesion are related to the conditions used for ECM scaffold production. For efficient fibulin-1 knockdown in SCP-1 cells, we used puromycin as the selection agent (Moffat et al., 2006). Puromycin is a very efficient antibiotic agent and the transduced cells should be resistant to the drug. It is possible that puromycin was integrated into ECM scaffolds. Under such conditions, HSPCs are exposed and susceptible to ECM-incorporated puromycin, which can also affect proliferation rate. Therefore, we were not able to elucidate the exact role of fibulin-1 within the ECM scaffold. Nevertheless, the importance of native-derived ECMs for *in vitro* HSPC culture has been further

invigorated by our experiments, as HSPC expansion remained higher compared to PCD suspension cultures.

Various components of the niche environment regulate hematopoiesis, maintain HSPCs within the bone marrow microenvironment, and give rise to several niches that increase overall complexity. We show that ITGβ3 surface expression is induced on HSPCs to an extent present in the BM using mechano-biological aspects and *ex vivo* biochemical cues from BM-mimetic ECM scaffolds derived from SCP-1 cells. Such ECMs, to the best of our knowledge, never been described in suspension cultures and indicate the feasibility of mimicing the BM niche environment. Integrin ITGβ3 was found to anchor HSPCs to ECM proteins that resulted in a migratory phenotype. The topographical and mechanical parameters of ECM scaffolds might be transduced through an outside-in signaling pathway via ITGαVβ3 that ultimately result in mechanical and functional adaptation of HSPCs. Such adaptation could be demonstrated by increased SDF-1 recognition and chemotactic migration. Further, ECM tension transduction through focal adhesion contacts was found to positively affect HSPC commitment, highlighting the importance of *in vitro* stroma modeling with respect to effective HSPC expansion and targeted lineage commitment in the context of regenerative medicine. Unfortunately, preliminary attempts to enhance HSPC-ECM interaction by uncovering cell adhesion sides within the macromolecular protein network via fibulin-1 knock down have failed. However, using targeted ECM modulation, either as an educated or unbiased approach, will help decipher HSPC-ECM interplay and elucidate ECM signaling in cell regulatory networks. This would allow a detailed study of signaling domains, adhesion ligands, and elasticity, to decipher the multitude of cell regulatory pathways derived from ECM contact. Finally, targeted ECM modulation will also increase the knowledge on design potentials for new biomaterials and accelerate the efficiency of cellular therapies in regenerative medicine.

6 Summary

As graft source for lymphoma or leukemia treatment, hematopoietic stem and progenitor cells (HSPCs) have been the focus of translational medicine for decades. HSPCs are defined by their self-renewing capacity and their ability to give rise to all mature blood cells. They are found anchored to a specialized microenvironment in the bone marrow (BM) called the hematopoietic niche. HSPCs can be enriched by sorting them based on the presence of the surface antigen CD34 before clinical or tissue engineering use. As these cells represent a minority in most graft sources and the amount of applicable cells is limited, *ex vivo* expansion-cultures were established using cytokine cocktails or small molecules. However, *in vitro* culture of HSPCs as suspension-cultures result in heterogeneous cell populations with undefined cellular identities. In the BM niche, HSPCs are not exclusively maintained by cytokines but also by cell-matrix adhesions mediated by integrins (ITGs). Thus, β1 and β2 ITGs were found to promote initial contact of HSPCs with mesenchymal stromal cells (MSCs) and ITGβ3 expression was shown to be a marker for long-term repopulating HSPCs *in vivo*. Consequently, *ex vivo* remodeling of the BM niche using co-cultures of HSPCs and niche cells like MSCs came into spotlight and was proven to be a promising tool for stem cell expansion. However, in clinical and research applications, direct contact of two cell populations necessitates HSPC post-culture purification.

To address these problems, we established a novel culture method for remodeling the BM extra cellular stroma *in vitro* wherein we used decellularized extracellular matrix (ECM) scaffolds derived from immortalized mesenchymal stromal cells (SCP-1). Such scaffolds were found to be highly reproducible and served as *in vitro* niche for HSPCs by being more effective for the expansion of CD34$^+$ cells, compared to classical suspension cultures. ECMs were shown to consist of multiple proteins including fibronectins, collagens, and a major niche chemokine responsible for BM homing and retention of HSPCs *in vivo,* namely, stromal derived factor 1 (SDF-1). SDF-1 is known to be secreted by MSCs and is anchored to matrix proteins. This reveals that ECM scaffolds produced by SCP-1 cells are a naïve reconstructed microenvironment. When CD34$^+$ cells were seeded, only around 20% of the cells adhered to the provided ECM scaffold. These cells recognized SDF-1 via C-X-C chemokine receptor type 4 (CXCR-4), as shown by laser scanning confocal microscopy. Thus, adhesive sides as they are present in the BM niche are provided. However, CD34$^+$ cells isolated from G-CSF mobilized peripheral blood of healthy donors were found to be heterogenous with respect to adhesion capacity. Nonetheless, it was similar to HSPC co-cultures with SCP-1 cells as feeder layer. Therefore, we separated and analyzed two cell fractions, the adherent (AT-cells) and the non-adherent supernatant (SN-cells) cells.

Summary

Other signals provided by the BM extracellular stroma to HSPCs are physical cues that control HSPC fate. HSPCs sense these physical features through focal contacts and accordingly remodel their morphological and biomechanical properties. Using real-time deformability cytometry (RT-DC) to uncover biomechanical phenotypes of freshly isolated HSPCs, SN-cells, AT-cells, and classical suspension cultured HSPCs in plastic culture dishes (PCD) were analyzed. We found freshly isolated cells to be less deformable and small. AT-cells displayed actin polymerization to stress fibers, and exhibited a stiffer mechanical phenotype compared to PCD-cultured or SN-cells. This might constitute the first hint of functional adaptation. Integrins are known to establish mechanosensing focal contacts. Thus, we analyzed ITG surface expression and identified ITGαIIb, ITGαV, and ITGβ3 to be enriched on AT-cells compared to freshly isolated cells or SN-cells. Active integrins need to form heterodimers consisting of one α- and one β subunit. Interestingly, the identified ITGs exclusively interact with each other to form RGD peptide receptors. RGD is a tripeptide consisting of the amino acids arginine, glycine, and aspartic acid and was identified as an adhesion sequence within fibronectin and other extracellular proteins. Consequently, we could confirm an important role for ITGαVβ3 in HSPC-ECM interaction with respect to adhesion and migration. However, we also identified ITGβ3 expression on a subset of CD34$^+$ cells either freshly isolated or ECM cultured cells, as a marker for erythrocyte differentiation. These findings demonstrate that, *in vitro*, the ECM compartment acts as a regulator of HSPC fate and portray mechanical recognition as a potent driver of differentiation.

In this context, targeted modulation of ECM scaffolds could enhance cell-ECM interactions and accelerate stem cell expansion or differentiation. These modulations could also provide further insights into HSPC-niche regulation. We demonstrate that ECMs derived from osteogenic differentiated SCP-1 cells increase HSPC expansion but do not lead to increased cell adhesion. As ECM adhesion preliminary alters HSPC function, we aimed at developing ECM scaffolds with increased adhesion capacity. Using lentiviral transduction, we generated a stable knock down of fibulin-1 in SCP-1 cells. Fibulin-1 is an ECM protein known to form anti-adhesion sites with fibronectin. However, we failed to increase adherent cell numbers or enhance HSPC expansion in the fibulin-1 knock down ECMs.

Taken together, SCP-1 cell-derived ECM protein scaffolds provide an *in vitro* niche for HSPCs capable of stem cell expansion. Integrin mediated signaling altered the biomechanical and functional properties of HSPCs and hints at suspension cultures as being inappropriate to study the physiological aspects of HSPCs. Targeted modulation of ECM scaffolds could theoretically generate suitable *ex vivo* environments with the capacity to gain detailed insight into HSPC

regulation within their niche. This will enhance the functionality of new biomaterials and will lead to improved regenerative therapies like BM transplantation.

7 Zusammenfassung

Als Quelle für die Behandlung von Lymphomen oder Leukämien stehen hämatopoetische Stamm- und Vorläuferzellen (HSVZs) seit Jahren im Fokus der translationalen Medizin. HSVZs sind durch ihre Fähigkeit der Selbsterneuerung und die Bildung aller Blutzellen definiert, wobei sie selbst fest im Knochenmark (KM) in sogenannten hämatopoetischen Stammzellnischen verankert sind. Für klinische oder regenerative Zwecke können sie mit Hilfe des Oberflächenantigens CD34 angereichert werden. Da der Anteil von HSVZs in gesunden Spendern im Vergleich zu anderen Zellen allerdings verschwindend gering ist, wurden *in vitro* Kultursysteme für ihre Expansion entwickelt. Diese Systeme nutzen zumeist regulative Zytokine oder niedermolekulare Verbindungen um die Stammzelleigenschaften aufrechtzuerhalten. Jedoch sind solche Suspensionskulturen meist ineffizient und führen zur Differenzierung der HSVZs und heterogenen Zellpopulationen, da in der KM-Nische das Stammzellpotential nicht ausschließlich durch Zytokine aufrechterhalten wird. Vor allem Zell-Matrix Interaktionen spielen eine wesentliche Rolle für die Regulation von HSVZs. Diese Interaktionen werden durch Integrine (ITG) vermittelt. So konnte beispielsweise gezeigt werden, dass ITG β1 und β2 benötigt werden um den Kontakt zu mesenchymalen Stromazellen herzustellen und ITG β3 wurde als Marker für sich selbst erneuernde HSVZs beschrieben. Dementsprechend wurde versucht, durch die Ko-kultur von HSVZs und MSZs, die Stammzellnische *ex vivo* zu modellieren. Es konnte gezeigt werden, dass Kokulturen ein vielversprechendes Werkzeug für die Expansion von HSVZs sind, allerdings erfordern diese eine nachträgliche Aufreinigung der HSVZs für klinische oder experimentelle Anwendungen.

In dieser Arbeit wurde ein neues Kulturverfahren etabliert, welches durch Dezellularizierung von imortalisierten mesenchymalen Stromazellen (SCP-1) die extrazellulären Bestandteile des KM-Stromas modelliert. Hierbei bleibt die sekretierte extrazelluläre Matrix (EZM) der SCP-1 Zellen erhalten und kann als Substrat für die Kultur von HSVZs verwendet werden. Wir konnten zeigen, dass diese dezellularisierten Matrices hoch reproduzierbar sind und durch eine verstärkte Expansion der HSVZs im Vergleich zu klassischen Suspensionskulturen als eine *in vitro* Nische fungieren. Die EZM besteht aus verschiedenen Proteinen, unteranderem Fibronektinen, Kollagenen und *stromal cell derived factor 1* (SDF-1). Das Zytokin SDF-1 wird im KM von MSZs sezerniert und in die EZM integriert. Wir konnten zeigen, dass SCP-1 sezernierte EZMs SDF-1 enthalten, was diese damit als natürliches Mikromilieu kennzeichnet. Interessanterweise war nur ein kleiner Teil (ca. 20%) frisch isolierter HSVZsin der Lage an die Proteinstrukturen der SCP-1 Matrices zu adhärieren. Fluoreszenzmikroskopische Aufnahmen verdeutlichten, dass diese Zellen in der Lage sind SDF-1 durch C-X-C chemokine receptor type 4 (CXCR-4) zu

internalisieren. Demnach werden adhäsive Bestandteile der KM-Nische durch die EZMs modelliert, wobei frisch isolierte HSVZs eine heterogene Zellpopulation hinsichtlich ihrer Adhäsionsfähigkeiten darstellt. Dieses Phänomen konnte auch in SCP-1-HSVZ Ko-kulturen bestätigt werden. Aus diesem Grund wurden die Zellen in zwei Gruppen eingeteilt und vergleichend untersucht: adhärente- (AT-Zellen) und Überstandszellen (SN-Zellen).

Weitere wichtige Parameter die durch das KM-Stroma auf die Regulation von HSVZs wirken sind physikalische Eigenschaften der Umgebung. Zellen können diese durch Fokalkontakte wahrnehmen und ihre morphologischen und biomechanischen Eigenschaften daran anpassen. Die Charakterisierung der biomechanischen Eigenschaften von frisch isolierten C34$^+$ Zellen, AT- und SN-Zellen sowie Zellen aus Suspensionskulturen erfolgte mit Hilfe der Echtzeit-Deformationszytometrie (RT-DC). Frisch isolierte HSVs waren deutlich kleiner und undeformierbarer als SN-Zellen. AT-Zellen hingegen wiesen durch ihre starke Aktinpolymerisierung einen deutlich steiferen Phänotyp im Vergleich zu SN- du Zellen aus Suspensionskultur auf. Das zeigt deutlich, dass die biomechanischen Eigenschaften der EZM Umgebung von adhärenten Zellen erkannt und deren Form und Mechanik an diese angepasst wird. Dies könnte ein erster Hinweis auf funktionelle Unterschiede zwischen AT- und SN-Zellen darstellen. Integrine sind dafür beschrieben mechanosensorische Fokalkontakte zu bilden. Durchflusszytometrische-Analysen zeigten eine verstärkte Expression der Integrine ITGαIIb, ITGαV und ITGβ3 auf der Oberfläche der AT-Zellen. Da Integrine Heterodimere aus einer α und einer β Untereinheit formen müssen um aktiv zu sein war es interessant, dass die gefundenen dafür bekannt sind, exklusive miteinander zu interagieren und RGD-Motiv Rezeptoren formen. RGD-Motive sind Tripeptide bestehend aus Arginin, Glycin und Asparaginsäure die als zell-adhäsive Strukturen in extrazellulären Proteinen wie Fibronektin detektiert wurden. Infolgedessen konnten wir zeigen das ITGαvβ3 eine entscheidende Rolle für die Adhäsion und für die Migration von AT-Zellen spielt. Allerdings, identifizierten wir auch die Oberflächenexpression von ITGβ3 auf einer Subpopulation aller CD34$^+$ isolierter (frisch isolierte, AT-Zellen und SN-Zellen) Zellen als einen Marker für Differenzierung in Richtung Erythrozyten. Diese Ergebnisse zeigen, dass die EZM Substrate primär durch ihre biomechanischen Eigenschaften eine regulatorische Wirkung auf die Differenzierung von HSVZs haben.

Daran anknüpfend könnte eine Veränderung der EZM modulare Substrate erzeugen, welche gezielt Einfluss auf die Proliferation und Differenzierung von HSVZs haben. Mit einer solchen modulierbaren Mikroumgebung könnten wichtige Einblicke in die Regulation von Stammzellen in ihrer Nische identifiziert werden. Wir konnten zeigen, dass Matrices osteogen differenzierter SCP-1 Zellen die Proliferation von HSVZs verbessern jedoch nicht die Menge an adhärenten Zellen verändert. Da vor allem die Adhäsion von HSZVs an die Matrix zu zellulären

Veränderungen führte, sollte ein EZM Substrat erzeugt werden, welches mehr Adhäsionsstrukturen bietet. Durch lentivirale Transduktion konnten wir einen stabilen *knock down* von Fibulin-1 in SCP-1 Zellen erzeugen. Fibulin-1 ist ein extrazelluläres Matrix Protein welches anti-adhäsive Komplexe mit Fibronektin bildet. Im Gegensatz dazu hatte der gezielte knockdown des extrazellulären Matrixproteins Fibulin-1 in den SCP-1 Zellen keinen Einfluss auf die Adhäsion und Proliferation der HSVZs.

Zusammenfassend konnten wir zeigen, dass EZM Substrate von SCP-1 Zellen eine geeignete *in vitro* Nische für die effektive Expansion von HSVZs darstellen. Durch die Induktion von Integrin-vermittelten Signalkaskaden wurde die Biomechanik und die Funktionalität der HSVZs verändert. Damit wurde möglicherweise gezeigt, dass Standard Suspensionskulturen für die Untersuchung von HSVZs *ex vivo* ungeeignet sind und nicht vollständig physiologische Effekte wiederspiegeln. Durch die gezielte Modulation der EZMs könnten *ex vivo* Umgebungen für HSVZs erzeugt werden, die genaue Einblicke in die Regulation der Zellen durch ihre Nische erlauben. Diese Erkenntnisse könnten zu neuen funktionellen Biomaterialen und zur Verbesserung von regenerativen Therapien wie beispielsweise der KM Transplantation führen.

Bibliography

Adams GB, Chabner KT, Alley IR, Olson DP, Szczepiorkowski ZM, Poznansky MC, Kos CH, Pollak MR, Brown EM, Scadden DT. 2006. Stem cell engraftment at the endosteal niche is specified by the calcium-sensing receptor. Nature 439:599–603.

Aiuti A, Webb IJ, Bleul C, Springer T, Gutierrez-Ramos JC. 1997. The chemokine SDF-1 is a chemoattractant for human CD34+ hematopoietic progenitor cells and provides a new mechanism to explain the mobilization of CD34+ progenitors to peripheral blood. J Exp Med 185:111–20.

Alakel N, Jing D, Mueller K, Bornhaeuser M, Ehninger G, Ordemann R. 2009. Direct contact with mesenchymal stromal cells affects migratory behavior and gene expression profile of CD133+ hematopoietic stem cells during ex vivo expansion. Exp Hematol 37:504–513.

Amable PR, Teixeira MVT, Carias RBV, Granjeiro JM, Borojevic R. 2014. Protein synthesis and secretion in human mesenchymal cells derived from bone marrow, adipose tissue and Wharton's jelly. Stem Cell Res Ther 5:53.

Arabanian LS, Fierro FA, Stölzel F, Heder C, Poitz DM, Strasser RH, Wobus M, Borhäuser M, Ferrer RA, Platzbecker U, Schieker M, Docheva D, et al. 2014. MicroRNA-23a mediates post-transcriptional regulation of CXCL12 in bone marrow stromal cells. Haematologica 99:997–1005.

Argraves WS, Tran H, Burgess WH, Dickerson K. 1990. Fibulin is an extracellular matrix and plasma glycoprotein with repeated domain structure. J Cell Biol 111:3155–64.

Arroyo a G, Yang JT, Rayburn H, Hynes RO. 1999. Alpha4 integrins regulate the proliferation/differentiation balance of multilineage hematopoietic progenitors in vivo. Immunity 11:555–566.

Arulmozhivarman G, Stoeter M, Bickle M, Kraeter M, Wobus M, Ehninger G, Sto lzel F, Brand M, Bornhaeuser M, Shayegi N. 2016. In Vivo Chemical Screen in Zebrafish Embryos Identifies Regulators of Hematopoiesis Using a Semiautomated Imaging Assay. J Biomol Screen 1087057116644163.

Asahara T, Takahashi T, Masuda H, Kalka C, Chen D, Iwaguro H, Inai Y, Silver M, Isner JM. 1999. VEGF contributes to postnatal neovascularization by mobilizing bone marrow-derived endothelial progenitor cells. EMBO J 18:3964–3972.

Bae YH, Mui KL, Hsu BY, Liu S-L, Cretu A, Razinia Z, Xu T, Puré E, Assoian RK. 2014. A FAK-Cas-Rac-lamellipodin signaling module transduces extracellular matrix stiffness into

mechanosensitive cell cycling. Sci Signal 7:ra57.

Banfi A, Bianchi G, Notaro R, Luzzatto L, Cancedda R, Quarto R. 2002. Replicative Aging and Gene Expression in Long-Term Cultures of Human Bone Marrow Stromal Cells. Tissue Eng 8:901–910.

Bara JJ, Richards RG, Alini M, Stoddart MJ. 2014. Concise Review: Bone Marrow-Derived Mesenchymal Stem Cells Change Phenotype Following In Vitro Culture: Implications for Basic Research and the Clinic. Stem Cells 32:1713–1723.

Barry ST, Ludbrook SB, Murrison E, Horgan CM. 2000. A regulated interaction between alpha5beta1 integrin and osteopontin. Biochem Biophys Res Commun 267:764–769.

Beacham DA, Amatangelo MD, Cukierman E. 2007. Preparation of Extracellular Matrices Produced by Cultured and Primary Fibroblasts. Current Protocols in Cell Biology, Hoboken, NJ, USA: John Wiley & Sons, Inc., p Unit 10.9.

Becker AJ, McCulloch EA, Till JE. 1963. Cytological Demonstration of the Clonal Nature of Spleen Colonies Derived from Transplanted Mouse Marrow Cells. Nature 197:452–454.

Beltrami AP, Barlucchi L, Torella D, Baker M, Limana F, Chimenti S, Kasahara H, Rota M, Musso E, Urbanek K, Leri A, Kajstura J, et al. 2003. Adult cardiac stem cells are multipotent and support myocardial regeneration. Cell 114:763–776.

Berridge M V, Ralph SJ, Tan AS. 1985. Cell-lineage antigens of the stem cell-megakaryocyte-platelet lineage are associated with the platelet IIb-IIIa glycoprotein complex. Blood 66:76–85.

Bianco P, Robey PG, Simmons PJ. 2008. Mesenchymal stem cells: revisiting history, concepts, and assays. Cell Stem Cell 2:313–9.

Blank U, Karlsson G, Karlsson S. 2008. Signaling pathways governing stem-cell fate Review article Signaling pathways governing stem-cell fate. Blood 111:492–503.

Bodine D, Seidel N, Orlic D. 1996. Bone marrow collected 14 days after in vivo administration of granulocyte colony-stimulating factor and stem cell factor to mice has 10-fold more repopulating ability than untreated bone marrow. Blood 88:89–97.

Boeker W, Yin Z, Drosse I, Haasters F, Rossmann O, Wierer M, Popov C, Locher M, Mutschler W, Docheva D, Schieker M. 2008. Introducing a single-cell-derived human mesenchymal stem cell line expressing hTERT after lentiviral gene transfer. J Cell Mol Med 12:1347–1359.

Boisset J-C, Clapes T, Linden R Van Der, Dzierzak E, Robin C. 2013. Integrin IIb (CD41) plays a role in the maintenance of hematopoietic stem cell activity in the mouse embryonic aorta. Biol

Open 2:525–532.

Brown NH. 2011. Extracellular Matrix in Development: Insights from Mechanisms Conserved between Invertebrates and Vertebrates. Cold Spring Harb Perspect Biol 3:a005082–a005082.

Broxmeyer HE, Kohli L, Kim CH, Lee Y, Mantel C, Cooper S, Hangoc G, Shaheen M, Li X, Clapp DW. 2003. Stromal cell-derived factor-1/CXCL12 directly enhances survival/antiapoptosis of myeloid progenitor cells through CXCR4 and G(alpha)i proteins and enhances engraftment of competitive, repopulating stem cells. J Leukoc Biol 73:630–8.

Bruder SP, Jaiswal N, Haynesworth SE. 1997. Growth kinetics, self-renewal, and the osteogenic potential of purified human mesenchymal stem cells during extensive subcultivation and following cryopreservation. J Cell Biochem 64:278–294.

Bryder D, Rossi DJ, Weissman IL. 2006. Hematopoietic stem cells: the paradigmatic tissue-specific stem cell. Am J Pathol 169:338–46.

Calvi LM. 2006. Osteoblastic activation in the hematopoietic stem cell niche.

Calvi LM, Adams GB, Weibrecht KW, Weber JM, Olson DP, Knight MC, Martin RP, Schipani E, Divieti P, Bringhurst FR, Milner LA, Kronenberg HM, et al. 2003. Osteoblastic cells regulate the haematopoietic stem cell niche. Nature 425:841–846.

Carow CE, Hangoc G, Broxmeyer HE. 1993. Human Multipotential Progenitor Cells (CFU-GEMM) Have Extensive Replating Capacity for Secondary CFU-GEMM: An Effect Enhanced by Cord Blood Plasma. Blood 81:942–949.

Carstanjen D, Gross A, Kosova N, Fichtner I, Salama A. 2005. The alpha4beta1 and alpha5beta1 integrins mediate engraftment of granulocyte-colony-stimulating factor-mobilized human hematopoietic progenitor cells. Transfusion 45:1192–1200.

Cashen AF, Nervi B, DiPersio J. 2007. AMD3100: CXCR4 antagonist and rapid stem cell-mobilizing agent. Futur Oncol 3:19–27.

Catton WT. 2012. Blood Cell Formation in Certain Teleost Fishes. Blood 6:39–60.

Chang K-H, Bonig H, Papayannopoulou T. 2011. Generation and Characterization of Erythroid Cells from Human Embryonic Stem Cells and Induced Pluripotent Stem Cells : An Overview. Stem Cells Int 2011:791604.

Cheuk DK. 2013. Optimal stem cell source for allogeneic stem cell transplantation for hematological malignancies. World J Transplant 3:99–112.

Choi S-C, Kim S-J, Choi J-H, Park C-Y, Shim W-J, Lim D-S. 2008. Fibroblast Growth Factor-2

and -4 Promote the Proliferation of Bone Marrow Mesenchymal Stem Cells by the Activation of the PI3K-Akt and ERK1/2 Signaling Pathways. Stem Cells Dev 17:725–736.

Colter DC, Class R, DiGirolamo CM, Prockop DJ. 2000. Rapid expansion of recycling stem cells in cultures of plastic-adherent cells from human bone marrow. Proc Natl Acad Sci U S A 97:3213–8.

Corbel C, Salauen J. 2002. AlphaIIb integrin expression during development of the murine hemopoietic system. Dev Biol 243:301–311.

Cordeiro-Spinetti E, Taichman RS, Balduino A. 2015. The bone marrow endosteal niche: how far from the surface? J Cell Biochem 116:6–11.

Coulombe L, Vuillet M, Leroy C, Tchernia G. 1988. Lineage- and stage-specific adhesion of human hematopoietic progenitor cells to extracellular matrices from marrow fibroblasts. Blood 71:329–334.

Coulombel L. 2004. Identification of hematopoietic stem/progenitor cells: strength and drawbacks of functional assays. Oncogene 23:7210–7222.

Covas DT, Panepucci RA, Fontes AM, Silva WA, Orellana MD, Freitas MCC, Neder L, Santos ARD, Peres LC, Jamur MC, Zago MA. 2008. Multipotent mesenchymal stromal cells obtained from diverse human tissues share functional properties and gene-expression profile with CD146+ perivascular cells and fibroblasts. Exp Hematol 36:642–654.

Csaszar E, Kirouac DC, Yu M, Wang W, Qiao W, Cooke MP, Boitano AE, Ito C, Zandstra PW. 2012. Rapid expansion of human hematopoietic stem cells by automated control of inhibitory feedback signaling. Cell Stem Cell 10:218–229.

Daley WP, Peters SB, Larsen M. 2008. Extracellular matrix dynamics in development and regenerative medicine. J Cell Sci 121:255–264.

Delaney C, Heimfeld S, Brashem-Stein C, Voorhies H, Manger RL, Bernstein ID. 2010. Notch-mediated expansion of human cord blood progenitor cells capable of rapid myeloid reconstitution. Nat Med 16:232–236.

Dexter TM, Allen TD, Lajtha LG. 1977a. Conditions controlling the proliferation of haemopoietic stem cells in vitro. J Cell Physiol 91:335–344.

Dexter TM, Moore MA, Sheridan AP. 1977b. Maintenance of hemopoietic stem cells and production of differentiated progeny in allogeneic and semiallogeneic bone marrow chimeras in vitro. J Exp Med 166:289–294.

Bibliography

Dias J, Gumenyuk M, Kang H, Vodyanik M, Yu J, Thomson JA, Slukvin II. 2011. Generation of Red Blood Cells from Human Induced Pluripotent Stem Cells. Stem Cells Dev 20:1639–1647.

Dominici M, Blanc K Le, Mueller I, Slaper-Cortenbach I, Marini F, Krause D, Deans R, Keating A, Prockop D, Horwitz E. 2006. Minimal criteria for defining multipotent mesenchymal stromal cells. The International Society for Cellular Therapy position statement. Cytotherapy 8:315–7.

Dor FJMF, Ramirez ML, Parmar K, Altman EL, Huang CA, Down JD, Cooper DKC. 2006. Primitive hematopoietic cell populations reside in the spleen: Studies in the pig, baboon, and human. Exp Hematol 34:1573–1582.

Eaves CJ. 2015. Hematopoietic stem cells: concepts, definitions, and the new reality. Blood 125:.

Ebihara Y, Ma F, Tsuji K. 2012. Generation of red blood cells from human embryonic/induced pluripotent stem cells for blood transfusion. Int J Hematol 95:610–616.

Ekpenyong AE, Whyte G, Chalut K, Pagliara S, Lautenschlaeger F, Fiddler C, Paschke S, Keyser UF, Chilvers ER, Guck J. 2012. Viscoelastic Properties of Differentiating Blood Cells Are Fate- and Function-Dependent. PLoS One 7:.

Emambokus NR, Frampton J. 2003. The glycoprotein IIb molecule is expressed on early murine hematopoietic progenitors and regulates their numbers in sites of hematopoiesis. Immunity 19:33–45.

Engler AJ, Sen S, Sweeney HL, Discher DE. 2006. Matrix Elasticity Directs Stem Cell Lineage Specification. Cell 126:677–689.

Evans M. 2011. Discovering pluripotency: 30 years of mouse embryonic stem cells. Nat Rev Mol Cell Biol 12:680–686.

Ferkowicz MJ, Starr M, Xie X, Li W, Johnson SA, Shelley WC, Morrison PR, Yoder MC. 2003. CD41 expression defines the onset of primitive and definitive hematopoiesis in the murine embryo. Development 130:4393–4403.

Ficko T. 2008. Platelet glycoprotein IIIa gene expression in normal and malignant megakaryopoiesis. Ann Hematol 87:131–137.

Finch AJ, Soucek L, Junttila MR, Swigart LB, Evan GI. 2009. Acute overexpression of Myc in intestinal epithelium recapitulates some but not all the changes elicited by Wnt/beta-catenin pathway activation. Mol Cell Biol 29:5306–15.

Fonseca AV, Freund D, Bornhaeuser M, Corbeil D. 2010. Polarization and migration of

hematopoietic stem and progenitor cells rely on the RhoA/ROCK I pathway and an active reorganization of the microtubule network. J Biol Chem 285:31661–31671.

Freedman MH, Saunders EF. 1981. Hematopoiesis in the human spleen. Am J Hematol 11:271–5.

Freund D, Bauer N, Boxberger S, Feldmann S, Streller U, Ehninger G, Werner C, Bornhaeuser M, Oswald J, Corbeil D. 2006a. Polarization of human hematopoietic progenitors during contact with multipotent mesenchymal stromal cells: effects on proliferation and clonogenicity. Stem Cells Dev 15:815–829.

Freund D, Oswald J, Feldmann S, Ehninger G, Corbeil D, Bornhäuser M. 2006b. Comparative analysis of proliferative potential and clonogenicity of MACS-immunomagnetic isolated CD34+ and CD133+ blood stem cells derived from a single donor. Cell Prolif 39:325–32.

Friedenstein AJ. 1976. Precursor Cells of Mechanocytes. p 327–359.

Friedenstein AJ, Petrakova K V, Kurolesova AI, Frolova GP. 1968. Heterotopic of bone marrow. Analysis of precursor cells for osteogenic and hematopoietic tissues. Transplantation 6:230–47.

Friedmann-Morvinski D, Verma IM. 2014. Dedifferentiation and reprogramming: origins of cancer stem cells. EMBO Rep 15:244–53.

Furuyama A, Mochitate K. 2000. Assembly of the exogenous extracellular matrix during basement membrane formation by alveolar epithelial cells in vitro. J Cell Sci 859–68.

Gattazzo F, Urciuolo A, Bonaldo P. 2014. Extracellular matrix: A dynamic microenvironment for stem cell niche. Biochimica et Biophysica Acta - General Subjects 8:250619

Geiger B, Spatz JP, Bershadsky AD. 2009. Environmental sensing through focal adhesions. Nat Rev Mol Cell Biol 10:21–33.

Giebel B, Corbeil D, Beckmann J, Hoehn J, Freund D, Giesen K, Fischer J, Koegler G, Wernet P. 2004. Segregation of lipid raft markers including CD133 in polarized human hematopoietic stem and progenitor cells. Blood 104:2332–2338.

Gilbert TW, Sellaro TL, Badylak SF. 2006. Decellularization of tissues and organs. Biomaterials 27:3675–3683.

Giordano GF, Lichtman MA. 1972. Marrow Cell Egress THE CENTRAL INTERACTION OF BARRIER PORE SIZE AND CELL MATURATION. J Clin Invest 52:1154–1164.

Giralt S, Costa L, Schriber J, DiPersio J, Maziarz R, McCarty J, Shaughnessy P, Snyder E, Bensinger W, Copelan E, Hosing C, Negrin R, et al. 2014. Optimizing Autologous Stem Cell

Mobilization Strategies to Improve Patient Outcomes: Consensus Guidelines and Recommendations. Biol Blood Marrow Transplant 20:295–308.

Gordon MY. 2008. Stem cells for regenerative medicine-Biological attributes and clinical application. Exp Hematol 36:726–732.

Greenbaum A, Hsu Y-MS, Day RB, Schuettpelz LG, Christopher MJ, Borgerding JN, Nagasawa T, Link DC. 2013. CXCL12 in early mesenchymal progenitors is required for haematopoietic stem-cell maintenance. Nature 495:227–230.

Hall W, Antonio S. 2001. Expression of Adhesion Molecules on CD34 + Cells in Peripheral Blood of Non-Hodgkin ' s Lymphoma Patients Mobilized with Different Growth Factors. 134–143.

Hattangadi SM, Wong P, Zhang L, Flygare J, Lodish HF. 2011.

Hergeth SP, Aicher WK, Essl M, Schreiber TD, Sasaki T, Klein G. 2008. Characterization and functional analysis of osteoblast-derived fibulins in the human hematopoietic stem cell niche. Exp Hematol 36:1022–1034.

Holst J, Watson S, Lord MS, Eamegdool SS, Bax D V, Nivison-Smith LB, Kondyurin A, Ma L, Oberhauser AF, Weiss AS, Rasko JE. 2010. Substrate elasticity provides mechanical signals for the expansion of hemopoietic stem and progenitor cells. Nat Biotechnol 28:1123–1128.

Horwitz E, Andreeff M, Frassoni F. 2006.

Horwitz EM, Blanc K Le, Dominici M, Mueller I, Slaper-Cortenbach I, Marini FC, Deans RJ, Krause DS, Keating A, International Society for Cellular Therapy. 2005. Clarification of the nomenclature for MSC: The International Society for Cellular Therapy position statement. Cytotherapy 7:393–395.

Huber TL, Kouskoff V, Joerg Fehling H, Palis J, Keller G. 2004. Haemangioblast commitment is initiated in the primitive streak of the mouse embryo. Nature 432:625–630.

Hutmacher DW. 2001. Scaffold design and fabrication technologies for engineering tissues-- state of the art and future perspectives. J Biomater Sci Polym Ed 12:107–24.

Hynes RO. 2002. Integrins: Bidirectional, allosteric signaling machines. Cell 110:673–687.

Hynes RO. 2012. The Extracellular Matrix : not just pretty fibrils. Science (80-) 1216–121:2009.

Hynes RO. 2014. Stretching the boundaries of extracellular matrix research. Nat Rev Mol Cell Biol 15:761–763.

Itkin T, Gur-Cohen S, Spencer JA, Schajnovitz A, Ramasamy SK, Kusumbe AP, Ledergor G,

Bibliography

Jung Y, Milo I, Poulos MG, Kalinkovich A, Ludin A, et al. 2016. Distinct bone marrow blood vessels differentially regulate haematopoiesis. Nature 1–19.

Jacobi A, Thieme S, Lehmann R, Ugarte F, Malech HL, Koch S, Thiede C, Mueller K, Bornhaeuser M, Ryser M, Brenner S. 2010. Impact of CXCR4 inhibition on FLT3-ITD-positive human AML blasts. Exp Hematol 38:180–190.

Jang YK, Jung DH, Jung MH, Kim DH, Yoo KH, Sung KW, Koo HH, Oh W, Yang YS, Yang SE. 2006. Mesenchymal stem cells feeder layer from human umbilical cord blood for ex vivo expanded growth and proliferation of hematopoietic progenitor cells. Ann Hematol 85:212–225.

Jansen LE, Birch NP, Schiffman JD, Crosby AJ, Peyton SR. 2015. Mechanics of intact bone marrow. J Mech Behav Biomed Mater 50:299–307.

Jiang Y, Jahagirdar BN, Reinhardt RL, Schwartz RE, Keene CD, Ortiz-Gonzalez XR, Reyes M, Lenvik T, Lund T, Blackstad M, Du J, Aldrich S, et al. 2002. Pluripotency of mesenchymal stem cells derived from adult marrow. Nature 418:41–49.

Jing D, Fonseca A V., Alakel N, Fierro FA, Mueller K, Bornhaeuser M, Ehninger G, Corbeil D, Ordemann R. 2010. Hematopoietic stem cells in co-culture with mesenchymal stromal cells - modeling the niche compartments in vitro. Haematologica 95:542–550.

Jung Y, Song J, Shiozawa Y, Wang J, Wang Z, Williams B, Havens A, Schneider A, Ge C, Franceschi RT, McCauley LK, Krebsbach PH, et al. 2008. Hematopoietic Stem Cells Regulate Mesenchymal Stromal Cell Induction into Osteoblasts Thereby Participating in the Formation of the Stem Cell Niche. Stem Cells 26:2042–2051.

Jung Y, Wang J, Schneider A, Sun Y-X, Koh-Paige AJ, Osman NI, McCauley LK, Taichman RS. 2006. Regulation of SDF-1 (CXCL12) production by osteoblasts; a possible mechanism for stem cell homing. Bone 38:497–508.

Kalinina N, Kharlampieva D, Loguinova M, Butenko I, Pobeguts O, Efimenko A, Ageeva L, Sharonov G, Ischenko D, Alekseev D, Grigorieva O, Sysoeva V, et al. 2015. Characterization of secretomes provides evidence for adipose-derived mesenchymal stromal cells subtypes. Stem Cell Res Ther 6:221.

Karp G. 2008. Cell and Molecular Biology: Concepts and Experiments. John Wiley. 662-682 p.

Kiel MJ, Yilmaz ÖH, Iwashita T, Yilmaz OH, Terhorst C, Morrison SJ. 2005. SLAM Family Receptors Distinguish Hematopoietic Stem and Progenitor Cells and Reveal Endothelial Niches for Stem Cells. Cell 121:1109–1121.

Bibliography

Kimbrel EA, Lu S-J. 2011. Potential Clinical Applications for Human Pluripotent Stem Cell-Derived Blood Components. Stem Cells Int 2011:1–11.

Klein G. 1995. The extracellular matrix of the hematopoietic microenvironment. Experientia 9-10:914-26

Klimanskaya I, Chung Y, Meisner L, Johnson J, West MD, Lanza R. 2005. Human embryonic stem cells derived without feeder cells. Lancet 365:1636–1641.

Kluge M, Mann K, Dziadek M, Timpl R. 1990. Characterization of a novel calcium-binding 90-kDa glycoprotein (BM-90) shared by basement membranes and serum. Eur J Biochem 193:651–659.

Kobayashi H, Butler JM, O'Donnell R, Kobayashi M, Ding B-S, Bonner B, Chiu VK, Nolan DJ, Shido K, Benjamin L, Rafii S. 2010. Angiocrine factors from Akt-activated endothelial cells balance self-renewal and differentiation of haematopoietic stem cells. Nat Cell Biol 12:1046–1056.

Kobayashi I, Katakura F, Moritomo T. 2016. Isolation and characterization of hematopoietic stem cells in teleost fish. Dev Comp Immunol 58:86–94.

Kostka G, Giltay R, Bloch W, Addicks K, Timpl R, Fässler R, Chu ML. 2001. Perinatal lethality and endothelial cell abnormalities in several vessel compartments of fibulin-1-deficient mice. Mol Cell Biol 21:7025–34.

Kräter M, Jacobi A, Otto O, Tietze S, Müller K, Poitz D, Palm S, Zinna V, Biehain U, Wobus M, Chavakis T, Werner C, et al. 2017. Bone marrow niche-mimetics modulate HSPC function via integrin signaling. Sci Rep. in press

Kretser D de. 2007. Totipotent, pluripotent or unipotent stem cells: a complex regulatory enigma and fascinating biology. J Law Med 15:212–8.

Lai T-H, Fong Y-C, Fu W-M, Yang R-S, Tang C-H. 2009. Stromal cell-derived factor-1 increase alphavbeta3 integrin expression and invasion in human chondrosarcoma cells. J Cell Physiol 218:334–42.

Lautenschlaeger F, Paschke S, Schinkinger S, Bruel A, Beil M, Guck J. 2009. The regulatory role of cell mechanics for migration of differentiating myeloid cells. Proc Natl Acad Sci U S A 106:15696–15701.

Lee-Thedieck C, Rauch N, Fiammengo R, Klein G, Spatz JP. 2012. Impact of substrate elasticity on human hematopoietic stem and progenitor cell adhesion and motility. J Cell Sci 125:3765–

Bibliography

3775.

Lee-Thedieck C, Spatz JP. 2014. Biophysical regulation of hematopoietic stem cells. Biomater Sci 2:1548–1561.

Lee HJ, Li N, Evans SM, Diaz MF, Wenzel PL. 2013. Biomechanical force in blood development: Extrinsic physical cues drive pro-hematopoietic signaling. Differentiation 86:92–103.

Lemoli RM, Tafuri A, Fortuna A, Catani L, Rondelli D, Ratta M, Tura S. 1998. Biological characterization of CD34+ cells mobilized into peripheral blood. Bone Marrow Transpl 22 Suppl 5:S47-50.

Li W, Johnson SA, Shelley WC, Ferkowicz M, Morrison P, Li Y, Yoder MC. 2003. Primary endothelial cells isolated from the yolk sac and para-aortic splanchnopleura support the expansion of adult marrow stem cells in vitro. Blood 102:4345–4353.

Lima M de, McNiece I, Robinson SN, Munsell M, Eapen M, Horowitz M, Alousi A, Saliba R, McMannis JD, Kaur I, Kebriaei P, Parmar S, et al. 2012. Cord-blood engraftment with ex vivo mesenchymal-cell coculture. N Engl J Med 367:2305–2315.

Liu X, Rahaman MN, Hilmas GE, Bal BS. 2013. Mechanical properties of bioactive glass (13-93) scaffolds fabricated by robotic deposition for structural bone repair. Acta Biomater 9:7025–7034.

Lodish H, Flygare J, Chou S. 2010. From stem cell to erythroblast: regulation of red cell production at multiple levels by multiple hormones. IUBMB Life 62:492–6.

Lord BI, Testa NG, Hendry JH. 1975. The relative spatial distributions of CFUs and CFUc in the normal mouse femur. Blood 46:65–72.

Lu P, Takai K, Weaver VM, Werb Z. 2011. Extracellular matrix degradation and remodeling in development and disease. Cold Spring Harb Perspect Biol 3:.

Lv F-J, Tuan RS, Cheung KMC, Leung VYL. 2014. Concise Review: The Surface Markers and Identity of Human Mesenchymal Stem Cells. Stem Cells 32:1408–1419.

Mendelson A, Frenette PS. 2014. Hematopoietic stem cell niche maintenance during homeostasis and regeneration. Nat Med 20:833–846.

Mietke A, Otto O, Girardo S, Rosendahl P, Taubenberger A, Golfier S, Ulbricht E, Aland S, Guck J, Fischer-Friedrich E. 2015. Extracting Cell Stiffness from Real-Time Deformability Cytometry: Theory and Experiment. Biophys J 109:2023–2036.

Miller PG, Al-Shahrour F, Hartwell KA, Chu LP, Jaerås M, Puram R V., Puissant A, Callahan KP, Ashton J, McConkey ME, Poveromo LP, Cowley GS, et al. 2013. InVivo RNAi Screening

Identifies a Leukemia-Specific Dependence on Integrin Beta 3 Signaling. Cancer Cell 24:45–58.

Mitjavila-Garcia MT, Cailleret M, Godin I, Nogueira MM, Cohen-Solal K, Schiavon V, Lecluse Y, Pesteur F Le, Lagrue AH, Vainchenker W. 2002. Expression of CD41 on hematopoietic progenitors derived from embryonic hematopoietic cells. Development 129:2003–2013.

Moffat J, Grueneberg DA, Yang X, Kim SY, Kloepfer AM, Hinkle G, Piqani B, Eisenhaure TM, Luo B, Grenier JK, Carpenter AE, Foo SY, et al. 2006. A Lentiviral RNAi Library for Human and Mouse Genes Applied to an Arrayed Viral High-Content Screen. Cell 124:1283–1298.

Mohammadi M, Olsen SK, Goetz R. 2005. A protein canyon in the FGF–FGF receptor dimer selects from an à la carte menu of heparan sulfate motifs. Curr Opin Struct Biol 15:506–516.

Mohle R, Murea S, Kirsch M, Haas R. 1995. Differential expression of L-selectin, VLA-4, and LFA-1 on CD34+ progenitor cells from bone marrow and peripheral blood during G-CSF-enhanced recovery. Exp Hematol 23:1535–1542.

Morrison SJ, Hemmati HD, Wandycz AM, Weissmant IL. 1995. The purification and characterization of fetal liver hematopoietic stem cells. Immunology 92:10302–10306.

Morrison SJ, Kimble J. 2006. Asymmetric and symmetric stem-cell divisions in development and cancer. Nature 441:1068–1074.

Naba A, Clauser KR, Whittaker CA, Carr SA, Tanabe KK, Hynes RO. 2014. Extracellular matrix signatures of human primary metastatic colon cancers and their metastases to liver. BMC Cancer 14:518.

Nagasawa T, Hirota S, Tachibana K, Takakura N, Nishikawa S, Kitamura Y, Yoshida N, Kikutani H, Kishimoto T. 1996. Defects of B-cell lymphopoiesis and bone-marrow myelopoiesis in mice lacking the CXC chemokine PBSF/SDF-1. Nature 382:635–638.

Naik UP, Parise L V. 1997. Structure and function of platelet alpha IIb beta 3. Curr Opin Hematol 4:317–22.

Nakagawa M, Koyanagi M, Tanabe K, Takahashi K, Ichisaka T, Aoi T, Okita K, Mochiduki Y, Takizawa N, Yamanaka S. 2007. Generation of induced pluripotent stem cells without Myc from mouse and human fibroblasts. Nat Biotechnol 26:101–106.

Nakamura Y. 2008. In vitro production of transfusable red blood cells. Biotechnol Genet Eng Rev 25:187–201.

Nayal A, Webb DJ, Brown CM, Schaefer EM, Vicente-Manzanares M, Horwitz AR. 2006. Paxillin phosphorylation at Ser273 localizes a GIT1-PIX-PAK complex and regulates adhesion and

protrusion dynamics. J Cell Biol 173:587–599.

Nilsson SK. 2005. Osteopontin, a key component of the hematopoietic stem cell niche and regulator of primitive hematopoietic progenitor cells. Blood 106:1232–1239.

Nilsson SK, Johnston HM, Whitty GA, Williams B, Webb RJ, Denhardt DT, Bertoncello I, Bendall LJ, Simmons PJ, Haylock DN. 2005. Osteopontin, a key component of the hematopoietic stem cell niche and regulator of primitive hematopoietic progenitor cells. Blood 106:1232–1239.

North TE, Goessling W, Walkley CR, Lengerke C, Kopani KR, Lord AM, Weber GJ, Bowman T V, Jang I-H, Grosser T, Fitzgerald GA, Daley GQ, et al. 2007. Prostaglandin E2 regulates vertebrate haematopoietic stem cell homeostasis. Nature 447:1007–11.

Notta F, Doulatov S, Laurenti E, Poeppl A, Jurisica I, Dick JE. 2011. Isolation of Single Human Hematopoietic Stem Cells Capable of Long-Term Multilineage Engraftment. Science (80-) 333:218–221.

Ogawa M. 1989. Effects of hemopoietic growth factors on stem cells in vitro. Hematol Oncol Clin North Am 3:453–64.

Ogawa M. 1993. Differentiation and proliferation of hematopoietic stem cells. Blood 81:2844–2853.

Ohmori T, Kashiwakura Y, Ishiwata A, Madoiwa S, Mimuro J, Furukawa Y, Sakata Y. 2010. Vinculin is indispensable for repopulation by hematopoietic stem cells, independent of integrin function. J Biol Chem 285:31763–73.

Osawa M, Hanada K -i., Hamada H, Nakauchi H. 1996. Long-Term Lymphohematopoietic Reconstitution by a Single CD34-Low/Negative Hematopoietic Stem Cell. Science (80-) 273:242–245.

Osawa M, Hanada KI, Hamada H, H N. 1996. Long-Term Lymphohematopoietic Reconstitution by a Single CD34-Low/Negative Hematopoietic Stem Cell. Science (80-) 273:3–6.

Oswald J, Boxberger S, Jørgensen B, Feldmann S, Ehninger G, Bornhäuser M, Werner C. 2004. Mesenchymal stem cells can be differentiated into endothelial cells in vitro. Stem Cells 22:377–384.

Otto O, Rosendahl P, Mietke A, Golfier S, Herold C, Klaue D, Girardo S, Pagliara S, Ekpenyong A, Jacobi A, Wobus M, Töpfner N, et al. 2015. Real-time deformability cytometry: on-the-fly cell mechanical phenotyping. Nat Methods 12:199-202

Peled A, Kollet O, Ponomaryov T, Petit I, Franitza S, Grabovsky V, Slav MM, Nagler A, Lider O,

Alon R, Zipori D, Lapidot T. 2000. The chemokine SDF-1 activates the integrins LFA-1, VLA-4, and VLA-5 on immature human CD34(+) cells: role in transendothelial/stromal migration and engraftment of NOD/SCID mice. Blood 95:3289–96.

Peled A, Petit I, Kollet O, Magid M, Ponomaryov T, Byk T, Nagler A, Ben-Hur H, Many A, Shultz L, Lider O, Alon R, et al. 1999. Dependence of human stem cell engraftment and repopulation of NOD/SCID mice on CXCR4. Science 283:845–8.

Pereira C, Clarke E, Damen J. 2007. Hematopoietic colony-forming cell assays. Methods Mol Biol 407:177–208.

Petit I, Szyper-Kravitz M, Nagler A, Lahav M, Peled A, Habler L, Ponomaryov T, Taichman RS, Arenzana-Seisdedos F, Fujii N, Sandbank J, Zipori D, et al. 2002. G-CSF induces stem cell mobilization by decreasing bone marrow SDF-1 and up-regulating CXCR4. Nat Immunol 3:687–694.

Peyton SR, Ghajar CM, Khatiwala CB, Putnam AJ. 2007. The emergence of ECM mechanics and cytoskeletal tension as important regulators of cell function. Cell Biochem Biophys 47:300–320.

Potocnik AJ, Brakebusch C, Fässler R. 2000. Fetal and Adult Hematopoietic Stem Cells Require β1 Integrin Function for Colonizing Fetal Liver, Spleen, and Bone Marrow. Immunity 12:653–663.

Pouget C, Peterkin T, Simões FC, Lee Y, Traver D, Patient R. 2014. FGF signalling restricts haematopoietic stem cell specification via modulation of the BMP pathway. Nat Commun 5:5588.

Prewitz MC, Seib FP, Bonin M von, Friedrichs J, Stißel A, Niehage C, Mueller K, Anastassiadis K, Waskow C, Hoflack B, Bornhäuser M, Werner C. 2013. Tightly anchored tissue-mimetic matrices as instructive stem cell microenvironments. Nat Methods 10:788–94.

Prewitz MC, Stißel A, Friedrichs J, Traeber N, Vogler S, Bornhaeuser M, Werner C. 2015. Extracellular matrix deposition of bone marrow stroma enhanced by macromolecular crowding. Biomaterials 73:60–69.

Prockop DJ. 1997. Marrow Stromal Cells as Stem Cells for Nonhematopoietic Tissues. Science (80-) 276:71–74.

Prosper F, Stroncek D, McCarthy JB, Verfaillie CM. 1998. Mobilization and homing of peripheral blood progenitors is related to reversible downregulation of alpha4 beta1 integrin expression and function. J Clin Invest 101:2456–2467.

Prosper F, Verfaillie CM. 2001. Regulation of hematopoiesis through adhesion receptors. J Leukoc Biol 69:307–316.

Qian H, Tryggvason K, Jacobsen SE, Ekblom M. 2006. Contribution of a6 integrins to hematopoietic stem and progenitor cell homing to bone marrow and collaboration with a4 integrins. Blood 107:3503–3510.

Quesenberry PJ, Abedi M, Aliotta J, Colvin G, Demers D, Dooner M, Greer D, Hebert H, Menon MK, Pimentel J, Paggioli D. 2004. Stem cell plasticity: an overview. Blood Cells Mol Dis 32:1–4.

Rahman S, Patel Y, Murray J, Patel K V, Sumathipala R, Sobel M, Wijelath ES. 2005. Novel hepatocyte growth factor (HGF) binding domains on fibronectin and vitronectin coordinate a distinct and amplified Met-integrin induced signalling pathway in endothelial cells. BMC Cell Biol 6:8.

Ranganathan V, De PK. 1996. Western Blot of Proteins from Coomassie-Stained Polyacrylamide Gels. Anal Biochem 234:102–104.

Reichert D, Friedrichs J, Ritter S, Kaeubler T, Werner C, Bornhaeuser M, Corbeil D. 2015. Phenotypic, Morphological and Adhesive Differences of Human Hematopoietic Progenitor Cells Cultured on Murine versus Human Mesenchymal Stromal Cells. Sci Rep 5:15680.

Rippon HJ, Bishop AE. 2004. Embryonic stem cells. Cell Prolif 37:23–34.

Roecklein BA, Torok-Storb B. 1995. Functionally Distinct Human Marrow Stromal Cell Lines Immortalized by Transduction With the Human Papilloma Virus E6/E7 Genes. Blood 85:997–1005.

Roskelley CD, Desprez PY, Bissell MJ. 1994. Extracellular matrix-dependent tissue-specific gene expression in mammary epithelial cells requires both physical and biochemical signal transduction. Cell Biol 91:12378–12382.

Ross TD, Coon BG, Yun S, Baeyens N, Tanaka K, Ouyang M, Schwartz MA. 2013. Integrins in mechanotransduction. Curr Opin Cell Biol 25:613–618.

Rosso F, Giordano A, Barbarisi M, Barbarisi A. 2004. From Cell-ECM interactions to tissue engineering. J Cell Physiol 199:174–180.

Rougier F, Cornu E, Praloran V, Denizot Y. 1998. IL-6 AND IL-8 PRODUCTION BY HUMAN BONE MARROW STROMAL CELLS. Cytokine 10:93–97.

Sahin AO, Buitenhuis M. 2012. Molecular mechanisms underlying adhesion and migration of hematopoietic stem cells. Cell Adh Migr 6:39–48.

Sánchez-Madrid F, Pozo MA Del. 1999. Leukocyte polarization in cell migration and immune interactions. EMBO J 18:501–511.

Scadden DT. 2006. The stem-cell niche as an entity of action. Nature 441:1075–9.

Schofield R. 1978. The relationship between the spleen colony-forming cell and the haemopoietic stem cell. Blood Cells 4:7–25.

Seib FP, Müller K, Franke M, Grimmer M, Bornhäuser M, Werner C. 2009a. Engineered extracellular matrices modulate the expression profile and feeder properties of bone marrow-derived human multipotent mesenchymal stromal cells. Tissue Eng Part A 15:3161–3171.

Seib FP, Prewitz M, Werner C, Bornhäuser M. 2009b. Matrix elasticity regulates the secretory profile of human bone marrow-derived multipotent mesenchymal stromal cells (MSCs). Biochem Biophys Res Commun 389:663–667.

Seita J, Weissman IL. 2010. Hematopoietic stem cell: self-renewal versus differentiation. Wiley Interdiscip Rev Syst Biol Med 2:640–53.

Shi Y, Massagué J. 2003. Mechanisms of TGF-beta signaling from cell membrane to the nucleus. Cell 113:685–700.

Sipkins DA, Wei X, Wu JW, Runnels JM, Côté D, Means TK, Luster AD, Scadden DT, Lin CP. 2005. In vivo imaging of specialized bone marrow endothelial microdomains for tumour engraftment. Nature 435:969–973.

Smith JNP, Calvi LM. 2013. Concise review: Current concepts in bone marrow microenvironmental regulation of hematopoietic stem and progenitor cells. Stem Cells 31:1044–50.

Spangrude GJ, Heimfeld S, Weissman IL. 1988. Purification and characterization of mouse hematopoietic stem cells. Science 241:58–62.

Spees JL, Lee RH, Gregory CA. 2016. Mechanisms of mesenchymal stem/stromal cell function. Stem Cell Res Ther 7:125.

Stewart SA, Dykxhoorn DM, Palliser D, Mizuno H, Yu EY, An DS, Sabatini DM, Chen ISY, Hahn WC, Sharp PA, Weinberg RA, Novina CD. 2003. Lentivirus-delivered stable gene silencing by RNAi in primary cells. RNA 9:493–501.

Stopp S, Bornhäuser M, Ugarte F, Wobus M, Kuhn M, Brenner S, Thieme S. 2013. Expression of the melanoma cell adhesion molecule in human mesenchymal stromal cells regulates proliferation, differentiation, and maintenance of hematopoietic stem and progenitor cells.

Haematologica 98:505–513.

Sun Yan-Xi, Fang Ming, Wang Jianhua, Cooper Carlton R, Kenneth Pienta J TRS. 2007. Expression andActivation of avb3 Integrinsby SDF-1/CXC12 Increases theAggressiveness of ProstateCancerCells. Prostate 67:61–73.

Taichman RS, Emerson SG. 1998. The role of osteoblasts in the hematopoietic microenvironment. Stem Cells 16:7–15.

Takahashi K, Okita K, Nakagawa M, Yamanaka S. 2007. Induction of pluripotent stem cells from fibroblast cultures. Nat Protoc 2:3081–3089.

Takahashi K, Yamanaka S. 2006. Induction of Pluripotent Stem Cells from Mouse Embryonic and Adult Fibroblast Cultures by Defined Factors. Cell 126:663–676.

Takai K, Hara J, Matsumoto K, Hosoi G, Osugi Y, Tawa A, Okada S, Nakamura T. 1997. Hepatocyte growth factor is constitutively produced by human bone marrow stromal cells and indirectly promotes hematopoiesis. Blood 89:1560–5.

Taupin P, Gage FH. 2002. Adult neurogenesis and neural stem cells of the central nervous system in mammals. J Neurosci Res 69:745–749.

Teitelbaum SL. 2000. Bone Resorption by Osteoclasts. Science (80-) 289:1504–1508.

Teixido J, Hemler ME, Greenberger JS, Anklesariat P. 1992. Role of beta 1 and beta 2 integrins in the adhesion of human CD34hi stem cells to bone marrow stroma. J Clin Invest 90:358–367.

Thon JN. 2014.

Till JE, McCulloch EA. 1961. A Direct Measurement of the Radiation Sensitivity of Normal Mouse Bone Marrow Cells. Radiat Res 14:213.

Trumpp A, Essers M, Wilson A. 2010. Awakening dormant haematopoietic stem cells. Nat Rev Immunol 10:201–209.

Twal WO, Hammad SM, Guffy SL, Argraves WS. 2015. A novel intracellular fibulin-1D variant binds to the cytoplasmic domain of integrin beta 1 subunit. Matrix Biol.

Uchida N, He D, Friera a M, Reitsma M, Sasaki D, Chen B, Tsukamoto a. 1997. The unexpected G0/G1 cell cycle status of mobilized hematopoietic stem cells from peripheral blood. Blood 89:465–472.

Umemoto T, Yamato M, Ishihara J, Shiratsuchi Y, Utsumi M, Tsukui H, Terasawa M, Shibata T, Nishida K, Kobayashi Y, Petrich G, Nakauchi H, et al. 2012. Integrin-αvβ3 regulates

thrombopoietin-mediated maintenance of hematopoietic stem cells. Blood 119:83–94.

Umemoto T, Yamato M, Shiratsuchi Y, Terasawa M, Yang J, Nishida K, Kobayashi Y, Okano T. 2006. Expression of Integrin beta3 is correlated to the properties of quiescent hemopoietic stem cells possessing the side population phenotype. J Immunol 177:7733–7739.

Umemoto T, Yamato M, Shiratsuchi Y, Terasawa M, Yang J, Nishida K, Kobayashi Y, Okano T. 2008. CD61 enriches long-term repopulating hematopoietic stem cells. Biochem Biophys Res Commun 365:176–182.

Vega S de, Iwamoto T, Yamada Y. 2009. Fibulins: Multiple roles in matrix structures and tissue functions. Cell Mol Life Sci 66:1890–1902.

Visnjic D. 2004. Hematopoiesis is severely altered in mice with an induced osteoblast deficiency. Blood 103:3258–3264.

Visnjic D, Kalajzic I, Gronowicz G, Aguila HL, Clark SH, Lichtler AC, Rowe DW. 2001. Conditional Ablation of the Osteoblast Lineage in Col2.3Δtk Transgenic Mice. J Bone Miner Res 16:2222–2231.

Wagers AJ, Allsopp RC, Weissman IL. 2002. Changes in integrin expression are associated with altered homing properties of Lin-/lo Thy1.1lo Sca-1+ c-kit+ hematopoietic Stem Cells Following Mobilization By Cyclophosphamide/Granulocyte Colony-Stimulating Factor. Exp Hematol 30:176–185.

Wagner W, Horn P, Castoldi M, Diehlmann A, Bork S, Saffrich R, Benes V, Blake J, Pfister S, Eckstein V, Ho AD. 2008. Replicative Senescence of Mesenchymal Stem Cells: A Continuous and Organized Process. PLoS One 3:e2213.

Whetton AD, Spooncert E. 1998. Role of cytokines and extracellular matrix in the regulation of haemopoietic stem cells. Curr Opin Cell Biol 10:721–726.

Whitaker B, Hinkins S. 2011. The 2011 National Blood Collection and Utilization Survery Report

Williams DA, Rios M, Stephens C, Patel VP. 1991. Fibronectin and VLA-4 in haematopoietic stem cell-microenvironment interactions. Nauture 6334:438-41

Wilson A, Trumpp A. 2006. Bone-marrow haematopoietic-stem-cell niches. Nat Rev Immunol 6:93–106.

Wolber FM, Leonard E, Michael S, Orschell-Traycoff CM, Yoder MC, Srour EF. 2002. Roles of spleen and liver in development of the murine hematopoietic system. Exp Hematol 30:1010–9.

Wright DE. 2001. Physiological Migration of Hematopoietic Stem and Progenitor Cells. Science

(80-) 294:1933–1936.

Wu AG, Michejda M, Mazumder A, Meehan KR, Menendez FA, Tchabo JG, Slack R, Johnson MP, Bellanti JA. 1999. Analysis and characterization of hematopoietic progenitor cells from fetal bone marrow, adult bone marrow, peripheral blood, and cord blood. Pediatr Res 46:163–169.

Xavier M, Rosendahl P, Herbig M, Kraeter M, Spencer D, Bornhaeuser M, Oreffo ROC, Morgan H, Guck J, Otto O. 2016. Mechanical phenotyping of primary human skeletal stem cells in heterogeneous populations by real-time deformability cytometry. Integr Biol (Camb) 10–12.

Xie X, Li Y, Pei X. 2014. From stem cells to red blood cells: how far away from the clinical application? Sci China Life Sci 57:581–585.

Yamaguchi DT. 2014. " Ins " and " Outs " of mesenchymal stem cell osteogenesis in regenerative medicine. World J Stem Cells 6:94–110.

Yang J, Plikus M V, Komarova NL. 2015. The Role of Symmetric Stem Cell Divisions in Tissue Homeostasis. PLoS Comput Biol 11:e1004629.

Yin a H, Miraglia S, Zanjani ED, Almeida-Porada G, Ogawa M, Leary a G, Olweus J, Kearney J, Buck DW. 1997. AC133, a novel marker for human hematopoietic stem and progenitor cells. Blood 90:5002–5012.

Yu H, Tay CY, Leong WS, Tan SCW, Liao K, Tan LP. 2010. Mechanical behavior of human mesenchymal stem cells during adipogenic and osteogenic differentiation. Biochem Biophys Res Commun 393:150–155.

Yu J, Vodyanik M, Smuga-Otto K, Antosiewicz-Bourget J, Frane J, Tian S, Nie J, Jonsdottir G, Ruotti V, Stewart R, Slukvin I, Thomson J. 2007. Induced Pluripotent Stem Cell Lines Derived from Human Somatic Cells. Science (80-) 318:1917–1920.

Zachos TA, Shields KM, Bertone AL. 2006. Gene-mediated osteogenic differentiation of stem cells by bone morphogenetic proteins-2 or -6. J Orthop Res 24:1279–1291.

Zamir E, Geiger B. 2001. Molecular complexity and dynamics of cell-matrix adhesions. J Cell Sci 114:3583–3590.

Zhang CC, Lodish HF. 2008. Cytokines regulating hematopoietic stem cell function. Curr Opin Hematol 15:307–11.

Zhang J, Niu C, Ye L, Huang H, He X, Tong W-G, Ross J, Haug J, Johnson T, Feng JQ, Harris S, Wiedemann LM, et al. 2003. Identification of the haematopoietic stem cell nic...[Nature. 2003] - PubMed Result. Nature 425:836–841.

Zhang Z, Luo X, Xu H, Wang L, Jin X, Chen R, Ren X, Lu Y, Fu M, Huang Y, He J, Fan Z. 2015. Bone marrow stromal cell-derived extracellular matrix promotes osteogenesis of adipose-derived stem cells. Cell Biol Int 39:291–299.

Zuk PA, Zhu M, Ashjian P, Ugarte DA De, Huang JI, Mizuno H, Alfonso ZC, Fraser JK, Benhaim P, Hedrick MH. 2002. Human Adipose Tissue Is a Source of Multipotent Stem Cells. Mol Biol Cell 13:4279–4295.

Danksagung

Die vorliegende Dissertation wurde am Uniklinikum Carl Gustav Carus an der Technischen Universität Dresden im Stammzelllabor 2 angefertigt.

Ich möchte mich ganz herzlich bei Prof. Dr. Martin Bornhäuser für die Aufnahme in seine Arbeitsgruppe, für seine wissenschaftliche Unterstützung und für die wissenschaftliche Freiheit, die ich während der Anfertigung dieser Promotion genießen durfte bedanken.

Ich danke Prof. Dr. Jochen Guck für die großartige Zusammenarbeit und die Freiheiten und Möglichkeiten die ich in seinem Labor hatte, ohne die ein Großteil dieser Dissertation und anderer Arbeiten während meiner Promotion nicht möglich gewesen wären.

Für die fachliche Unterstützung im Labor, für die motivierenden und kritischen Gespräche, für das Interesse am Fortgang meiner Arbeit und für unsere Freundschaft möchte ich mich herzlich bei Dr. Angela Jacobi bedanken. Für die freundliche Betreuung dieser Arbeit und die hilfreichen Hinweise im Labor danke ich Dr. Manja Wobus.

Ich danke allen Kollegen, dem gesamten Team der Arbeitsgruppe um Prof. Dr. Martin Bornhäuser und dem gesamten Team der Arbeitsgruppe um Prof. Dr. Jochen Guck für das konstruktive und freundliche Arbeitsklima. Besonderer Dank geht an Dr. Oliver Otto, Dr. Stefanie Tietze, Dr. David Poitz, Maik Herbig, Guruchandar Arulmozhivarman und Katrin Müller, für eure tatkräftige und unermüdliche Unterstützung, eure kritischen und fachlichen Anregungen und für die gute und freundschaftliche Zusammenarbeit. Ohne euch wäre die Arbeit nicht halb so schön gewesen und wahrscheinlich auch noch nicht fertig.

Für die Bereitstellung der Arbeitsmaterialien und Labore im Max Bergman Zentrum danke ich Prof. Dr. Carsten Werner. Ein besonderer Dank geht in diesem Zusammenhang an Dr. Marina Prewitz für die Einführung in das Thema ECM-Präparation sowie an Aline Stißel und Nelly Rein für ihre Unterstützung im Labor.

Ich danke Prof. Dr. Sebastian Thieme für die Bereitstellung seines Labors zur Durchführung der lentiviralen kock down Experimente. Für die Unterstützung bei der Durchführung der knock down Experimente möchte ich mich besonders bei Dr. Sebastian Brenner und Katrin Navratiel bedanken. Ich danke auch Prof. Dr. Frank Buchholz für die Bereitstellung der shRNA Vektoren.

Für fachliche Anregungen, kritische Kommentare und spannende Diskussionen möchte ich mich bei Prof. Dr. Triantafyllos Chavakis bedanken.

Gerne möchte ich allen Mitgliedern des Promotionsausschusses danken. Besonderer Dank geht dabei an Prof. Angela Rösen-Wolff für die Übernahme des Vorsitzes. Ich danke Prof. Dr. Martin

Anlagen

Erklärung zur Eröffnung des Promotionsverfahrens [Formblatt 1.2.1]

Erklärung zur Einhaltung rechtlicher Vorschriften [Formblatt 1.1]